UCLA HENRY SAMUELI SCHOOL OF ENGINEERING AND APPLIED SCIENCE

Passive Tactile Sensing

Masters Design Study

Eric K. Sender

Spring 2012

Capstone course in the UCLA Masters of Engineering program. Advised by Professor Christopher S. Lynch.

TABLE OF CONTENTS

FIGURES

TABLES

ABSTRACT

Sensing—whether it be pressure, temperature, heat, or light—is critical to life. A creature which keenly senses can evade danger, discern physical limits, and become resourceful by measuring their efforts. In many ways, achieving greater abilities to sense has been a race to the top for living creatures. Like a fly that senses the change in air pressure and gets away before being swatted, or a dolphin which senses the acoustic waves from sonar to find its way in any dark environment, sensing has proven itself an invaluable trait.

Now, in the realm of artificial endeavors, the ability to sense impact, strain, and temperature can equally offer this high value. It simply follows that any device which allows a user to measure and understand their environment will be of great value, biological or not.

The most basic example of a passive-like sensor is skin. Skin will sense strain and temperate and communicate this almost instantly. But, skin is biological and technically alive. What if there were non-biological, inert materials that can react to heat and strain? Unlike skin which communicates via a nervous system, this other material would need to communicate via electromagnetic (EM) means.

As it turns out, a family of these materials exists, both in artificial and natural form. This family of materials is called ferroelectrics. Within the family of ferroelectrics are piezoelectric and pyroelectric materials; respectively, these materials react to changes in strain and heat with an EM response.

Imagine that, a material that generates an EM field when deformed or heated. Can materials like these be used as an artificial skin? Will these materials crack, melt, or breakdown after only slight disturbances—after all, as frail as humans are, we can withstand a fair amount of pressure and temperature; we do not crack when a baseball hits us, though we do bruise of course.

This master's study focuses on a specific subset of the ferroelectric materials: piezoelectric polymers. The specific study of the pyroelectric effect, as well as piezoelectric crystals and others are of great interest, but the specific goal in this study is to examine how a piezoelectric polymer can be used as a dielectric in a passive tactile sensor.

The principal question: can the electric field generated by an impact be funneled into an antenna, transmitted to a middleware receiver, and data-processed? Although there are many more questions to address, the question forms the basis of this master's study. The answer to this question will be attempted with a combination of theory based off of modern research as well as an Ansys simulation.

If a passive, wireless, skin-like sensor can be made with efficiency and low cost, it could find itself in a slew of applications, from coverings of aerospace payloads, where impacts need to be known quickly, to edges of composites where sudden delamination needs to be known immediately, to even high value consumer products, such as the fender of expensive cars—owners may want this to be notified right away if their parked car gets hit. There could also be a large number of uses in the medical device field as well, such as a wireless, batteryless pump that could be activated on demand in a patient's heart for resuscitation; the list goes on.

INTRODUCTION

The study of transducers, or rather devices that convert energy from one form to another, is nothing new. Windmills convert air flow to electricity, LCD's convert electric current into precise photons, and audio speakers convert EM signals into air vibrations. In this design study, the goal is to convert the tactile energy of an impact into a radio frequency (RF) signal. Unlike the most well-known tactile sensors, such as smartphones or touchpads which requires a power source, the tactile sensor studied here is one that will not require an active power source—the impact itself will be the power source. But, to be clear, this tactile sensor is not meant to be a replacement technology for smartphones or touchpads; rather, this technology could be used in conjunction with them as this tactile sensor will detect impacts of high magnitude—sizes that would crack a touchpad—and send an RF chirp to a "smart" middleware.

This is a multidisciplinary study involving the mechanical analysis of a multilayered, thin device, the EM field it produces, and the middleware it communicates with. Therefore, this design study has been split into two separate reports. This report done by myself, Eric Sender, focuses on the sensor; the other report done by Chris Yang—a fellow UCLA Masters of Engineering student—will focus on the RF, application specific integrated circuit (ASIC) system. We will both collaborate on the antenna design eventually, as the antenna will need to be embedded in the sensor either intrinsically or extrinsically. But, for the purposes of this report, the antenna will be assumed, as there is much to cover until then.

Upon completion, we hope to combine studies to form a basis for a passive, wireless sensor system that works in an Ansys simulation environment, a SPICE environment, and is based off of realistic materials, physical tolerances, and well below damage thresholds.

OTHER APPLICATIONS

Many other studies have inspired this paper, including research on using piezoelectric materials as generators and wireless surface acoustic wave (SAW) sensors. The idea of using piezoelectric materials is an active area of research, as many scientists see refined uses of piezoelectric sensors, along with advanced communication equipment, as a strong combination. A particular paper discussing this is "A Review of Wireless SAW Sensors" by Alfred Pohl. In this paper, Dr. Pohl discusses one popular arrangement called the one-port wideband SAW delay line (DL):

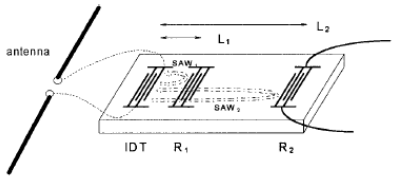

FIGURE 1 - ONE-PORT WIDEBAND SAW DL[i]

The function of the SAW DL sensor is that a receiving signal (called an interrogator) gets received by an antenna which funnels the current to an inter-digital transducer (IDT) which then vibrates in response (this is the piezoelectric effect). That vibration causes the entire substrate to vibrate as well, thus creating a SAW; this saw traverses across the substrate at a known speed and reaches the end IDT, where the signal is convoluted. This signal, as it's convoluted by the second IDT, causes another SAW to develop on the material, unique from the first SAW. The second SAW travels back across the substrate, to the first IDT where it is passed into the antenna and transmitted back to the interrogator. Thus, from a known input signal, traveling into a substrate with a known delay time, and a known convolution, an identification system can be implemented—and on top of that, if the substrate stretches or contracts—for example, if the sensor is measuring compression or expansion—the change in size will change the delay time of the returning signal, thus allowing an engineer to measure the strain[ii].

In the above system, careful study of the impedance matching, resistivity and arrangement of the IDT must be made—this concept is similar to impedance matching in transmission lines and in antennas, as a wave will experience much distortion if it is not "seen through clear lenses"—to put it metaphorically—as impedance matching minimizes wave reflections and standing waves.

Another application for piezoelectrics is described in a paper titled "Piezoelectric Generator as Power Supply for RFID-Tags and Application" by researchers in Tamagawa University, Japan.

The target application is any low power, active electrical unit and the most practical example of this is an active RFID tag. The goal of these piezoelectric energy harvesters is to acts as a battery replacement and, especially in a one-time use active RFID assembly, life cycle extension. The specific example taken in this paper if an RFID system which requires 20-30 microwatts over a 2 second duration per each use of the RFID[iii].

The source of the energy is expected to be children walking—the vibrations of walking will shake the piezoelectric harvester in a child's backpack. The energy from the walking will be fed into an RFID tag that transmits ID information. The researchers found it to work for fast walking, but not reliable for slow walking—but this could depend on the specifics of the device set up. Their design is shown as follows:

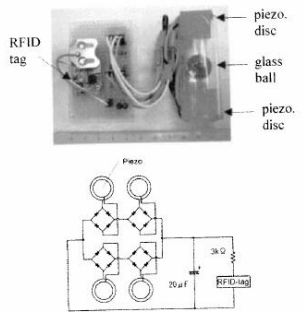

FIGURE 2 - CONSTRUCTED GENERATOR[iv]

The idea is a glass ball will bounce in the cylinder which holds a piezoelectric disc at both ends. As the ball bounces up and down, current is dumped into a 20 microfarad capacitor, which acts as a low-pass filter, extracting out high frequency components of the generator while letting the low frequency (especially DC) components of the generator pass onto the RFID-tag load.

There are many more examples of how to use piezoelectric materials in applications—another common use in signal processing is SAW filters, which utilize the time delay aspect of a SAW to make it into a high quality FIR (finite impulse response) filter, which is built on memory and delays; if a SAW will delay a signal by 1 unit of time, it is like having a memory span of 1 unit—cascade this delay across many more units of time and then one will have an equivalent, almost analog-like FIR filter without the use of active memory modules.

DESIGN OVERVIEW

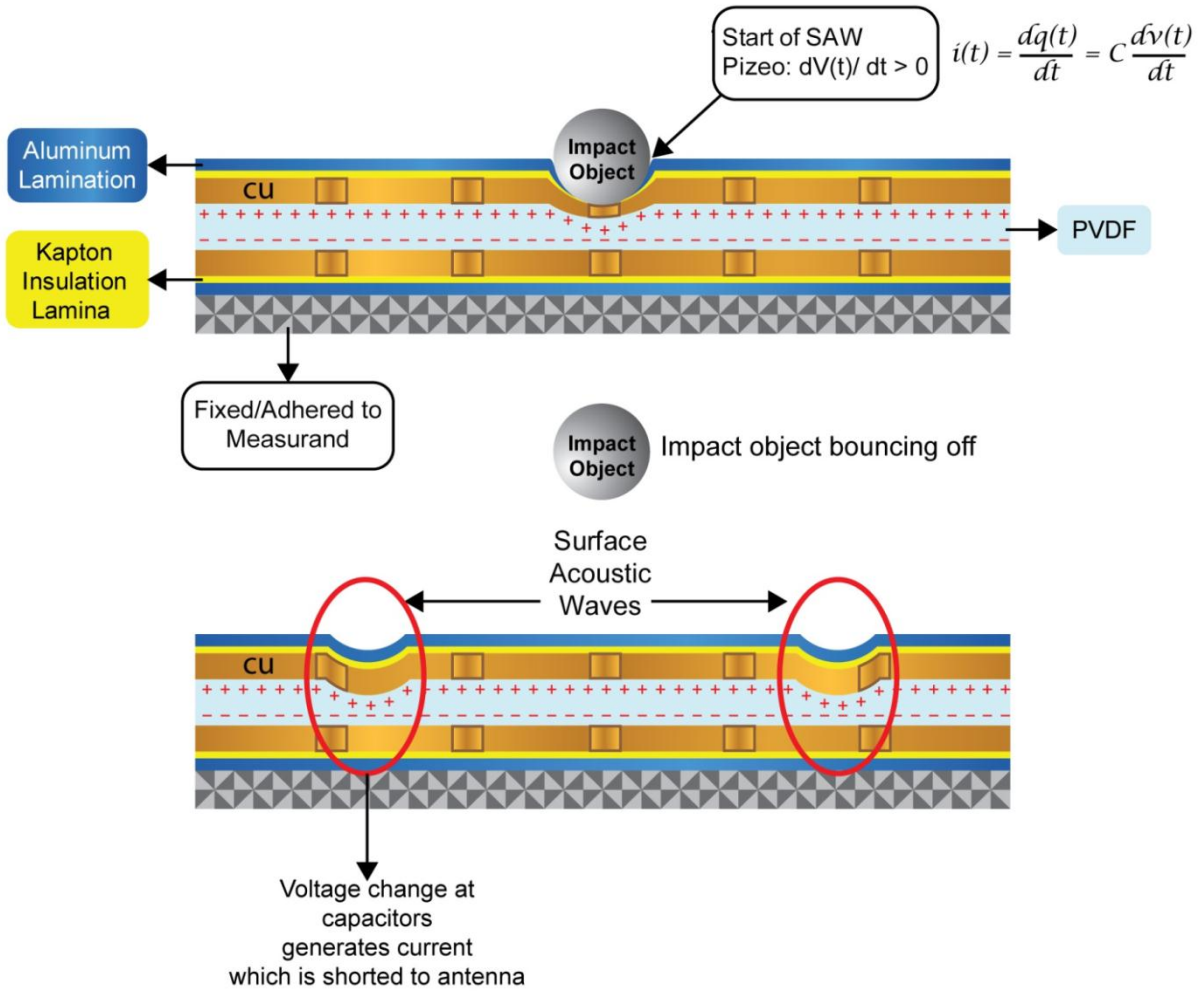

FIGURE 3- SENSOR DESIGN SIDE VIEW

The basic design is that of a parallel plate capacitor. In words, imagine a parallel plate capacitor, about 1" wide by 2" long made up of a middle dielectric layer and a top and bottom copper layer. That middle dielectric layer is piezoelectric, so if any strain is placed on it, a temporary electromagnetic field will occur as well, and this field will drain onto the copper, thus creating a medium for charge carriers to build up. This forms the basis of the sensor: a copper-piezo-copper sandwich. With that, a proper design must be in place to ensure the charge carriers (i.e., current) from the copper is funneled into an antenna and each layer is protected from the damage inflicted by impacts.

To ensure protection in the normal direction, an aluminum lamination will be sandwiched above and below the copper layers; however, to ensure the aluminum protection layer is electrically separated from the copper, a layer of kapton will be placed between the copper and aluminum as well. This amounts to a total of seven layers; starting from the top: aluminum, kapton, copper, piezo, copper, kapton, and aluminum. In addition to this, a strip of metal (most likely copper) will be placed around the sensor to act as a loop antenna. Because of the aluminum lamination, one will be limited in terms of antenna design (unless the aluminum itself is to act as a crude antenna). However, if a large amount of current flows into the antenna, even for a very short period of time, a large enough RF chirp can be produced, even if it gets highly attenuated.

Visually, the non-copper layers may look like this:

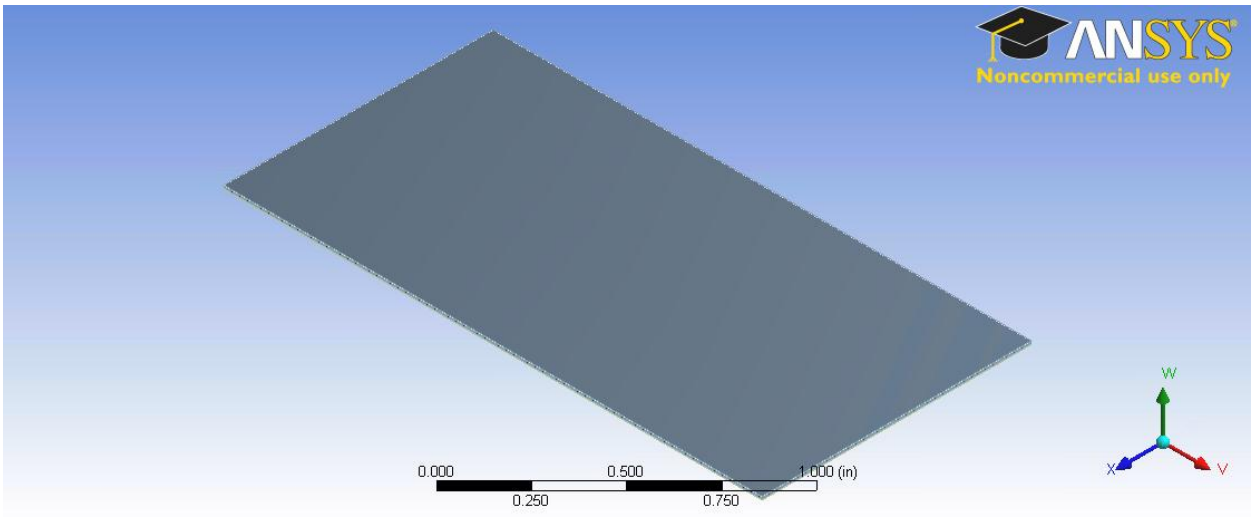

FIGURE 4 - SENSOR TOP VIEW (CAD MODEL)

Take note, that although the typical layer is bland and uniform, it is the properties of the materials and how it interacts with its environment which produces the interesting effects. The next view is of the side, here one can see the different layers sandwiched around the thicker piezoelectric layer:

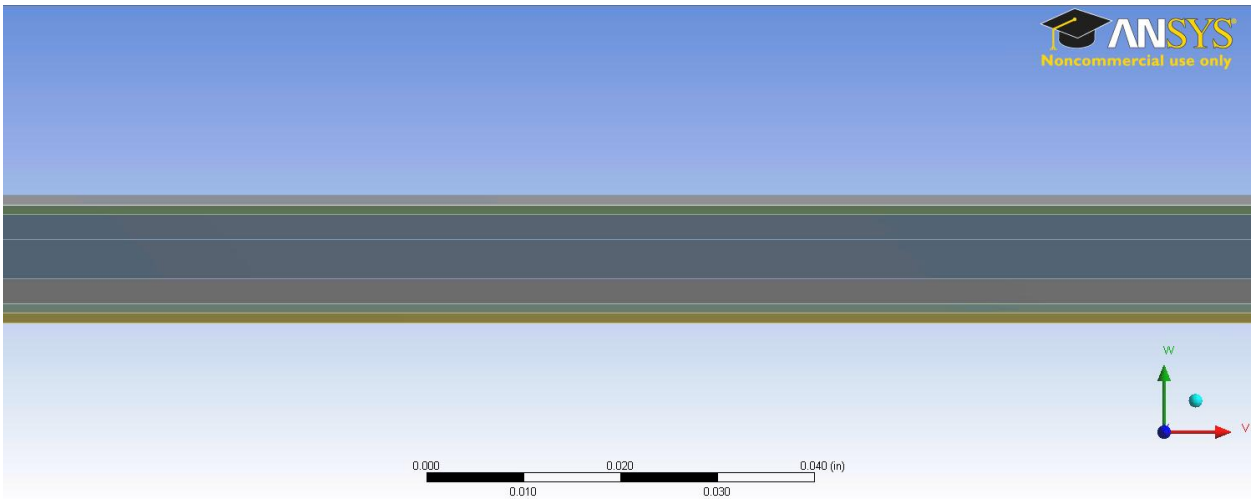

FIGURE 5 - SENSOR THICKNESS VIEW (CAD MODEL)

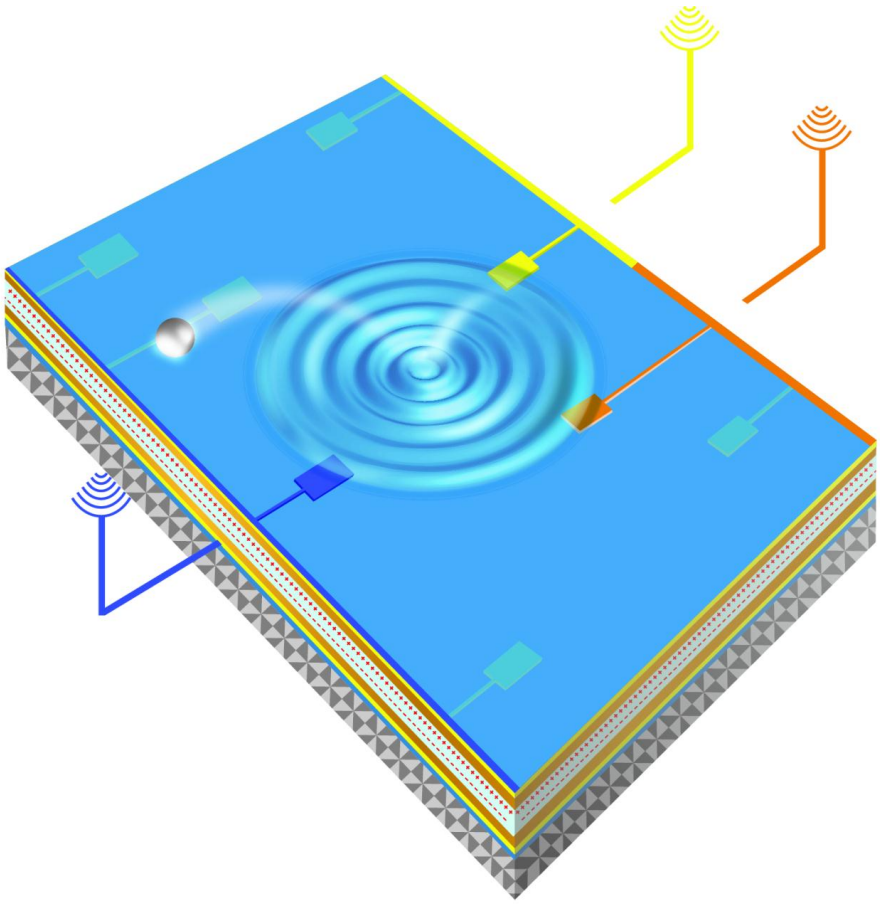

FIGURE 6 - SENSOR IN ACTION – ARTISTIC RENDITION

The above figure demonstrates artistically how the sensor will perform in action. First, one should notice a ball leaving the sensor surface, leaving behind a surface wave. This surface wave, known as a Rayleigh wave, will activate the piezoelectric effect in the middle layer; that is, each crest of the wave will represent a voltage spike. As the wave travels, it will reach the designated islands, or capacitive nodes. When the nodes are activated by the voltage spike, current is released and will travel through the conducting lines, releasing an identifiable RF chirp. The above figure is not drawn to scale; each layer will be considerably thin, on the order of a thousandth of an inch.

At this point, the sensor system is described; each layer has been given an overview and the antenna releases RF chirps at known frequencies. Now, a proper middleware system needs to be designed that can pick up this chirp and process it. The design of this system is the subject of my fellow classmate, Chris Yang's, master's project. But, in summary, the middleware will run as a state machine. The state machine will activate when the end user switches it on, then remain in a listening → action→ listening status until the user switches it off.

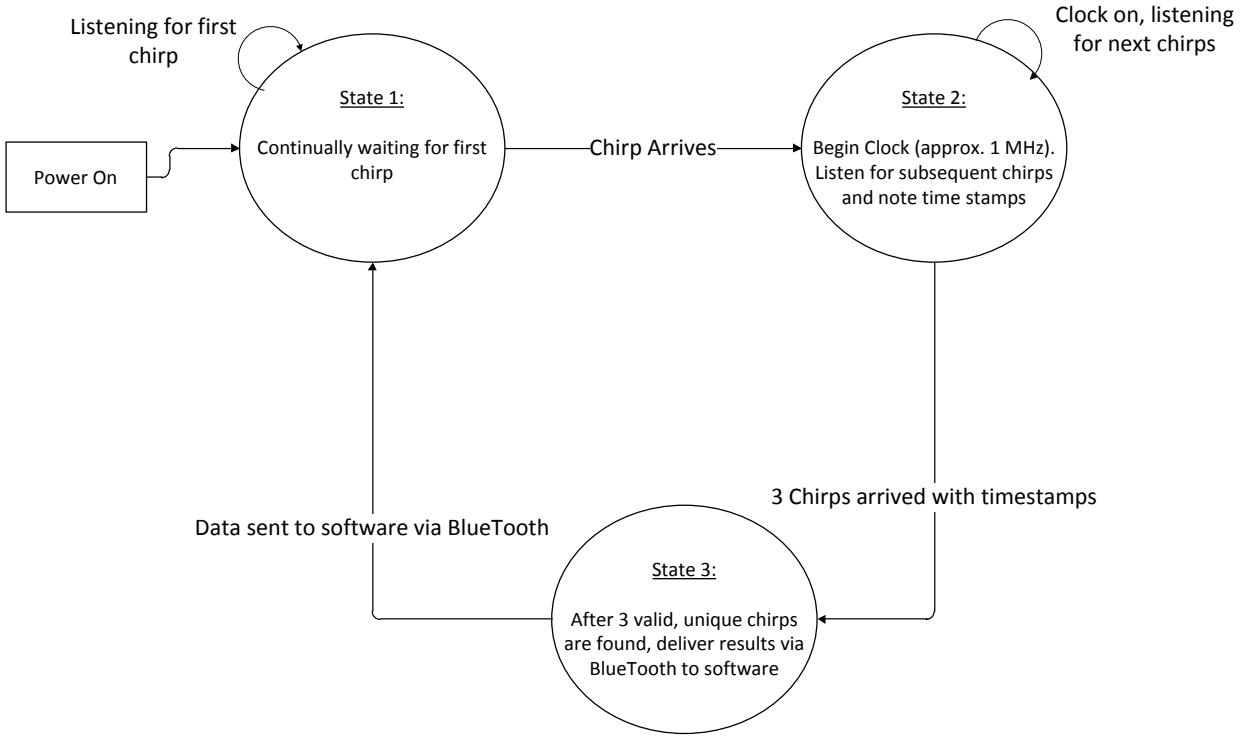

FIGURE 7 - MIDDLEWARE STATE MACHINE CONFIGURATION #1

The above state machine is just one option that could be used. Another combines State 2 and State 3 in that it continually sends information to the software.

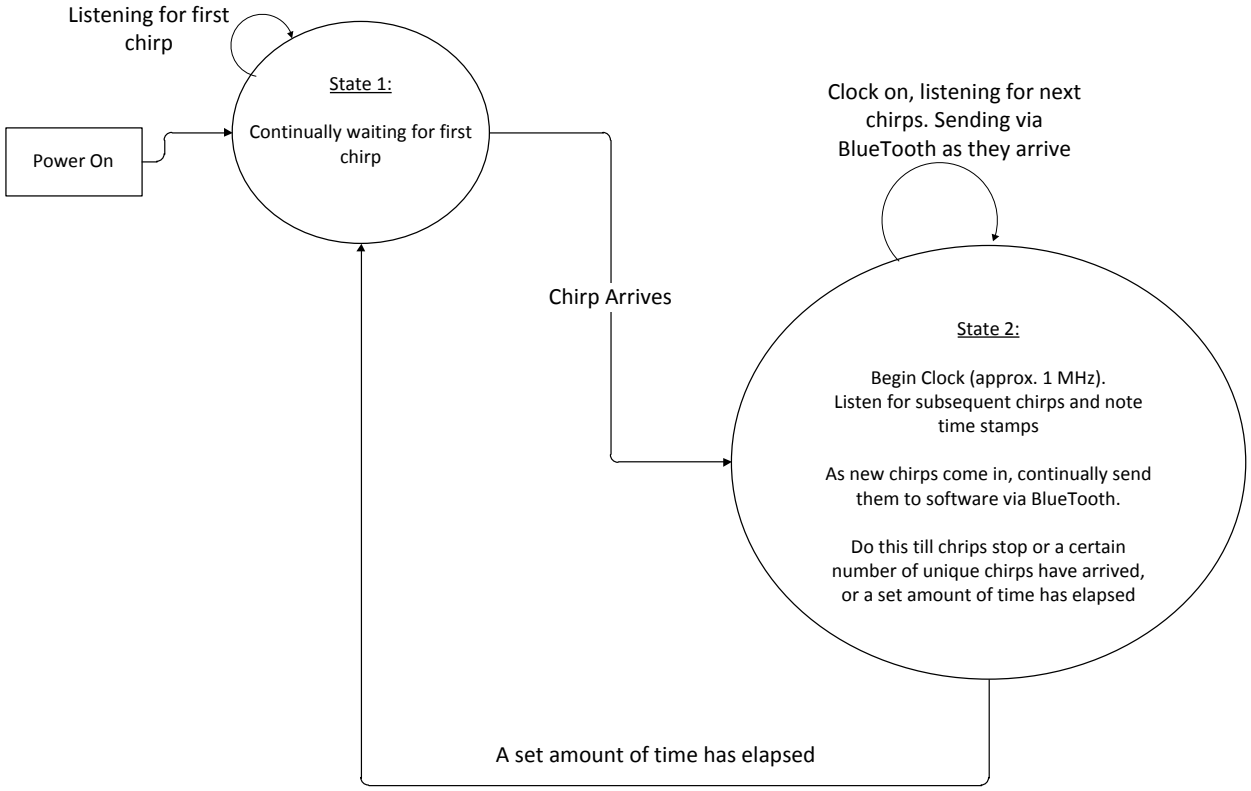

FIGURE 8 – MIDDLEWARE STATE MACHINE CONFIGURATION #2

Configuration 2 contains less complexity, but relies more heavily on software to do filtering and checking, while configuration 1 does that work. Configuration 2 may require more battery power since it will continually send Bluetooth signals whereas configuration 1 only sends the signal when a confirmed three chirps have arrived. The deeper details of this state machine will be in Chris Yang's report.

MATERIALS, MECHANICS, AND PIEZOELECTRICITY

The following section may require a review of the design figures above. The below descriptions are an overview of the high level design and material needs for this proposed device.

Since the sensor is essentially a specialized set of parallel plate capacitors, the materials must have specific conductive, dielectric, and piezoelectric properties. In addition to that, the sensor will require protective layers to reduce the risk of damage, delamination, or any shifting of the geometry. The proposed protective layer is a lamination of aluminum on the top and bottom of the sensor; the aluminum will be exposed to the direct impact of the object and will cushion the blow to the internal sensor materials.

Referring to figure 1, between the aluminum layers will be kapton. kapton will serve as an insulation barrier between the aluminum protective layers and the eventual copper that will make up the capacitive island nodes.

Between the kapton layers will be the copper islands. Now, the construction of the copper is something that will require experimentation in a lab and some calibration in Ansys. The main question is whether there should be a full copper layer spanning the whole area of the sensor, with electrically separated islands representing the nodes, or if there should only be copper nodes and simply add more kapton between the capacitive islands. This will be need to be investigated in a laboratory. The main concern is parasitic capacitive effects of having too much copper.

The piezoelectric layer, made up of ferroelectric polymer Polyvinylidene Fluoride (PVDF) will serve as the charge generator when impacts occur. This layer will be a film and according to manufactures, on the order of 0.001" (1-mil) at its thinnest to 5-mil at its thickest.

Lastly, as will be discussed in the electrical loading section, there will be a need to electrically separate each capacitive island in the sensor. In its current form, with each island connected straight to the antenna, each island will be essentially in parallel, since the antenna would act as an electrical bus-line. This will cause current to not only go through the antenna, but also immediately drain into the other capacitive islands. This will not only have a negative effect on the RF transmission, but it will also stimulate the PVDF causing additional strain through the inverse piezoelectric effect; that is, while the original impact is traversing through the sensor at relatively slow acoustic speeds, the first node to be stimulated will have already drained charges on

the other capacitive islands, causing other SAWs to traverse through the sensor, perhaps destructively interfering with the original SAW and worst of all, causing bad data to emit from the antenna. Therefore, the best way to avoid these scenarios is to ensure the capacitive islands are electrically separated and the most straightforward way to do this is with a polymer based PN-Junction diode that could be injected at each entrance to the antenna.

The concept of diodes and discussion of polymer based diodes will be discussed later.

Although not a layer, the final material to discuss briefly is the antenna itself. This antenna will be designed by Chris Yang, as it must be tuned and accurate for his RF middleware system, however the most likely option is to have the antenna loop around the sensor either once, or a number of times. Loop antennas are a known antenna configuration and in this way, it will be separated from the aluminum and copper layers and safer from potential damage from normal-oriented impacts. The specific material type is not determined yet, but it will need to be such that its electrical length is on the order of the wanted wavelengths of the RF chirps and will allow for a large enough signal amplitude for a middleware to pick up the chirp within 4 to 6 feet from the sensor.

MATERIAL PROPERTIES

To make sense of the piezoelectric effect, one must know a material's stiffness or compliance tensor, as well as its electrical permittivity tensor; of course, one must also know the piezoelectric coefficients.

The Young's modulus, in its most general form, is a tensor with components for every direction and orientation stress possible: normal, tangential, shearing. For isotropic materials, the value of the Young's modulus is the same for every orientation and thus it is given as a single number. But this is too simplistic for the analysis to be performed here. Putting the Young's modulus in a matrix form will allow its usage in electromagnetic coupling equations and Classical Lamination Theory. To give some background, orthotropic materials may help shed light on the direction taken in analysis.

$$S = \begin{bmatrix} \frac{1}{E_x} & -\frac{\nu_{yx}}{E_y} & -\frac{\nu_{zx}}{E_z} & 0 & 0 & 0 \\ -\frac{\nu_{xy}}{E_x} & \frac{1}{E_y} & -\frac{\nu_{zy}}{E_z} & 0 & 0 & 0 \\ -\frac{\nu_{xz}}{E_x} & -\frac{\nu_{yx}}{E_y} & \frac{1}{E_z} & 0 & 0 & 0 \\ 0 & 0 & 0 & \frac{1}{G_{yz}} & 0 & 0 \\ 0 & 0 & 0 & 0 & \frac{1}{G_{zx}} & 0 \\ 0 & 0 & 0 & 0 & 0 & \frac{1}{G_{xy}} \end{bmatrix}$$

The above matrix is the Young's modulus for an orthotropic materials. There, one can discern how the matrix is arranged mathematically, where shearing is placed and how Poisson's ratio comes into play. This matrix reduces considerably for isotropic materials. That is, when $E_x = E_y = E_z$, it becomes straight forward to simply state a material's Young's modulus and Poisson ratio to obtain a filled Stiffness/Compliance tensor. So, for the below materials mentioned, only a single number is given for the Young's modulus is given. From there, the Poisson ratio is given that will

allow the extraction of the Shear modulus, $G = E/2(1+\nu)$. The reduced stiffness tensor would thus be:

$$S = \begin{bmatrix} \frac{1}{E} & -\frac{\nu}{E} & -\frac{\nu}{E} & 0 & 0 & 0 \\ -\frac{\nu}{E} & \frac{1}{E} & -\frac{\nu}{E} & 0 & 0 & 0 \\ -\frac{\nu}{E} & -\frac{\nu}{E} & \frac{1}{E} & 0 & 0 & 0 \\ 0 & 0 & 0 & \frac{2(1+\nu)}{E} & 0 & 0 \\ 0 & 0 & 0 & 0 & \frac{2(1+\nu)}{E} & 0 \\ 0 & 0 & 0 & 0 & 0 & \frac{2(1+\nu)}{E} \end{bmatrix}$$

To go one step further, if one assumes plane strain—i.e., effects in the normal, z, direction are negligible—then the modulus reduces to:

$$S = \begin{pmatrix} \frac{1}{E} & -\frac{\nu}{E} & 0 \\ -\frac{\nu}{E} & \frac{1}{E} & 0 \\ 0 & 0 & \frac{2(1+\nu)}{E} \end{pmatrix}$$

With this stiffness matrix at hand, obtaining the values for E and ν will be needed for all materials; in addition to this, applying Classical Lamination Theory will be straight forward. See appendix section 4 for Classical Lamination Theory.

The goal of this section is not to solve for an exact value of voltage or impulse response of the sensor, it is to serve as an impact location detector. Thus, the goal is calibration and understanding of the piezoelectric effect in the hopes of setting up a reasonable design in a laboratory.

ALUMINUM

Aluminum[v] is an isotropic material and thus, its Young's modulus is straightforward. The Young's modulus is known to be 70 GPa, its shear modulus is 26 GPa, Poisson ratio of 0.35, density of 2.7 g/cc and Bulk modulus is 76 GPa. Depending on the specific aluminum used (6061-O, 6061-T4, 6061-T6), the tensile strength is 125 MPa, 207 MPa, and 300 MPa respectively[vi].

KAPTON

Kapton[vii,viii] is an isotropic material with a Young's modulus of 2.5 GPa, Poisson ratio of 0.34, Ultimate tensile strength of 231 MPa, and density of 1.42g/cc, dielectric constant of 3.5, resistivity of 1.5×10^{17} Ω-cm—all values given at room temperature.

COPPER

Copper[ix,x,xi] is an isotropic material with a Young's modulus of 110 – 128 GPa (assume 119 GPa as the average), a shear modulus of 48 GPa, a Poisson ratio of 0.34, and an ultimate tensile strength of 220 MPa. Furthermore, its electrical resistivity at room temperature is 16.78 nΩ-m, which is nearly negligible.

PVDF

PVDF[xii,xiii,xiv], along with the others, will be treated as an isotropic material with Young's modulus of 3.2 ± 20% GPa, tensile strength of 240 ± 15% MPa, and a Poisson ratio of 0.35. It has a density of 1.42 g/cc. Along with this, its piezoelectric coefficients are d_{33} = 15 ± 20% pC/N, d_{31} = 6 ± 20% pC/N, d_{32} = 1 ± 20% pC/N, g_{33} = 0.14 ± 20% V-m/N at 1 kHz, and p_3 =-25 ± 25% μC/m^{2}K.

PVDF[xv] is a fluoropolymer with a high piezoelectric response. Although the exact science describing why PVDF exhibits a piezoelectric response is not known, research has been done to empirically describe the electrical and structural changes in the PVDF. Ultimately, a dipole is created in the PVDF material due to the atomic arrangement of the polymers, but since it is not crystalline with a lattice structure, a deeper story must explain the physics behind its piezoelectric response.

The following image shows the structural change of PVDF while it is floating (no applied voltage) and when it is grounded to 0V.

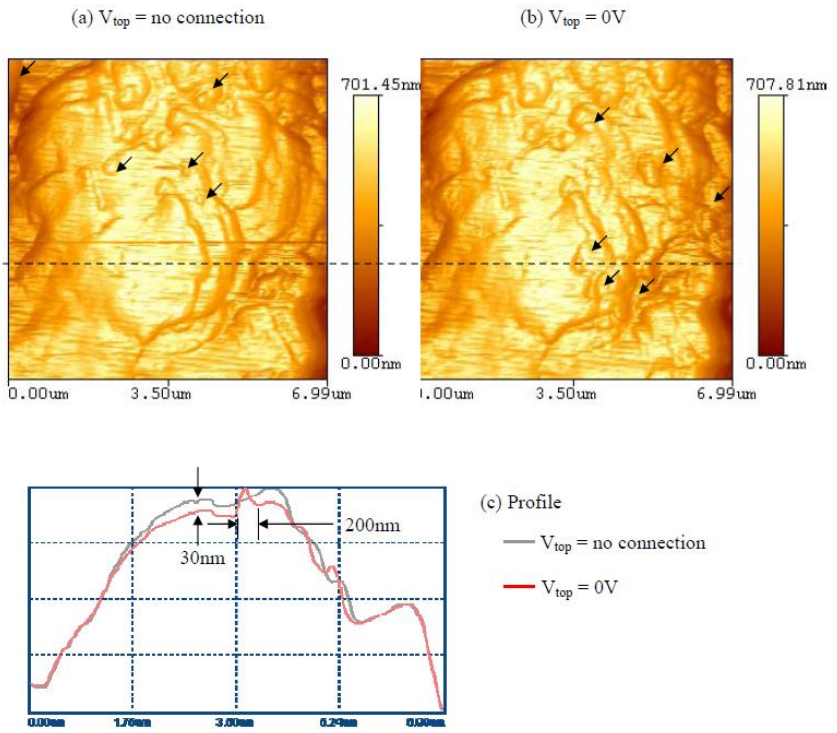

FIGURE 9 - MICROSCOPY OF 110 UM THICK PVDF. (A) FLOATING (B) 0V CONTROL (C) PROFILE[xvi]

This experiment, done with Atomic Force Microscopy, a procedure which enables one to characterize surface morphology at the nano-scale, shows that when grounded a floating PVDF area, it experiences an internal shift, as shown in the arrows in the above figure and the profile image in (c).

Further experiments were performed in 5V increments.

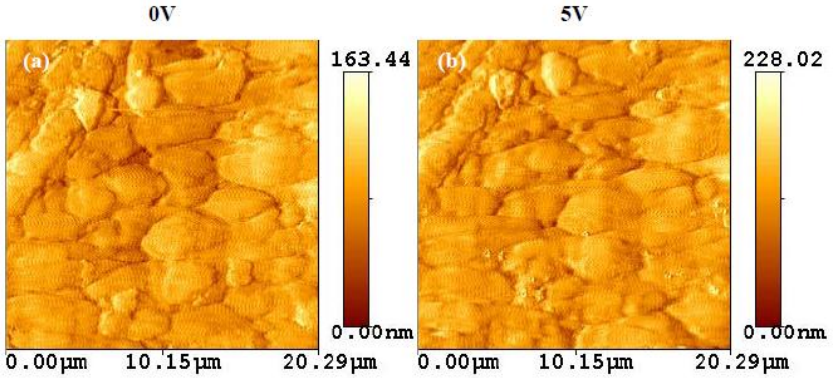

FIGURE 10 - MICROSCOPY OF 110 UM THICK PVDF. (A) 0V CONTROL (B) 5V[xvii]

As seen above, based on the color scale changes, the PVDF is squeezed by the increased voltage. The increased height is believe to be caused by dipole realignment within the PVDF structure.

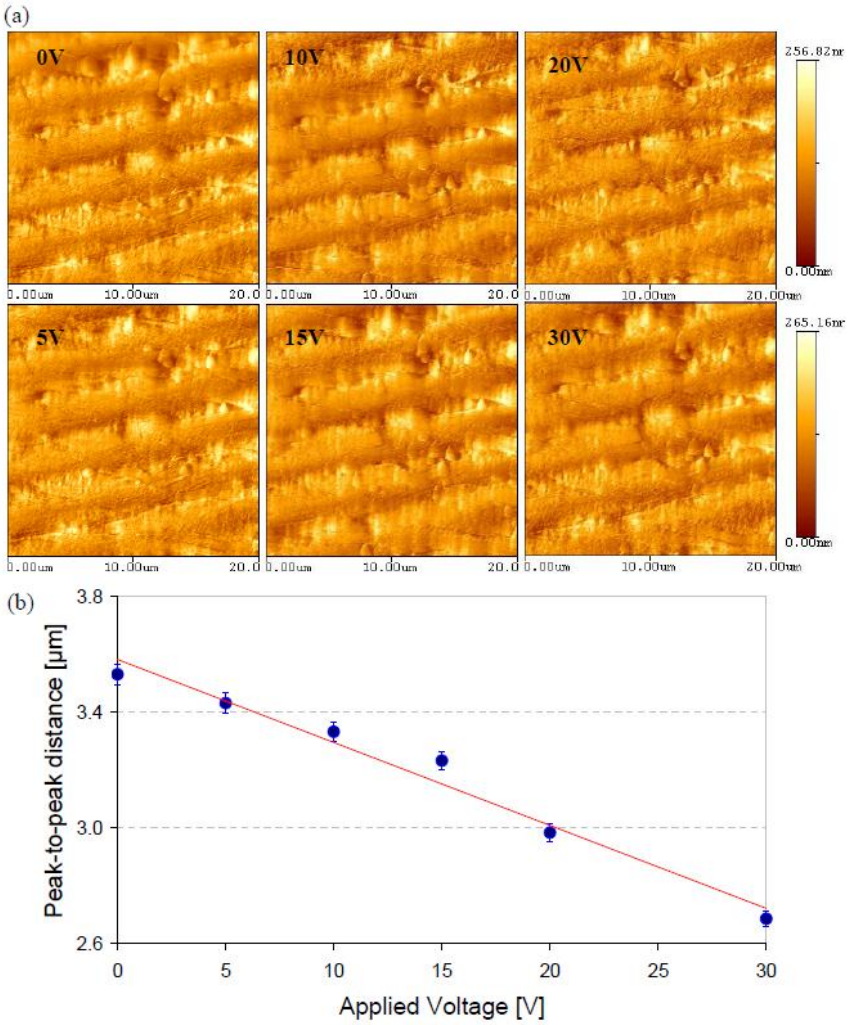

FIGURE 11 – (A) MICROSCOPY IN 5V INCREMENTS (B) VOLTAGE VS. PEAK-PEAK DISTANCE[xviii]

The above figure demonstrates that as voltage increases, the PVDF contracts at a fairly predictable linear rate. When no potential is applied, the dipoles inside the PVDF were not aligned and the nano-structure was randomly oriented such that all their polarity canceled out. However once a potential gradient was applied, the dipoles began to align.

Another angle to study PVDF is on the molecular arrangement of the molecule. The following figure shows the known orientations:

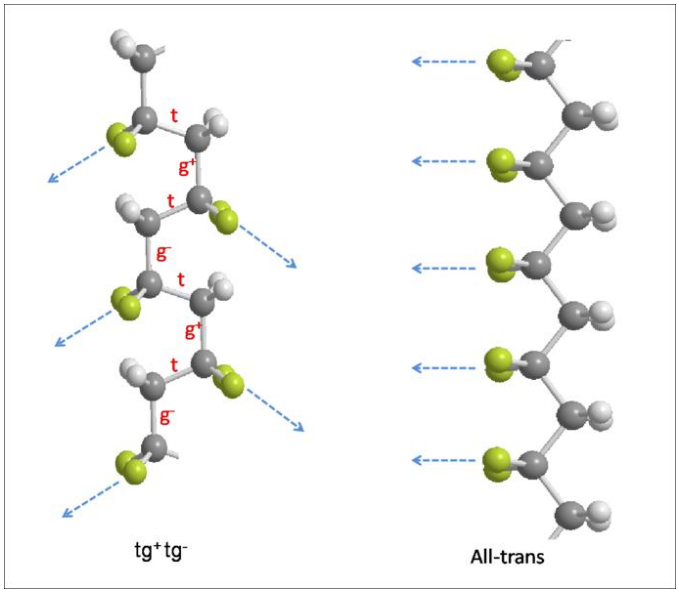

FIGURE 12 – MOLECULAR ORIENTATIONS OF PVDF[xix]

The structure to the left, tg^+tg^-, the molecules are 180° from each other while in the all-trans orientation, they are 60°. In either case, the separation of charged molecules forms the basis of the piezoelectric effect, and when strain (either compression or stretching of the bonds) occurs, an electric field is produced in response to the changed distance. Vice versa when an electric field is applied to the structure, the bond distance will change and thus strain occurs[xx].

In either case, the expectation in this study is an impact will occur on the PVDF, which will result in strains, and thus transient changes the PVDF bond structure. These changes will result in a temporarily electric field—and this field will funnel into copper layers (a capacitor and conducting lines) where current will be produced and sent out through an antenna as a unique chirp. Thus, PVDF that is polarized in the normal direction will be required, otherwise the impact strain will not produce this electric effect.

SUMMARY OF MATERIALS

TABLE 1 - MATERIAL PROPERTIES

	Aluminum	Copper	Kapton	PVDF
Young's Modulus (GPa)	70	119	2.5	3.2
Poisson Ratio	0.35	0.34	0.34	0.35
Tensile Strength (MPa)	125	220	231	240
Density (g/cc)	2.7	8.94	1.42	1.42
Dielectric Constant at 1 kHz	NA	NA	3.9	11

TABLE 2 - PVDF PIEZOELECTRIC TABLE

d_{33}	15 ± 20% pC/N
d_{31}	6 ± 20% pC/N
d_{32}	1 ± 20% pC/N
g_{33}	0.14 ± 20% V-m/N at 1 kHz
p_3	25 ± 25% μC/m²K

THE PIEZOELECTRIC EFFECT

As explained above, the piezoelectric effect relates mechanical stress and strain to an electromagnetic field. The following equation system was derived from Hamilton's Principles[xxi], which is the practice of containing all dynamics of a physical system into a single function called a Lagrangian[xxii].

$$\begin{bmatrix} S_1 \\ S_2 \\ S_3 \\ S_4 \\ S_5 \\ S_6 \end{bmatrix} = \begin{bmatrix} s_{11}^E & s_{12}^E & s_{13}^E & 0 & 0 & 0 \\ s_{21}^E & s_{22}^E & s_{23}^E & 0 & 0 & 0 \\ s_{31}^E & s_{32}^E & s_{33}^E & 0 & 0 & 0 \\ 0 & 0 & 0 & s_{44}^E & 0 & 0 \\ 0 & 0 & 0 & 0 & s_{55}^E & 0 \\ 0 & 0 & 0 & 0 & 0 & s_{66}^E = 2\left(s_{11}^E - s_{12}^E\right) \end{bmatrix} \begin{bmatrix} T_1 \\ T_2 \\ T_3 \\ T_4 \\ T_5 \\ T_6 \end{bmatrix} + \begin{bmatrix} 0 & 0 & d_{31} \\ 0 & 0 & d_{32} \\ 0 & 0 & d_{33} \\ 0 & d_{24} & 0 \\ d_{15} & 0 & 0 \\ 0 & 0 & 0 \end{bmatrix} \begin{bmatrix} E_1 \\ E_2 \\ E_3 \end{bmatrix}$$

$$\begin{bmatrix} D_1 \\ D_2 \\ D_3 \end{bmatrix} = \begin{bmatrix} 0 & 0 & 0 & 0 & d_{15} & 0 \\ 0 & 0 & 0 & d_{24} & 0 & 0 \\ d_{31} & d_{32} & d_{33} & 0 & 0 & 0 \end{bmatrix} \begin{bmatrix} T_1 \\ T_2 \\ T_3 \\ T_4 \\ T_5 \\ T_6 \end{bmatrix} + \begin{bmatrix} \varepsilon_{11} & 0 & 0 \\ 0 & \varepsilon_{22} & 0 \\ 0 & 0 & \varepsilon_{33} \end{bmatrix} \begin{bmatrix} E_1 \\ E_2 \\ E_3 \end{bmatrix}$$

FIGURE 13 - PIEZOELECTRIC/MECHANICAL COUPLING RELATION[xxiii,xxiv,xxv]

$[D_i]$ and $[E_i]$ are the electric charge density and electric field vectors. They only contain 3 components as electric fields are described in 3 physical dimensions. $[T_i]$ and $[S_i]$ are stress and strain tensors, where the first 3 terms represent the <11>, <22> and <33> directions and latter 3 terms describe the symmetric <12>, <13>, and <23> shear orientations of stress and strain; since it can be reduced to 6 terms, it can be manipulated like a vector in linear algebra and thus presents itself as a vector. $[\varepsilon_{ij}]$, $[d_{ij}]$ are the dielectric and piezoelectric coefficient tensors. The dielectric tensor has 3 components per each dimension of the electric field—hence 9 terms; most materials are known to have just 1 value for the dielectric constant, but exotic materials could have different electrical properties depending on the polarization of the electric field; so, usually $[\varepsilon_{ij}]$ is not a tensor but a scalar ε_r.

Most importantly for this discussion is the piezoelectric tensor, $[d_{ij}]$. The piezoelectric tensor has the potential for 6 contributing factors for each dimension of stress (and there are 6 dimensions to stress as stated earlier in this paragraph); thus there are 18 terms. Like most tensors describing physical events and materials, it can be reduced. This reduction is possible by taking the crystallographic symmetry into account[xxvi]. The electrically dependent values of $d_{31}E_3$, $d_{32}E_3$, $d_{33}E_3$,

$d_{24}E_2$, $d_{15}E_1$ are the values that contribute to strain on a material. Likewise, the mechanically dependent values $d_{31}T_1 + d_{32}T_2 + d_{33}T_3$, $d_{24}T_4$, $d_{15}T_5$ contribute to the charge density.

Specifically, since the <3> subscript describes the normal direction and the normal direction is the most relevant direction for our purposes, it follows that $D = d_{31}T_1 + d_{32}T_2 + d_{33}T_3 + \varepsilon_r E$, and since there is no applied electric field, the E term is 0; furthermore, since it is assumed that the contributions in the mechanical contributions in the <1> and <2> direction are negligible in the simplest model, $D = d_{33}T_3$. Of course, there will be shearing forces and forces in the <1> and <2> directions since an impact will have a beam-bending effect on the material, but for this simplification, only one term is left behind.

This is significant because it allows the straight forward coupling of Gausses' Law with normal stress. Further, since stress is related to strain by the Poisson ratio and Young's modulus[xxvii], it allows one to correlate the electric charge density with the amount of displacement placed on the material.

$$\oint_S D \cdot dA = Q$$

For a parallel plate system, this reduces to D×Area = Q. Therefore, $d_{33}T_3 \times A = Q$. Using the classical model for current as $i = \frac{dq}{dt}$ it follows that $i = \frac{d}{dt}\left(d_{33}T_3 A\right) = d_{33}A\frac{dT_3}{dt}$ so, the current is found to be limited by the "speed" of the stress application, as well as proportional to the piezoelectric coefficient, area, and magnitude of the stress. I.e., a very quick, strong stress applied to the piezoelectric material will allow a larger current. This is a very interesting, though at first almost counter intuitive result, but it makes perfect sense when looking at the piezoelectric effect as related to the capacitive effect. In the realm of capacitors, if the input is a DC voltage, the effect is a sharp current spike—i.e., the initial spike at the start of a DC input—followed by a decay in current, $i(t) = \frac{V_0}{R}\exp\left(-\frac{t}{RC}\right)$. In this situation, the impact is like the voltage input to the capacitor.

$$i(t) = d_{33}A\frac{dT_3}{dt} = C\cdot\frac{dv}{dt}$$

$$\int_0^{T_3} d_{33}A\frac{dT_3}{dt} = \int_0^{V} C\cdot\frac{dv}{dt}$$

$$d_{33}A\cdot T_3 = C\cdot V$$

$$\frac{d_{33}A\cdot T_3}{C} = \underbrace{V = IR}_{\text{Ohm's Law}}$$

$$I = \frac{d_{33}A\cdot T_3}{RC} = d_{33}A\frac{dT_3}{dt}$$

$$\int_0^{t}\frac{dt}{RC} = \int_{T_{3-0}}^{T_3}\frac{dT_3}{T_3}$$

$$\frac{t}{RC} = \log\left(\frac{T_3}{T_{3-0}}\right) = -\log\left(\frac{T_{3-0}}{T_3}\right)$$

$$T_{3-0} = T_3\exp\left(-\frac{t}{RC}\right) \rightarrow \frac{dT_{3-0}}{dt} = \frac{d}{dt}\left(T_3\exp\left(-\frac{t}{RC}\right)\right)$$

$$\underbrace{i(t) = d_{33}A\frac{dT_{3-0}}{dt}}_{\text{Derived Earlier}} = d_{33}A\cdot\frac{d}{dt}\left(T_3\exp\left(-\frac{t}{RC}\right)\right)$$

$$\boxed{i(t) = -\frac{d_{33}A\cdot T_3}{RC}\exp\left(-\frac{t}{RC}\right)}$$

The above derivations, although many constants are filtered out (such as assuming the starting stress is negligible in the first integral), leads to the relation that the transient current is a function of the normal stress, the piezoelectric coefficients, as well as a decaying time function. The term $T_{3\text{-}0}$ specifies the initial stress in the <3> direction. Since it is in the <3> direction, it is also a function of current and allows the viewing of the above relationship. But the main conclusion is that an impulse of stress will cause a current spike, but that current spike will die down quite rapidly as a function of the RC time constant.

$$i(t) = d_{33}A\frac{dT_3}{dt} = C\cdot\frac{dv}{dt} = \frac{V_0}{R}\exp\left(-\frac{t}{RC}\right)$$

$$\int d_{33}A\frac{dT_3}{dt}dt = \int\frac{V_0}{R}\exp\left(-\frac{t}{RC}\right)dt$$

$$d_{33}AT_3 = -RC\frac{V_0}{R}\exp\left(-\frac{t}{RC}\right) = -RC\cdot i(t)$$

$$i(t) = -\frac{d_{33}A}{RC}T_3$$

In the above derivation, current is solved in another fashion as well, though the solution is purely based on the initial conditions. The second derivation is not as clear as the first, but it's interesting to see how the general solution can be discerned by relating the piezoelectric effect to capacitance directly and by relating it to Ohm's law. The Ohm's law approach is more fundamental and this may be why it gives a fuller solution more readily.

CONTACT MECHANICS

In physics, momentum transfer between two bodies is simplified to the equation $m_1v_1 = m_2v_2$ but contact has proven to be a highly advanced topic, as the specific ways a body can deform during the extremely small contact duration is unique and requires great attention to the specifics of the geometry. Heinrich Hertz solved much of the foundational work in contact mechanics and gave a solution to the forces acting on two colliding bodies of various shapes[xxviii].

The specific Hertzian contact solution used here will be the sphere and elastic half-plane and it is such:

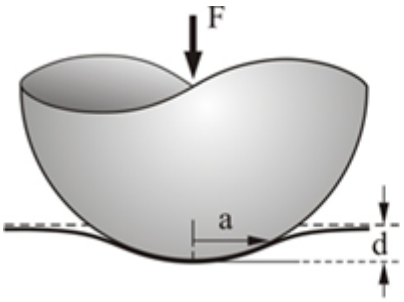

$$\begin{bmatrix} F = \frac{4}{3}E^{*}R^{1/2}d^{3/2} \\ \frac{1}{E^{*}} = \frac{1-\nu_1^2}{E_1} + \frac{1-\nu_2^2}{E_2} \\ a = \sqrt{Rd} \end{bmatrix}$$

FIGURE 14 – HERTZIAN CONTACT SOLUTION FOR A SPHERE AND ELASTIC HALF-PLANE[xxix]

This equation for "F", the force, will be solved for "d" to extract the deformation which will be used to find the strain on the laminate. Since the laminate is so thin and each layer is adhered to each other, it will be assume that the same strain permeates through the entire laminate.

IMPACT STRAIN

$$d = \left(\frac{3}{4} \cdot \frac{F}{E^{*}R^{1/2}} \right)^{2/3}$$

The above equation is simply solving for "d" in the Hertzian contact equation in the previous section. The Young's modulus for the laminate will be found using a concept adopted from the Micromechanics of a Lamina section of Robert M. Jones' "Mechanics of Composite Materials" as well as taught in UCLA's MAE 166C course by Professor Carmen. The idea is the effective Young's modulus can be found by analyzing the volume fraction of each material in a ply[xxx]:

$$\frac{1}{E_{eff}} = \frac{V_1}{E_1} + \frac{V_2}{E_2} + \ldots + \frac{V_n}{E_n}$$

$$E_{eff} = \frac{E_1 E_2 \ldots E_n}{V_1 E_2 .. E_n + V_2 E_1 E_3 .. E_n + \ldots V_n E_1 E_2 \ldots E_{n-1}}$$

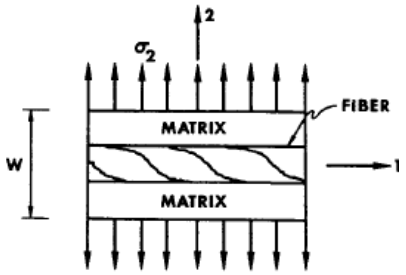

FIGURE 15 - REPRESENTATIVE VOLUME ELEMENT LOADED IN THE 2-DIRECTION[xxxi]

In the realm of fibers, this goes deeper because composite materials are anisotropic and thus one treats the fiber direction differently than the transverse direction. In the fiber direction (i.e., the Young's modulus when looking at the materials down the length of the fiber), one must find the weighted volume average instead. Since that is not the case, the pressure is coming from the top, the transverse is used.

Further, volume fractions can be simplified looking at the differences in thickness between the layers since each layer has the same area; this is like factoring out least common multiples. Therefore, the following Matlab code will find the fractions:

```
in = 0.0254;     % 1 inch = 0.0254 meters
za = 0.001 *in; % thickness of Aluminum
zc = 0.0026*in; % thickness of Copper
zk = 0.001 *in; % thickness of Kapton
zp = 0.004 *in; % thickness of PVDF

thick = 2*(za + zc + zk) + zp;

Frac_al = 2*za/thick; % 0.1515
Frac_cu = 2*zc/thick; % 0.3939
Frac_ka = 2*zk/thick; % 0.1515
Frac_pv =   zp/thick; % 0.3030
```

And the following Matlab code will determine the effective Young's modulus:

```
% Material properties - All units in SI.
Ea = 70e9;  % Aluminum
va = 0.35;
```

```
Ec = 119e9; % Copper
vc = 0.34;

Ek = 2.5e9; % Kapton
vk = 0.34;

Ep = 3.2e9; % PVDF
vp = 0.35;

Eeff = 1/(Frac_al/Ea + Frac_cu/Ec + Frac_ka/Ek + Frac_pv/Ep) % = 6.22 GPa
```

And the effective Young's modulus is 6.22 GPa. Then next value to find is the effective Poisson ratio. Again, this must be found for the transverse direction and it is done using a weighted averages approach[xxxii].

$$\nu_{eff} = \nu_1 V_1 + \nu_2 V_2 + \ldots + \nu_n V_n$$

```
veff = Frac_al*va + Frac_cu*vc + Frac_ka*vk + Frac_pv*vp % = 0.3445
```

Now that this value is found, it can be used to determine the deformation length using Hertzian Contact Mechanics.

$$\frac{1}{E^*} = \frac{1+\nu_{eff}^2}{E_{eff}} + \frac{1+\nu_{AL}^2}{E_{AL}}$$

In this equation, it is assumed that the half sphere will be an ice cube. The Young's modulus and Poisson ratio of ice is given in the this endnote[xxxiii].

```
E_ice = 10e9; v_ice = 0.33;
E_hertz = 1/((1+veff^2)/Eeff + (1+v_ice)^2/E_ice) % = 2.8 GPa
```

When taking this value of the Young's modulus and applying it into the depth equation above, one gets:

```
F     = 1e6;
R_ice = 0.25*in;
d     = @(E,R,F) (F/(4/3*E*sqrt(R)))^(2/3)
depth = d(E_hertz,R_ice,F)*in  % = 0.00056954 inches = 1.4452e-005 meters
```

And so, the expected depth of the impact is 0.00057 inches. This represents a strain of 0.6987.

IMPACT DURATION

Impact duration is a highly variable topic since an impact is a function of so many factors, including topology, friction, angle of impact, etc. That is, nothing is perfectly elastic, some amount energy is always lost[xxxiv]. However, there are a few viewpoints that can help one analyze impacts and get a rough idea of the impact details. One viewpoint is based on J. P. A. Tillett's "A study of the Impact on Spheres of Plates" done in 1954. This study relates impact velocity and material parameters to impact duration. Another viewpoint is based on the study of a material's pressure wave and resonant frequencies. The third, and possibly most reliable—though most expensive and time consuming—is a statistical analysis by observing impacts with a high speed camera and measure the number of frames required to encapsulate the impact time zone.

Impact duration will prove to be extremely important during the electromechanical sections of this report, namely the frequency response—the shorter the impact duration, the higher the possible bandwidth.

VELOCITY AND MATERIAL PERSPECTIVE

J. P. A. Tillett's paper studied the coefficient of restitution, $e = \sqrt{h_1/h_0}$, which is the square-root of the ratio of a ball's height before a drop and after it rebounds. For impact duration, Tillett gives a relation found by Clarence Zener[xxxv] which relates time of contact and pressure-time for perfectly elastic bodies:

$$\frac{d^2\sigma}{d\tau^2} + \left(1 + \lambda \frac{d}{d\tau}\right)\sigma^{3/2} = 0$$

$$\lambda = \frac{\pi^{3/5}}{3^{1/2}} \left(\frac{R}{2h}\right)^2 \left(\frac{v_0}{v'}\right)^{1/3} \left(\frac{\rho_1}{\rho_2}\right)^{3/5} \left(\frac{E_1'}{E_1' + E_2'}\right)^{2/3}$$

$$E_1' = \frac{E_1}{1 - \nu_1^2}$$

$$E_2' = \frac{E_2}{1 - \nu_2^2}$$

$$v' = \sqrt{E_2' / \rho_2}$$

FIGURE 16 – ZENER RELATION BETWEEN RELATIVE DISPLACEMENT AND TIME[xxxvi]

Where σ and τ are dimensionless variables, with σ proportional to the relative displacement of the plate and sphere and τ to the time from the beginning of impact. λ is termed by Zener as the inelasticity parameter with R is the radius of the sphere, 2h is the thickness of the plate, v_0 is the velocity of impact, ρ_1 and ρ_2 are the densities of the sphere and plate, and ν_1, E_1, ν_2, and E_2 are the respective Poisson ratio and Young's modulus of the respective materials.

This system has been solved by A.E.H. Love in 1927 and is[xxxvii]:

$$T_H = 2.94\left(\frac{5}{4}\pi\rho_1 \cdot \left(\frac{1}{E_1'} + \frac{1}{E_2'}\right)\right)^{2/5} \frac{R}{v_0^{1/5}}$$

However, nothing is perfectly elastic so this equation is a reference. Using values for E_1 and E_2 found in pervious sections, 58 GPa and 10 GPa, and using an impact velocity of approximately 100 miles per hour (or 44 m/s), a value to T_H is 51 μs.

```
E1 = 5.8833e+010;   % [Pa]
E2 = 1e10;          % [Pa]
p  = 1000;          % [kg/m^3]
v  = 44;            % [m/s]
R  = 0.0127;        % [m]
Th = 2.94*((5/4)*pi*p*(1/E1 + 1/E2))^(2/5)*R/v^(1/5) % [s]
% Th =
%
%   5.1092e-005
```

Tillett conducted experiments with steel balls that would active a circuit only while the ball was in contact with the designated impact surface. The following was generated:

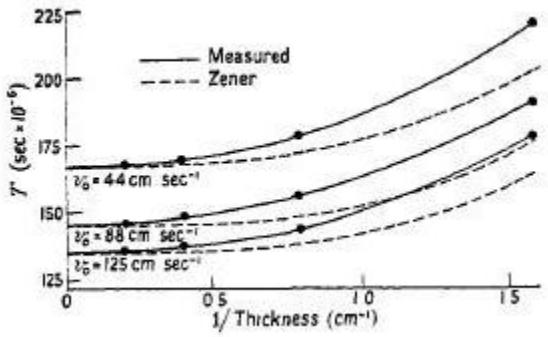

FIGURE 17 – PLOT OF CONTACT TIME OF A ½" DIAMETER BALL WITH VARIABLE SPECIMEN THICKNESS[xxxviii]

This demonstrates that the impact duration, according to Tillett's derivation, will be in the 100-200 μs range. These values will be taken later in the report.

RESONANT FREQUENCY PERSPECTIVE

There are other factors that can help shed light on impact duration that were not taken into account by Tillett, and that is the object's resonant frequency. Resonant frequencies are the vibrational modes an object can sustain after it has been impacted by a significant impulse[xxxix].

$$f = \frac{n \cdot v}{4 \cdot L} \qquad [1/\mathrm{s}]$$
$$v = \sqrt{E/\rho} \qquad [\mathrm{m/s}]$$
$$\Delta T \propto 1/f \qquad [\mathrm{s}]$$

FIGURE 18 - RESONANT FREQUENCY AND PERIOD RELATIONS[xl]

For extremely short periods of time, an object will vibrate, and this vibration is essentially the movement of acoustic waves internal to the body. This internal pressure will deform the body and upon restoration, projectile motion will result. Taking this information into Matlab:

```
E_ice = 10e9;              % [Pa]
p_ice = 1000;              % [kg/m^3]
Vs    = sqrt(E_ice/p_ice)  % [m/s]
f     = 1*Vs/(4*R)         % [1/s]
DT    = 5*1/f              %  = 80 us
```

And so, taking 5x for the proportionality term, a factor discussed by my advisor, a value of about 80 μs is obtained. This is promising, as it is roughly the same order of magnitude as Tillett's results above.

OBSERVATIONAL PERSPECTIVE

Lastly, and probably the most reliable though most expensive method of determining impact duration is direct observation.

By knowing how many frames per second a video is filmed at, and counting the number of frames, one can find the amount of time an impact takes place. Conversely, by counting the real time the impact duration is on video and dividing that by the FPS, impact duration can be extrapolated. Doing this on a survey of YouTube videos, impact durations on the order of 50-100 μs is found.

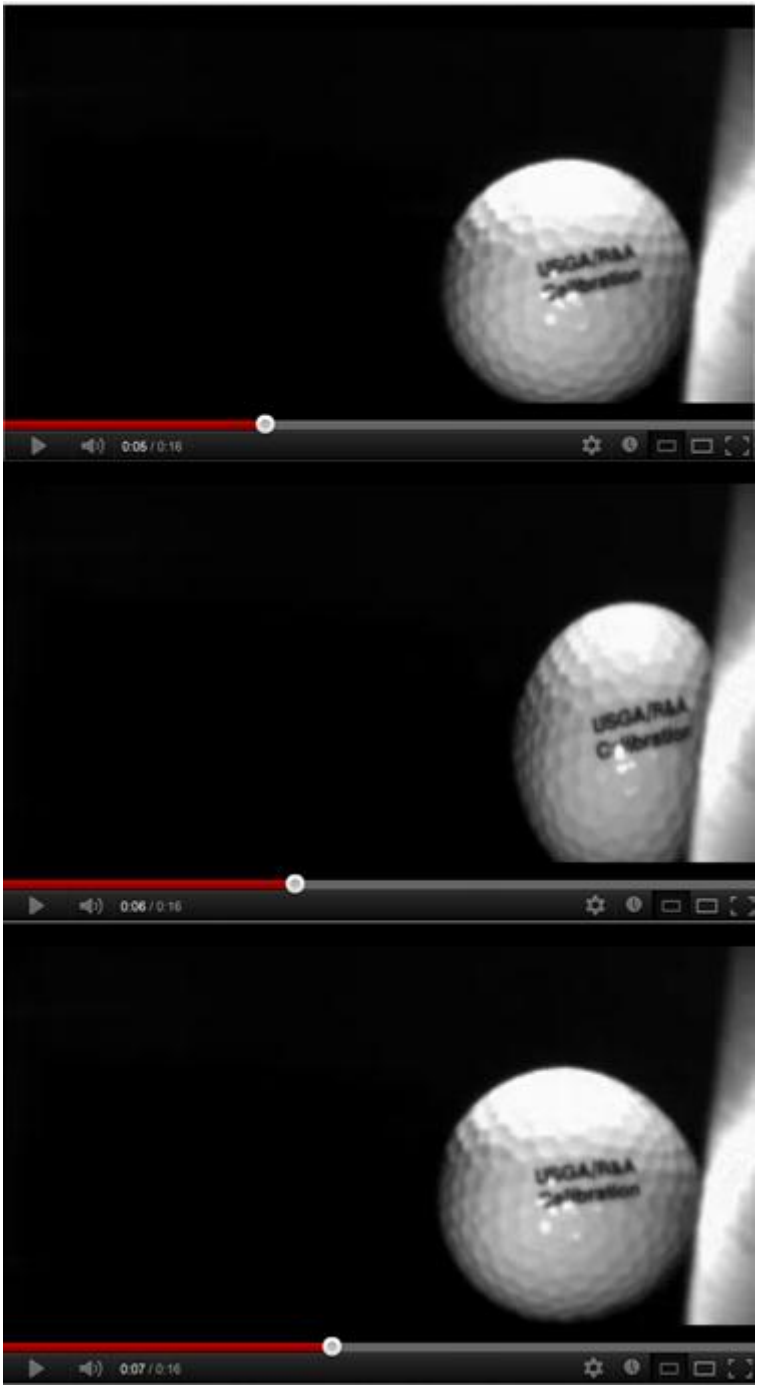

FIGURE 19 – YOUTUBE VIDEO OF A GOLF BALL IMPACTING A SURFACE AT 40,000 FPS[xli]

The above figure shows a golf ball, a prevalent video on YouTube, unfortunately, ice or hail impact videos could not be located. With a roughly 2 second impact duration shown in the video, and 40,000 FPS, the impact duration is roughly 2/40000 = 50 μs, which is also a very similar number to the ones found above.

MECHANICAL FAILURE

Mechanical failure, as expressed by the Huber-Von Mises-Hencky theory is stated as:

> *Failure is predicted to occur in the multi-axial state of stress when the distortion energy per unit volume becomes equal to or exceeds the distortion energy per unit volume at the time of failure in a simple uniaxial stress test using a specimen of the same material*[xlii].

What this means is the energy causing the change in shape (distortion) is the main focus of failure—other aspects are irrelevant. What this theorem does is takes the stress contributions in all three axial directions and relates them to the single uniaxial failure strength, σ_f[xliii]. If the following statement is true, then failure is predicted:

$$\frac{1}{2}\left[\left(\sigma_1-\sigma_2\right)^2+\left(\sigma_2-\sigma_3\right)^2+\left(\sigma_3-\sigma_1\right)^2\right]\geq\sigma_f^2$$

This theory of failure is the exact same result as the octahedral shearing stress theory, which states that:

$$\tau_0=\frac{1}{3}\sqrt{\left(\sigma_1-\sigma_2\right)^2+\left(\sigma_2-\sigma_3\right)^2+\left(\sigma_3-\sigma_1\right)^2}$$

$$\tau_{o,f}=\frac{1}{3}\sqrt{2\cdot\sigma_f^2}$$

Where τ_0 is the octahedral shearing stress. Visually, the following figure shows how this looks in a geometric-like adaptation.

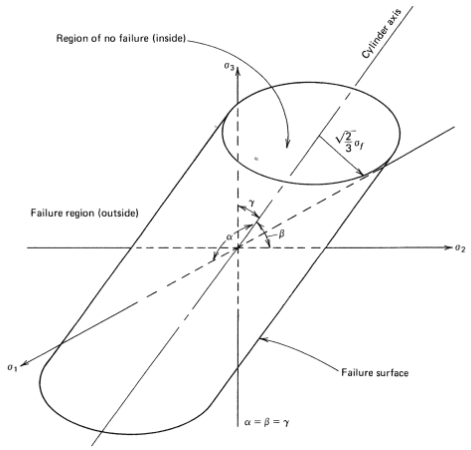

FIGURE 20 - GRAPHICAL REPRESENTATION OF DISTORTION ENERGY THEORY OF FAILURE[xliv]

In the above figure, if one takes their location on the stress axis and they appear outside the cylinder, failure is predicted. The values of σ_i will be taken from the estimated 1 MPa input stress but also the maximum stress will be found numerically. Lastly, σ_f is given as the ultimate strength. This will be compared in Matlab.

DISTORTION ENERGY ANALYSIS – MATLAB

The following code evaluates the distortion energy theory:

```
P = 1e6; % [Pa]
stress_al   = [1 0 0].*P;
stress_kap  = [1 0 0].*P;
stress_cu   = [1 0 0].*P;
stress_pvdf = [1 0 0].*P;

distortion_energy = @(s) 1/2*((s(1)-s(2))^2+(s(2)-s(3))^2+(s(3)-s(1))^2);
sf_al = 125e6; % When squared: 1.5625e+016
sf_cu = 220e6; % When squared: 4.8400e+016
sf_ka = 231e6; % When squared: 5.3361e+016
sf_pv = 240e6; % When squared: 5.7600e+016
fail_al_t = distortion_energy(stress_al);  % 1.7860e+012
fail_ka_t = distortion_energy(stress_kap); % 2.2858e+009
fail_cu_t = distortion_energy(stress_cu);  % 3.5041e+012
fail_pv   = distortion_energy(stress_pvdf);% 1.6619e+009

does_al_t_fail = fail_al_t >= sf_al^2 % False
does_ka_t_fail = fail_ka_t >= sf_ka^2 % False
does_cu_t_fail = fail_cu_t >= sf_cu^2 % False
does_pvdf_fail = fail_pv   >= sf_pv^2 % False
```

When comparing the commented out squared strength and results of the fail theorem function, it is clear to see that impacts of 1 MPa magnitude are nowhere near the failure range. However, after running the Matlab script through many values of pressure, the following is found for failure:

```
P_al_fail   = 1.28014e8;
P_cu_fail   = 2.29202e8;
P_ka_fail   = 2.34585e8;
P_pvdf_fail = 2.43902e8;
```

Which means, if the stress exceeds 128 MPa, the aluminum will fail, 229 MPa, the copper will fail, 234 MPa the kapton will fail and 243 MPa, the PVDF will fail. Thus, as long as the pressure is below 128 MPa, failure is a non-issue.

SURFACE ACOUSTIC WAVE

Seismic-Wave[xlv] is the overarching name of waves traveling through a body and it is split into two main subcategories: body waves and surface waves. Body waves are described by p-waves and s-waves, or rather longitudinal/compress waves and transverse/shear waves. P-waves generally travel faster since they are function of the bulk modulus and S-waves are a function of the shear modulus. Shear modulus is always less than the bulk modulus in a homogeneous, isotropic material by the simple relation[xlvi]:

$$E = \underbrace{2G(1+\nu)}_{\text{Shear}} = \underbrace{3K(1-2\nu)}_{\text{Bulk}}$$

$$\frac{G}{K} = \frac{3}{2}\cdot\frac{1-2\nu}{1+\nu}$$

$$\left\{2(1+\nu) > 3(1-2\nu)\right\} \forall \left[\nu > 0\right]$$

$$\therefore G > K$$

The subset of surface waves are Rayleigh waves, Love waves, and Stonely waves. Stonely waves are a subset of Rayleigh waves and deal with solid-fluid boundary (and thus, not important here). Love waves are transverse surface waves and cause material to shift side to side. Rayleigh waves, however, is the rolling motion associated with the surface acoustic wave (SAW)[xlvii].

An image from Ken-ya Hashimoto's textbook "Surface Acoustic Wave Devices in Telecommunications" portrays the bulk acoustic wave (BAW) and SAW:

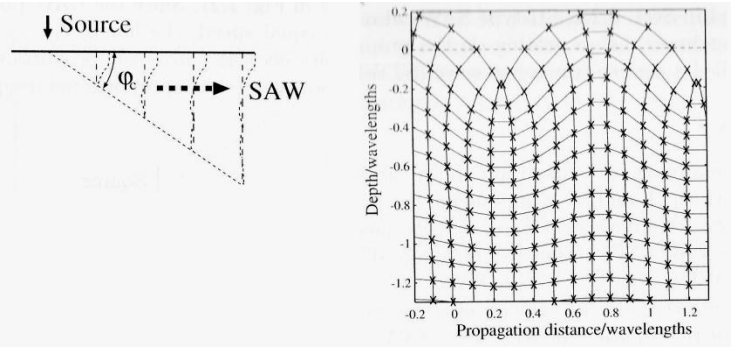

FIGURE 21 - SAW AND BAW IN MATERIALS[xlviii]

In left figure, $\phi_c = \cos^{-1}\left(V_S/V_B\right)$[xlix], where V_S is the SAW velocity and V_B is the BAW velocity. This relation tells a few things: that the BAW velocity is fundamentally greater than the SAW velocity and that V_S and V_B can't realistically be equal. The figure on the right shows the field distribution of a Rayleigh-type SAW. The X-axis is the propagation distance as a factor of wavelength and the Y-axis is the depth as a factor of wavelength and it is clear the bulk of energy is located at the surface[l].

Rayleigh waves are the main wave of focus because the rolling motion described will essentially cause the rolling strain in the normal direction through the sensor. The other waves (Love, P, S-waves, etc.) are of particular interest in geodynamics, but are of little use here.

The rolling strain caused by the Rayleigh wave is the desired effect wanted. It is expected that an object hitting the sensor will cause this wave through the piezoelectric polymer layer, and at each crest of the wave generate charges. As the wave travels past the capacitive islands, an electric field is expected to generate on the piezoelectric layer, creating current on the top and bottom copper layers, based off the law $i(t) = C \cdot dv/dt$. See the above section on the piezoelectric effect where the relationship between voltage and stress is shown.

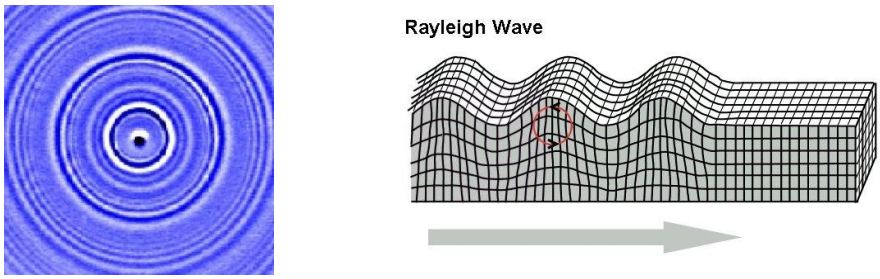

FIGURE 22 - IMAGES OF RAYLEIGH WAVES[li,lii]

The velocity of this wave is given by the relation $v_s = \sqrt{E/\rho}$ where E is the Young's modulus—and since the material is isotropic, only one number for the modulus is required—and ρ is the density. Since velocity is a function of only material properties, it is expected to always be the same, no matter how strong an impact is. Therefore, knowing this value a priori will solve one of the triangulation equations, as will be discussed later in this study.

ELECTRICAL LOADS

The electrical loads of the sensor follow from the explanation in the Material Characteristics section and the introduction. The electrical load is related to the input stress transduced into a voltage.

$$\left[\begin{array}{l} i(t) = -\frac{d_{33}A\cdot T_3}{RC}\exp\left(-\frac{t}{RC}\right) \\ \int_0^t C\frac{dv}{dt}\,dt = \int_0^t -\frac{d_{33}A\cdot T_3}{RC}\exp\left(-\frac{t}{RC}\right)dt \\ \quad i(t)=C\frac{dv}{dt} \\ C\cdot\left(v(t) - \underbrace{v(0)}_{\text{Assume 0 V}}\right) = -\frac{d_{33}A\cdot T_3}{RC}\left(\exp\left(-\frac{t}{RC}\right)(-RC) - K\right) \\ v(t) = \frac{d_{33}A\cdot T_3}{C}\exp\left(-\frac{t}{RC}\right) - \underbrace{K/C}_{d_{33}A\cdot T_3} \end{array}\right] \quad \left[v(t) = \frac{d_{33}A\cdot T_3}{C}\left(\exp\left(-\frac{t}{RC}\right) - 1\right)\right]$$

In the above, it is assumed that there is 0 voltage at steady state and with this boundary condition, V_0 is offset to make sure v(0) = 0. The following sections details this further with Matlab.

The following sections also attempt to describe the sensor with a SPICE circuit model. Since the sensor is an electromechanical device, the mechanical aspects of it can be represented as an input voltage passing into the circuit. Furthermore, each capacitive island within the sensor can be thought of as an RC circuit[liii]. This model follows from Ken-ya Hashimoto's book on SAW devices, and it makes logical sense, as a flat, separated island is what a parallel plate capacitor is. Hashimoto takes it a step further and applies an inductor to the circuit, but I neglect the inductor's effect since there are no current loops (except possibly in the antenna) and Hashimoto was using his model to explain the circuit model in the context of piezoelectric gratings. Below is a quick example of a grating.

FIGURE 23 - EXAMPLE OF A PIEZOELECTRIC GRATING[liv]

IMPACT AND VOLTAGE RESPONSE

Leading from the previous discussion on the material properties and piezoelectric effect, the following Matlab simulation is run that demonstrates the piezoelectric effect using reasonable numbers found for PVDF, as well as 1 MPa as the load. The code of this run can be found in the appendix, section 1.

The following equations are applied:

$$T_3(t) = T_{3-n} \cdot \exp\left(-\frac{(t - t_m)^2}{2 \cdot \sigma} \right) \quad \left\{ \begin{array}{l} T_{3-n} = 10^6 \,\text{Pa} \\ t_m = 0.5 \,\text{ms} \\ \sigma = 10 \,\text{ns} \end{array} \right\}$$

In this equation, $T_{3\text{-}n}$ is the 1 MPa input stress applied to the system, but it is applied as a Gaussian centered at 0.5 milliseconds. Centering at 0.5 ms was chosen because it would be unrealistic if the peak of the Gaussian started at t = 0 s. The standard deviation was chosen as 10 ns to ensure that the pulse-width would be with 0.1 ms in total. In short, this representation of impact is a natural approximation, but in reality, it will need to be found experimentally or with advanced contact mechanics (as discussed in the Contact Mechanics section).

$$V(t) = \frac{d_{33} A}{C} \left[\exp\left(-\frac{t}{RC} \right) - 1 \right] \cdot T_3(t) \quad \left\{ \begin{array}{l} d_{33} = 15 \cdot 10^{-12} \,\text{C/N} \\ A = 0.00129032 \,\text{m}^2 \\ C = 4.947 \cdot 10^{-9} \,\text{F} \\ R = 1\Omega \end{array} \right\}$$

In this equation, the piezoelectric effect is applied around the $T_3(t)$ equation. Lastly, the frequency response is found by utilizing Matlab's Fast Fourier Transform algorithm, with a sampling frequency of 1 MHz and a time bin of 0 – 1 ms. The specifics are all in the code, located in appendix, section 1.

The below sections are split up by the PVDF thickness and pulse widths. The thickness of the PVDF are critical to the piezoelectric equations, specifically the capacitance aspect of it. The capacitance value finds itself not just part of the RC time constant, but also as the front coefficient of the voltage equation. Graphs made with a pulse width of 0.01 ms is generated in comparison as well.

PVDF THICKNESS – 0.001”

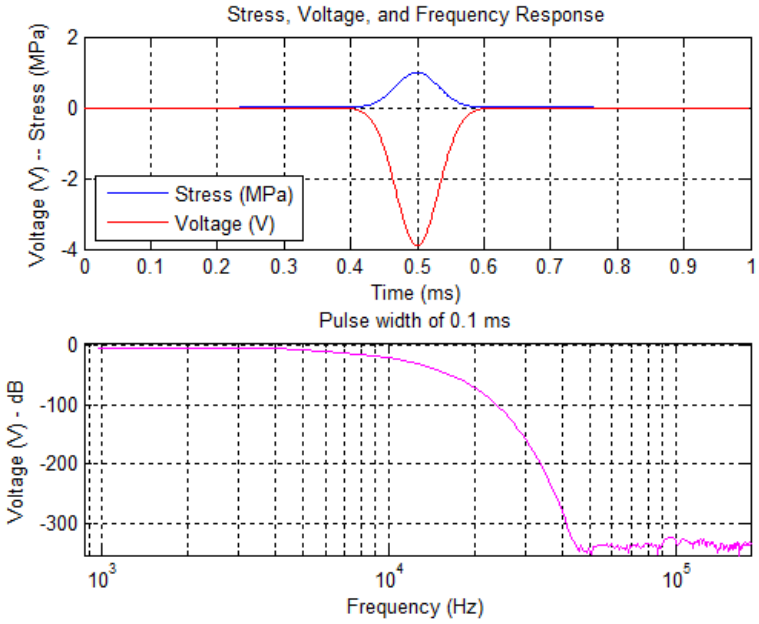

FIGURE 24 - STRESS, VOLTAGE, FREQ. RESPONSE – PVDF – 1 MIL, 0.1 MS PULSE

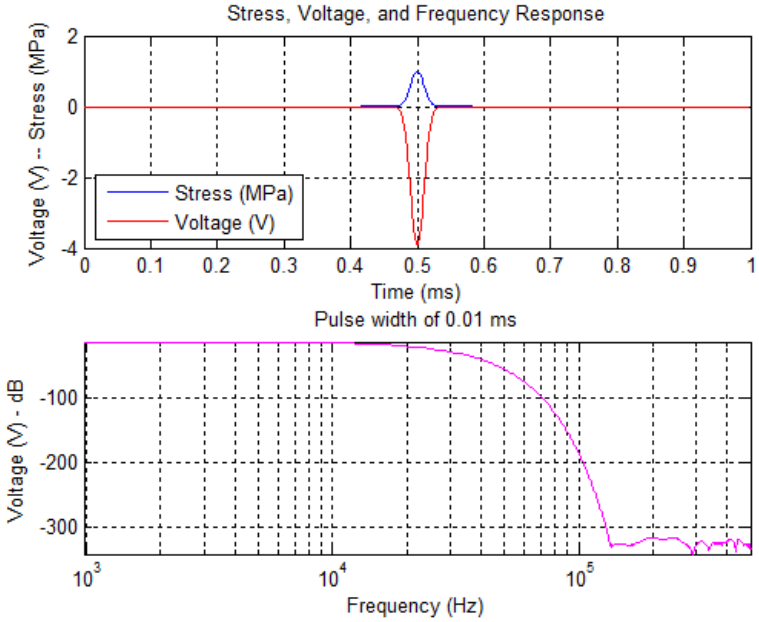

FIGURE 25 - STRESS, VOLTAGE, FREQ. RESPONSE – PVDF – 1 MIL, 0.01 MS PULSE

PVDF THICKNESS – 0.004”

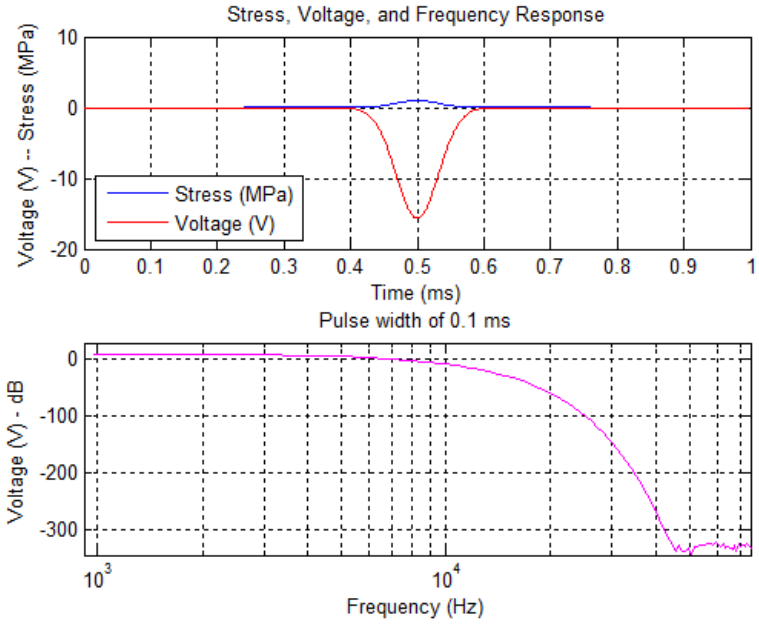

FIGURE 26 - STRESS, VOLTAGE, FREQ. RESPONSE – PVDF – 4 MIL, 0.1 MS PULSE

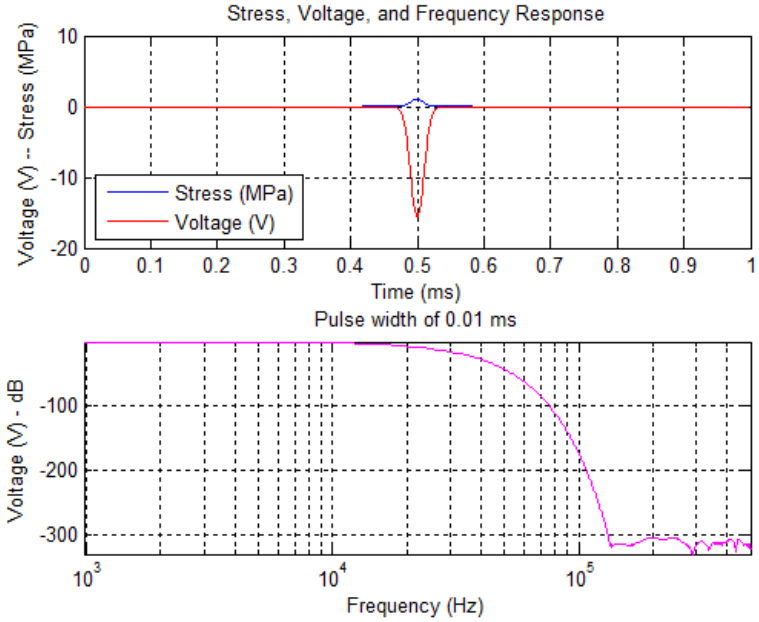

FIGURE 27 - STRESS, VOLTAGE, FREQ. RESPONSE – PVDF – 4 MIL, 0.01 MS PULSE

PVDF THICKNESS – 0.01”

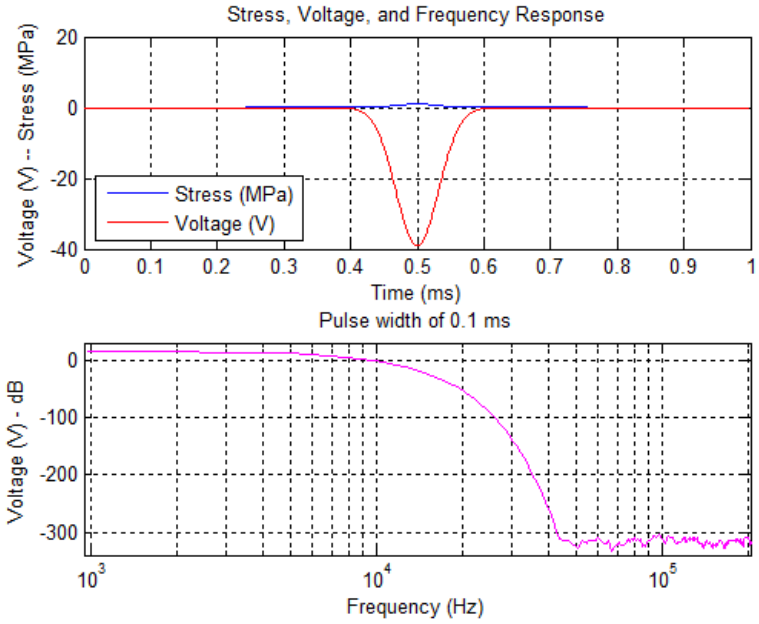

FIGURE 28 - STRESS, VOLTAGE, FREQ. RESPONSE – PVDF – 10 MIL, 0.1 MS PULSE

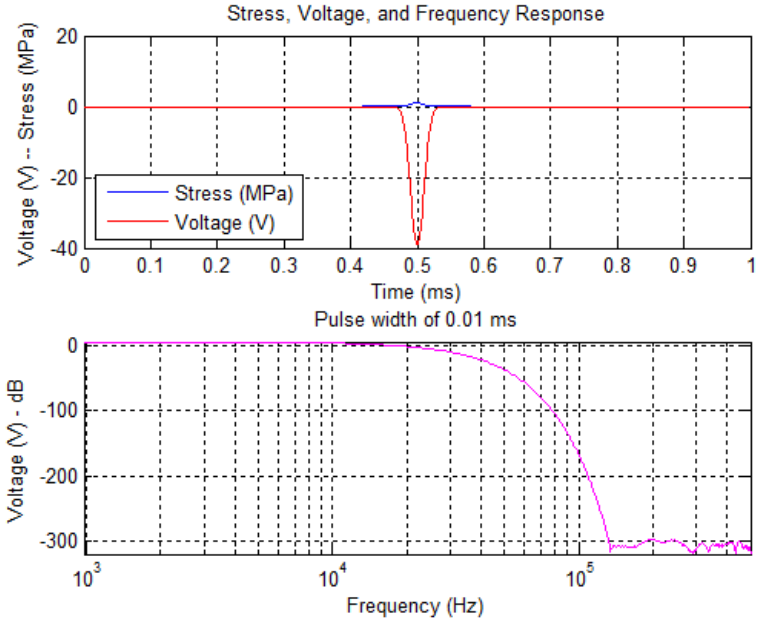

FIGURE 29 - STRESS, VOLTAGE, FREQ. RESPONSE – PVDF – 10 MIL, 0.01 MS PULSE

VOLTAGE RESPONSE DISCUSSION

This model demonstrates that, given the piezoelectric, dielectric, and other such constants, a reasonable response is attained. One can see a stress that is applied as a Gaussian and a voltage response which shows almost a linear relationship with stress. This is desired—having an easily discernible relationship between stress and voltage is expected.

The frequency response is greatly a function of impact duration, and as expected, its frequency response is in the acoustic range. There is roughly a 0 dB loss up to 2 KHz and then it begins to drop exponentially. Though it is mostly irrelevant, in the 100 KHz range, its loss oscillates between nodes, but since the loss is -150 dB, it is not important. The fact is, the frequency range (i.e., bandwidth) expected is in the 0 – 10 KHz range. One thing to notice, in the frequency graph, nothing is shown below 1 KHz, this is because of the sampling length—it is expected to be in the 0-7 dB range all the way from 0 – 10 KHz depending on the PVDF thickness.

While the pulse width of the impact determines the shape of the frequency response, the thickness of the PVDF greatly determines the amplitude of the voltage response. The thicker the PVDF, the more of a voltage response. This makes sense when looking back at the math:

$$V(t) = \underbrace{\frac{d_{33}A}{C}}_{V_0}\left[\exp\left(-\frac{t}{RC}\right)-1\right]\cdot T_3(t)$$

$$V_0 = \frac{d_{33}A}{C} = \frac{d_{33}A}{\varepsilon\frac{A}{d}} = \left\{d\cdot\frac{d_{33}}{\varepsilon}\right\}$$

$$V(t) = d\cdot\left\{\frac{d_{33}}{\varepsilon}\cdot\left[\exp\left(-\frac{t}{RC}\right)-1\right]\right\}\cdot T_3(t)$$

The thickness, d, becomes directly correlated to the V_0 voltage value. Therefore, the more the thickness, the more the voltage. And the more the voltage, the more frequency can be extracted. So, there is a high incentive to use as thick of a PVDF as possible, though that would come at the cost of adding extra weight and bulk to the sensor itself.

A thickness of 10 mil and pulse width of 0.1 ms will be used in the SPICE simulation below.

SPICE MODEL

Simulation Program with Integrated Circuit Emphasis[lv] (SPICE), is a common environment which gives the user the ability to simulate electrical systems. In the case of the sensor, the input load is a relatively large, though highly transient strain which causes very specific voltage drops at specific nodes. This impact can be approximately simulated by a Gaussian pulse, taken directly from the Matlab simulation in the above section, traveling with low electrical impedance, but delayed before reaching each node.

This delay is the SAW in effect, and electrically the delay can be modeled by a transmission line. Transmission lines forms an entire study in electrical engineering, especially in high frequency signals moving distances comparable to its wavelength[lvi]. However, although transmission line physics is derived for different applications, its properties of delay can be used very accurately in acoustic modeling[lvii]. Simply put, an acoustic wave is rather slow compared to the relatively near instantaneous speed of electricity. Since the SAW travels at roughly 300 meters per second, instead of 300,000,000 meters per second, transmission lines are employed with a time delay set at about 1 micro-second (this delay is meant just to keep the graph relatively tight) and the load impedance is set to 1Ω in order to match the impedance of the simulated lines.

Since the electrical analysis is focused primarily on the very short term, transient effects of the impact, acoustic wave reflections are ignored. Although those scenarios can occur, they will not serve a purpose in the electrical stimulation.

SPICE DIAGRAM AND RESULTS

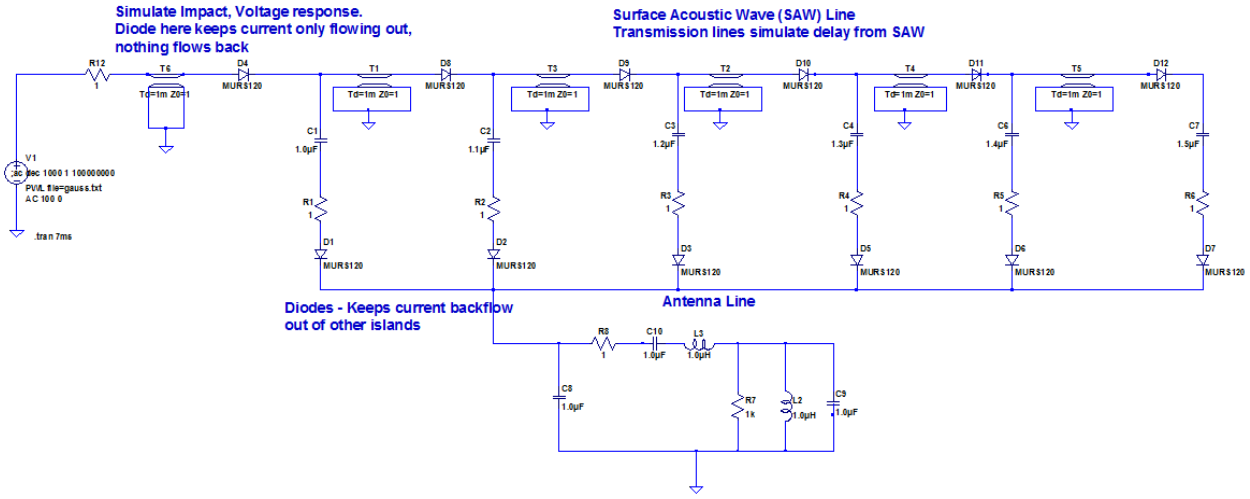

FIGURE 30 - SPICE REPRESENTATION OF SENSOR

From a circuit perspective, the above design outlines all the non-parasitic aspects of the sensor. Do note, the exact values are not presented here; this is a conceptual view point:

1. The pulse at the far left simulates the piezoelectric voltage spike (Gaussian) produced by the impact
2. The diodes ensure the flow of charges is similar to that of the sensor. I.e., current will flow into the antenna and dissipate, not back into the nodes.
3. The transmission lines simulate the delay caused by the SAW.
4. The 1Ω resistance at each step signifies the low resistivity, as current will be flowing through copper.
5. The capacitor in each branch represents each island on the sensor.
    a. Each capacitor is unique, which results in a unique center frequencies[lviii].
6. The produced chirps are very short lived, but the goal is for a receiver to pick up the chirp, discern is center frequency, and log its time of arrival.

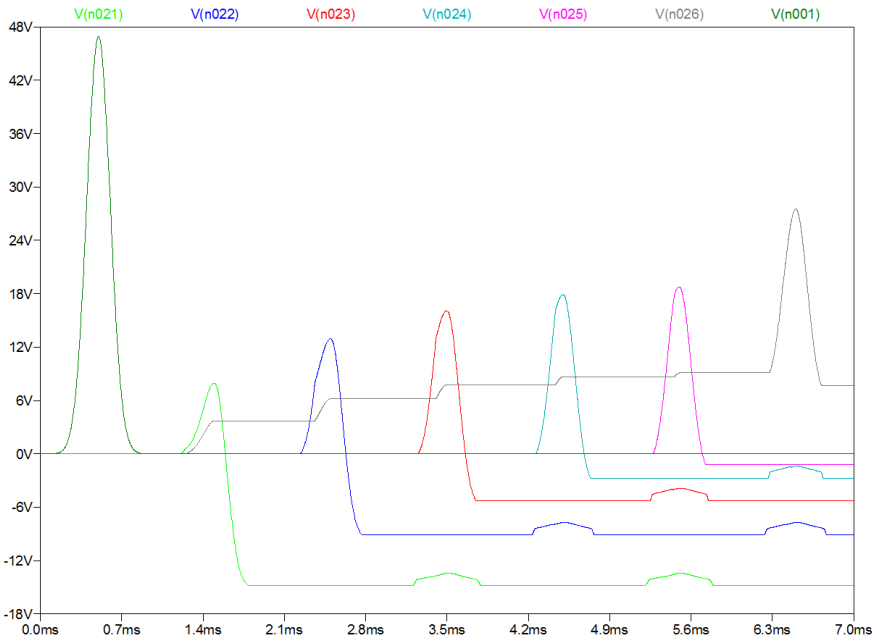

FIGURE 31 – PULSES SEEN BY EACH CAPACITIVE ISLAND (TIME DOMAIN)

7. The pulses shown in the above graph come from each branch separately. The 5 micro-second delays can be discerned from the graph itself.
    a. The Gaussian at the far left is the input voltage, whose values are taken directly from Matlab and imported into SPICE.

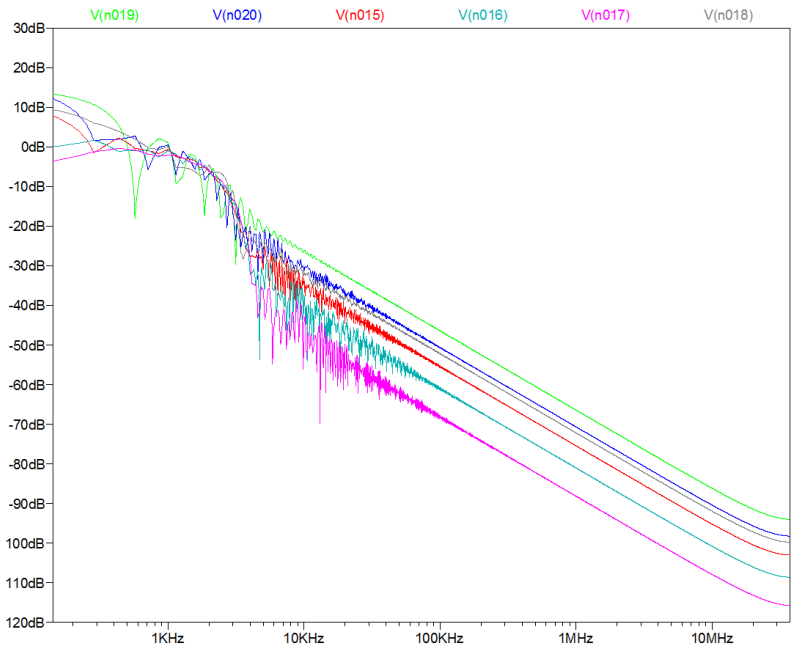

FIGURE 32 – SPICE OUTPUT ESTIMATION (FREQUENCY DOMAIN) – 0 – 30 MHZ

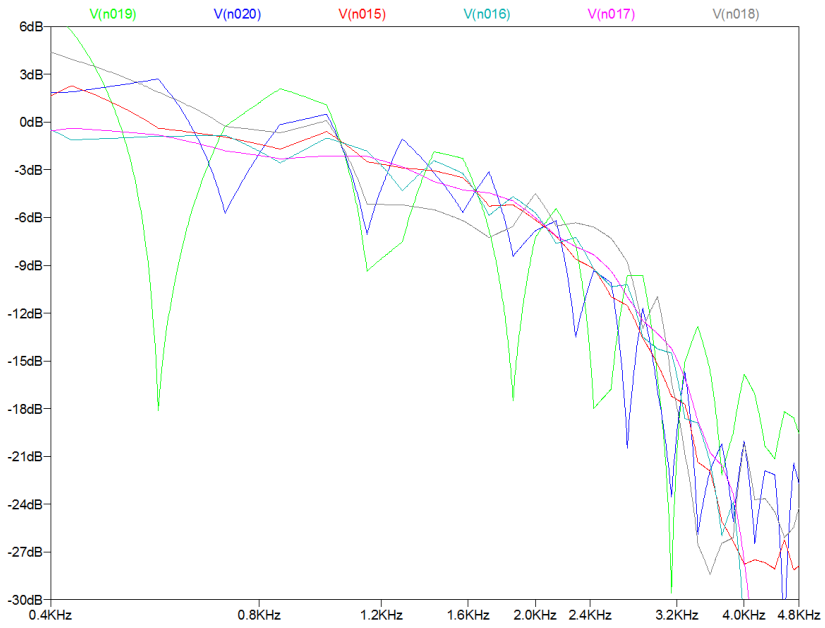

FIGURE 33 – SPICE OUTPUT ESTIMATION (FREQUENCY DOMAIN) – 0.4 – 4.8 KHZ

8. This frequency transform graph (found using the fast Fourier transform function, FFT, common to almost all spectrum analyzers) shows the various resonant points and will lead us to figuring out how to best tune the receiver circuit.

FREQUENCY EXPLANATION

Point 8 and the figure above exemplify the most important aspect of the electrical analysis: the expectation that each node will be identifiable by a unique center frequency. The following two figures are the time domain view of the expected output of the antenna, and a frequency view of the antenna output. The expectation is each chirp is sufficiently unique such that a properly tuned receiver system can distinguish one chirp from the next, thus allowing one to mark the time difference of arrive between sequential chirps.

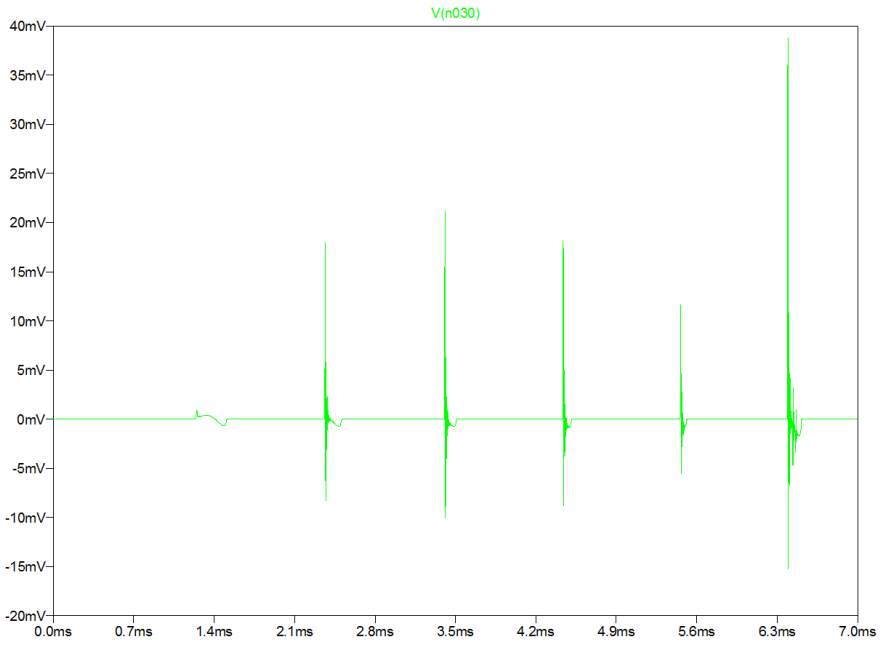

FIGURE 34 - EXPECTED ANTENNA OUTPUT (CHIRPS)

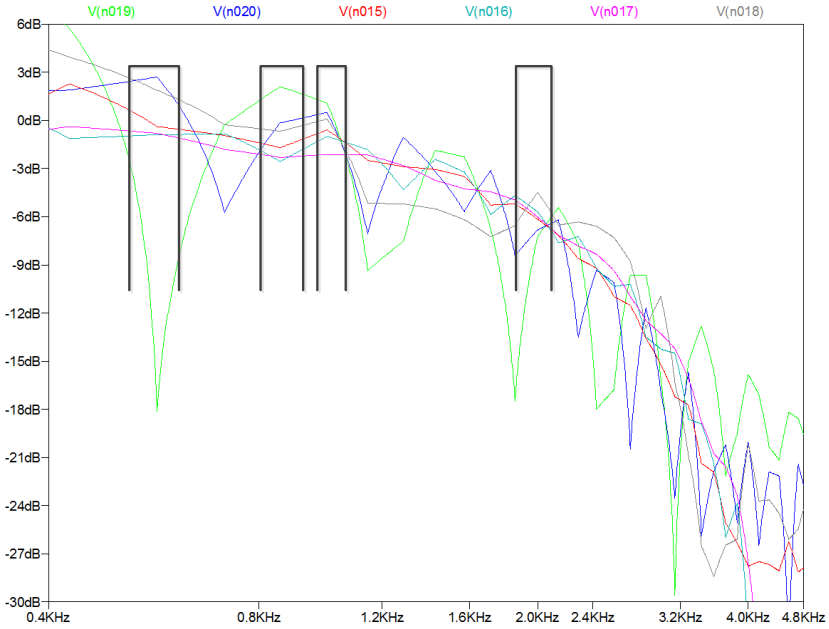

FIGURE 35 - FREQUENCY WINDOWS

The above figure shows the strategy a radio frequency (RF) engineer would employ in identifying one chirp from the next—identify specific windows and observe if an RF chirp contains a peak at those levels. Although this SPICE experiment is just a model that will help calibrate and refine further laboratory design, it demonstrates that a sensor which reduces down into a set of

these electrical elements will have discernible frequency windows for each node and this may be the most straightforward approach to identifying one location (i.e., capacitive island) from another.

DESIGN CAVEATS

One main caveat to this design is the current behavior after it reaches the antenna. In other words, when the impact induces the piezoelectric effect, and current from the capacitive islands is drained onto the antenna, what will it do next? The answer is, without proper design, signal will both emit from the antenna and also drain into all the other capacitive islands. The reason for this is each island is connected to the antenna through a copper line in the layer; if each copper line is shorted to the same antenna (which in itself is a conducting medium), it will drain current into the other islands as if each island were connected in parallel.

Although it was not mentioned in the material section, thought must be given to a material which can be placed between the antenna and all the capacitive island nodes which will enforce directionality in the current—i.e., only allow current to flow into the antenna, never flow out (except as an RF chirp). If current were to flow back into capacitive islands, unintended mechanical effects could occur, such as additional SAW's generated by the reverse piezoelectric effect, as well as additional chirps draining onto the antenna. This would hurt accuracy, introduce extra noise, and possibly decrease the life of the sensor.

DIODES AS A SOLUTION

As can be seen in the SPICE diagram, diodes are placed on each line. Diodes are a non-linear circuit element with the following two well-known properties: enforce directionality in current flow and rectification of oscillating current flow. The latter property is relevant in diodes' use in power regulation and converting alternating current into direct current. Other uses of diodes—such as surge protection and light generation (LED)[lix]—are not relevant here.

In this design, diodes are meant to keep the current flowing only in one direction—towards the antenna. While diodes are fairly simple elements to put into an IC circuit, as they are PN junctions, their implementation in this sensor will not be as straight forward. Since silicon is known to be very brittle[lx] and thus, even in small quantities, it may be unwise to use it within the sensor for fear of cracking (which could cut the current line).

So, while a diode is desired, the traditional silicon base diode may not work. At the end of the day, what is truly desired is a PN Junction. PN Junction physics[lxi] explain how diodes work—namely, a P-type material (a material with many positive ions) is placed in juxtaposition with an N-type material (a material with many negative ions), and when placed together, almost analogous to a magnet which only lets other magnets touch at one pole, current also can pass through one direction—the other direction, it is "repelled." Classically, silicon is used because of its abundance and good economics, as well as its low band gap energy, 1.11 eV at room temperature[lxii,lxiii].

If not silicon, another option for a diode could be polymer based diodes. These materials are commonly used in organic LEDs[lxiv]. Specifically, the use of organic semiconductors, doped as P and N could serve as the solution. The expectation is that, like common polymers, it will not be brittle or crack under the normal loading conditions. Organic materials conduct only when π-bonds overlap, allowing for a path for current to flow—all other paths are insulating, or contain large resistances. Organic semiconductors are doped with organic compounds as well, namely polyaniline (Ormecon) and PEDOT:PSS—these compounds are also termed organic metals[lxv].

The synthesis and design of the diodes would be beyond the scope of this paper. Ideally, N-type and P-type raw materials can be synthesized and injected into each conducting line within the sensor and have the right tolerance level to withstand the voltage spike as well as pass through the relevant frequency levels.

It may be found, however, that common silicon based diodes could be used as well, since the lamination layers and the expected small cross-section of the silicon used in the diode may render its brittle properties irrelevant. This would need to be confirmed with experimentation. If silicon would work, it may be ideal since the technology is well known and relatively cheap.

TRIANGULATION AND SOFTWARE SIMULATION

So far, this study has focused on the physical and electrical aspects of the sensor; an object impacts the sensor and unique RF chirps are emitted. Now the question is—how will one use those chirps to determine the impact location.

The algorithm used in this report is called Time Difference of Arrival (TDOA), which comes from a geometric family of location algorithms related to multilateration and triangulation. The results of the algorithm are exceedingly long, but are detailed in a paper title "A Synthesizable Low Power VHDL Model of the Exact Solution of the Three Dimensional Hyperbole Position System" by Ralph Bucher and D. Misra. That paper solves the 3-D case, whereas this sensor only requires the 2-D solution. Although that paper does not discuss wattage and actual power figures, the reason this method is "low power" is because it breaks down into a set of additions, multiplications and divisions which, to a modern processing chip, can be completed very quickly. This paper will demonstrate this fact.

This TDOA algorithm can also be applied to many other sensor systems as well. As will be discussed in the final sections of this report, there are other implementations of the sensor. One proposed version is an embedded sensor based of the piezoelectric nodes. This implementation would also rely on this same TDOA algorithm to locate points of impact. So, this section details the backbone of the entire locating goal, and therefore great care was used to model is and confirm its usefulness.

2D MULTILATERATION AND TIME DIFFERENCE OF ARRIVAL

In order to solve a TDOA problem, the following information must be known beforehand: the location of each sensor, a high resolution timestamp of each sensor's activation, knowledge of the acoustic wave speed inside the sensors' medium (such as air, water, or a solid body), and at least 3 sensors. Further, the acoustic wave speed needs to be isotropic. Beyond these physical requirements, software is required that will resolve all these givens in a reasonable amount of time.

To start, one should look at three circle equations:

$$\begin{aligned}(x-x_1)^2+(y-y_1)^2-R_1^2&=0\\(x-x_2)^2+(y-y_2)^2-R_2^2&=0\\(x-x_3)^2+(y-y_3)^2-R_3^2&=0\end{aligned}$$

$$\begin{aligned}R_i &= v_d\cdot\Delta t_{0-i}\\ \Delta t_{0-i} &= t_0-t_i\\ v_d &= \sqrt{E/\rho}\end{aligned}$$

Each equation above represents a circle, centered at x_i, y_i and with a radius R_i that is equal to $v_d\cdot\Delta t_{0-i}$. In this equation, v_d is the acoustic wave speed in the medium; it is constant for any type of impact or environment—as discussed in the section on Surface Acoustic Waves, acoustic speed is a function of a materials Young's modulus and density—and it is further simplified if the material is isotropic. The time value, $\Delta t_{0\text{-}i}$ represents the time difference between the first hit and the current hit. To put another way, when the sensor is hit, the following happens:

1. Impact occurs – acoustic wave (SAW) is triggered.
2. SAW touches first sensor and the "clock starts"
    a. This first touch of the sensor implies that $\Delta t_{0\text{-}0} = 0$, and thus $R_1 = 0$. So the first circle is actually just a point, centered at x_1, y_1.
3. The wave continues to spread and it touches the second sensor
    a. When the second sensor is touched, its time of arrival is known relative to the first sensor's "clock start" time.
    b. That is, if $\Delta t_{0\text{-}0} = 0$, then $\Delta t_{0\text{-}2} = |0 - t_2|$. Or, the amount of time passed between the first and second sensor being touched by the wave.

c. For the third sensor, it is similar to the second—the amount of time passed between the first sensor and third sensor being touched by the wave.
d. Thus, $\Delta t_{0\text{-}0} = 0$, always, and $\Delta t_{0\text{-}2} < \Delta t_{0\text{-}3}$.

Visually, the following figures exemplifies this:

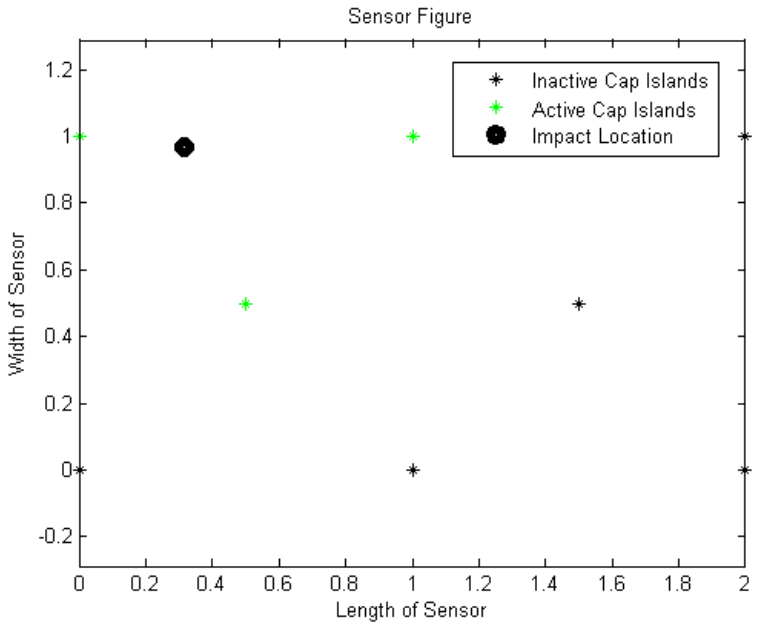

FIGURE 36 - NODAL VIEW OF SENSOR

The above figure generated by Matlab shows 3 rows of sensors, 3x2x3, laid out on a 1" x 2" surface. These sensors are represented by black or green asterisks. The green asterisks are the closest sensors to the impact, represented as the dark, black dot near the top left. The closest sensors will feel the acoustic wave first, before any of the others; in theory, all the sensors will feel the wave, but only the first 3 matter for location derivation.

At this stage, the software should be collecting the TDOA between each of the 3 sensors, thus deriving R_1 (which is trivially 0), R_2, and R_3.

In the following figure, what is shown is two blue circles surrounding the further two sensors and a red dotted circle around the impact. The blue circles are the locus of all points the wave could be located when the wave touched the first sensor. That is, when all the TDOA's are known and each radius is derived, one can draw a circle around each respective sensor with that radius; each point of that circle is a possible location the SAW could have been located as it was touching the first sensor. The red dotted line represents a snapshot of the edge of the SAW as it is

touching the first sensor; on the middle left, notice that the red dotted circle is intersecting the green asterisks. At the same time, the red dotted circle is touching one point of each blue circle. Of course, the red dotted circle is imaginary and would never be known in real life, but for this simulation, it represents where the surface wave is located when the "clock starts."

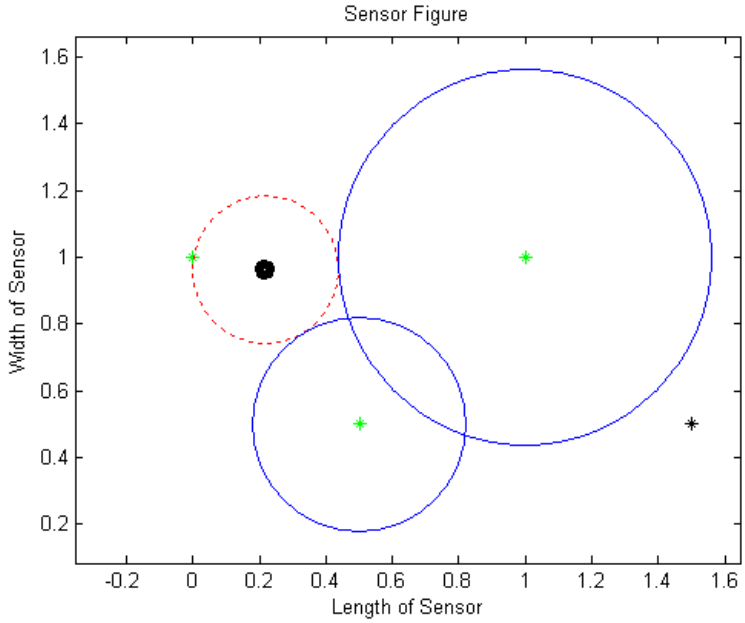

FIGURE 37 - TDOA "CLOCK STARTS" IMAGE

At this point, what is known is that the top left sensor got touched first by the SAW and the other two sensors got touched at a time $\Delta t_{0\text{-}2}$ and $\Delta t_{0\text{-}3}$ from the first sensor's touch, thus producing radiuses $R_2 = v_d * \Delta t_{0\text{-}2}$ and $R_3 = v_d * \Delta t_{0\text{-}3}$. At this point, the most straight forward method of solving for the impact location is increase each radius, with R_1 starting at 0, and R_2 and R_3 starting at their respective $v_d * \Delta t_{0\text{-}2,3}$ values, and note at what location does each of the three circles have a real intersection (as opposed to an imaginary one).

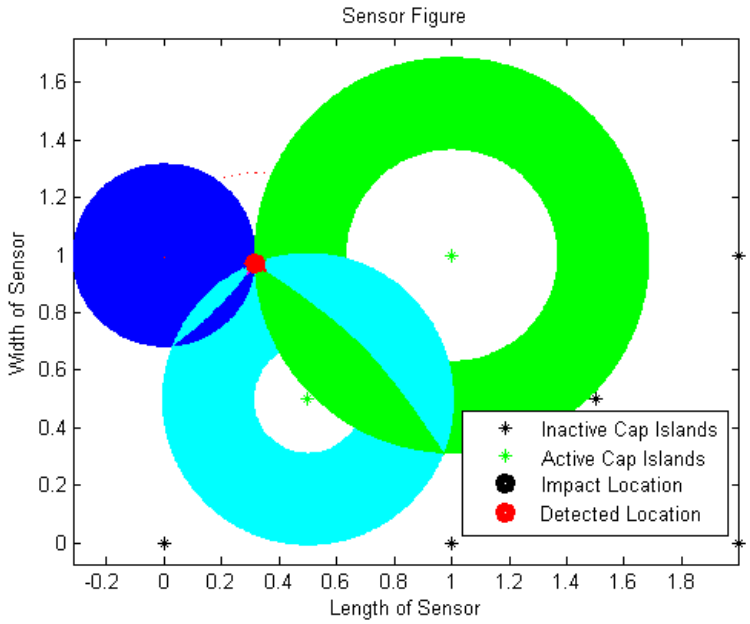

FIGURE 38 - TDOA LOCATION DETERMINATION

The above figure shows this theory in action. It shows 3 circles, the green and turquoise one are donut shaped because these circles start off with initial radius of $v_d * \Delta t_{0\text{-}2,3}$. However, the blue circle starts from R = 0 and thus is completely full.

Algorithmically, a loop is made that solves the three-circle equations for all 12 values, 6 possible x-intersections and 6 possible y-intersections. All that is needed for a satisfactory answer is 3 solutions from both x and y.

The basis of this algorithm is the expectation that all solutions prior to the real one are imaginary. So, the algorithm is based on checking if there are at least 3 real solutions for each intercept, then checking if each intercept represents the same location (within a healthy error bound). Once 3 real intersections are found, the algorithm is completed. Although this may seem like a cumbersome solution, the average solution time in a 30,000 Monte Carlo set was 0.0637 seconds, with a range of 0.0003 seconds to 0.3467 seconds. So at worst, it took about a 1/3 of a second and at best about 3 ten-thousandths of a second. These statistics will be analyzed deeper in the following sections.

See appendix, section 2, for the complete solution and a Matlab script that will produce all 12 solutions.

CAVEATS TO SOLUTION

One caveat is that the location needs to be within the sensor itself—theoretically, a surface wave could be located anywhere, even beyond the sensor, but values from there could receive a false positive solution since there could be more than one intersection of the three circles. One expectation to this solution is that the very first mathematical intersection represents the true, physical impact location. To ensure this, the impact should occur within the boundaries of the sensors. This means care must be made in the sensor's environment to ensure it is covering the measurand completely and SAWs caused by neighboring materials should be avoided; or, more sophisticated software could be written to run checks on the chirps. For example, if the first three chirps have come from edge nodes, it could imply the impact occurred outside the sensor.

Another caveat is the sensors must be placed in such an order to avoid a dual solution situation. That is, if each sensor was arranged perpendicularly to each other, there could be points where the circles intersect at two different locations at the same time. To overcome this, situating the sensors such that they are not all perpendicular to each other will avoid this.

The final caveat to mention is the size of the sensors. In the algorithm, the size of the sensor itself was neglected and taken for a point. However, the sensors will have a size associated with them; in fact, this size is very seriously taken into account in determining the capacitance of the islands in the electrical and piezoelectric sections of this report. In effect, the larger the sensor is in relation to the sensor size, the more uncertainty there will be in the location. This is because it is not known at what side the surface wave touched the sensor. Although this error is not focused on in this algorithm or report, this caveat could be mitigated by taking further action in the software by determining radius of the sensors themselves and factoring that back into the found solution. In general, the smaller the sensors, the less complex this algorithm will be.

MATLAB SIMULATION

In order to test the algorithm, an object oriented Matlab program was written, giving the end user the ability to test the algorithm in a variety of scenarios and run large Monte Carlo sets. Since the code consists of multiple files, it has been uploaded to the following UCLA website: http://esender.bol.ucla.edu/masters/TDOA.zip

For now, the main algorithm, besides the solution to the 3 circle system, is written out in the appendix, section 3. What that code amounts to is looping through each radius value, incrementing slightly at each loop iteration until 3 real solutions are found. Beyond this, the code was also written to count the specific time the algorithm takes to run, as well as calculate the error between the actual hit location and the resolved hit location.

EXAMPLE RUN AND ERROR RECONCILIATION

The following example takes off from earlier in this section with the following situation:

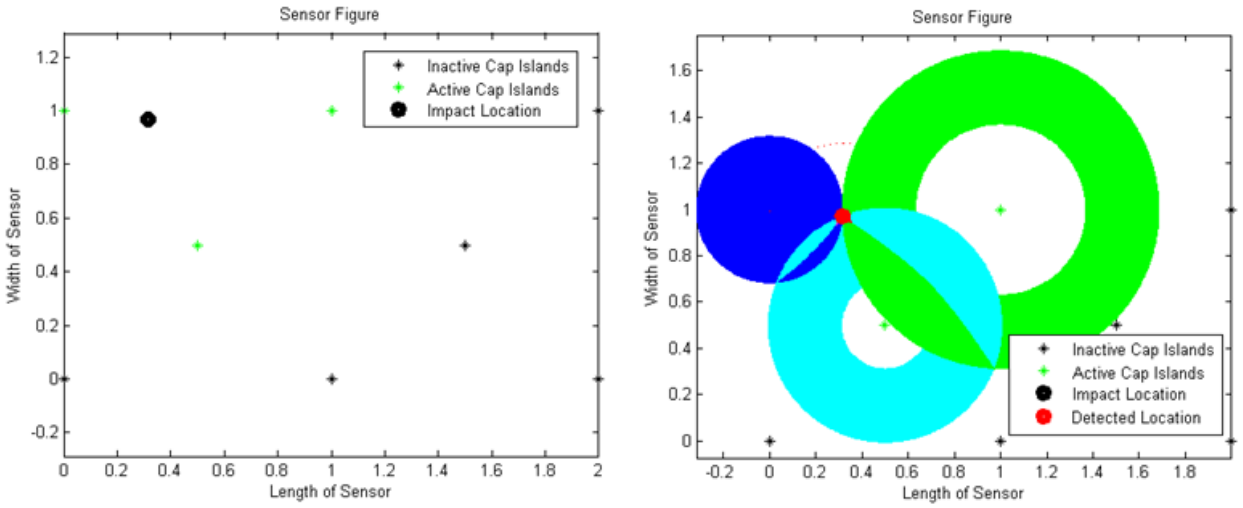

In the above figure, the example impact occurs on the top left and is resolved on the right. To run this solution, it required 354 loop iterations and took 0.0827 seconds to run. It resolved with an error of 0.001".

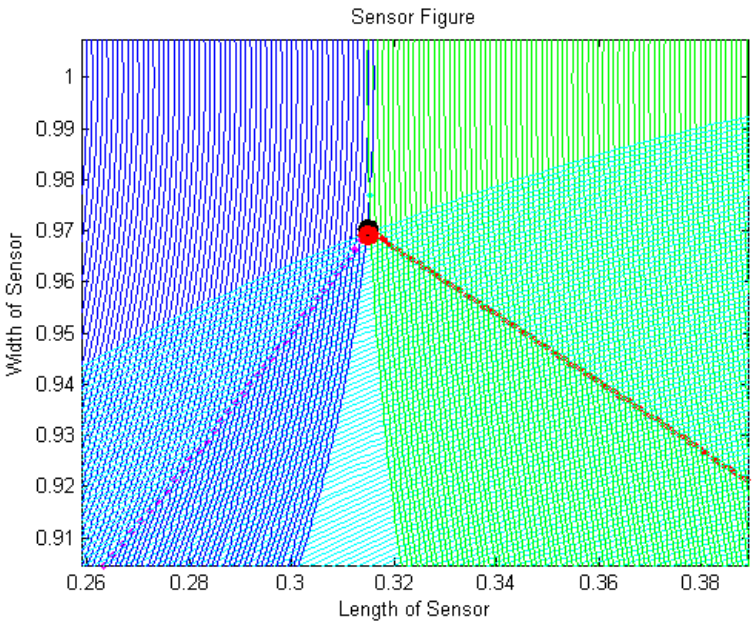

FIGURE 39 - ZOOMED IN RESOLVED IMPACT LOCATION

As can be seen, the red dot (the resolved location) and the black dot (the real hit location) are slightly off. During the testing and coding phase of this program, it was found that rarely did the 3-circles overlap exactly. This is because of the resolution of the numbers and the magnitude of the increments. If the increments were infinitesimal and the precision was 100+ digits long, then exact solutions would be found nearly every time, but it would also take too long to resolve location. Because of this, the precision of digits is set to 0.001 and the increments of the radius are also set to 0.001.

So, when looking at the solution set, checking to find the first real intercepts, a problem emerges—there will always be some imaginary part.

To resolve this, one can look at the modulus of $X_i - X_j$ and $Y_i - Y_j$. In other words, one can subtract the intercepts and looks for when $X_i - X_j = 0$. However, since an exact 0 will rarely come up, one should look for the modulus, or absolute value, and discard the complex argument. The logic is such: if the difference between $X_i - X_j = a + ib$, then the modulus is $\sqrt{a^2 + b^2}$ and the complex argument is $\arctan(b/a)$, and the full form is $a + ib = \sqrt{a^2 + b^2}\exp\left(i2\pi \cdot \arctan\left(b/a\right)\right)$. Since the arctangent is placed inside an exponential anyway, its contribution can be no more than a value of 1 since[lxvi]

$$\exp(i\phi) \equiv \cos(\phi) + i\sin(\phi)$$

- $|\cos(\phi)| \le 1$
- $|\sin(\phi)| \le 1$
- $|\exp(i\phi)| = |\cos(\phi) + i\sin(\phi)| = \sqrt{\cos^2(\phi) + \sin^2(\phi)} = 1 \quad \forall\ \phi$

Therefore, looking at just the modulus will suffice. On the complex plane (similar to the polar plane), the modulus represents a circle, whose radius is the absolute value of the complex number and whose angle is the complex argument[lxvii].

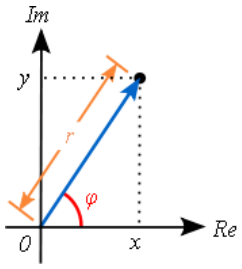

FIGURE 40 - COMPLEX NUMBER ON PLANE (SRC: WIKIPEDIA)[lxviii]

Looking at the above figure, as long as "r", the modulus of the complex number is small, it is irrelevant how big φ is.

MONTE CARLO RUN – 30,000

This Matlab program was written in the fairly new object oriented structure, introduced into Matlab in version 2008A. The advantage of object oriented is the ease of taking an algorithm and running it in multiple scenarios without rechecking the integrity of the code; the classical way of putting this is "object oriented design separates interface from implementation."

With this in mind, the program can be run in multiple modes. The obvious mode is giving the program an explicit location to resolve. The next mode is to allow the user to click on a graph, signaling the hit location. And lastly, the program can be commanded to use random impact locations. And with this random location feature, Matlab can be programming to run the simulation in a loop as many times as wanted with those random inputs.

The Matlab function used to generate the random numbers is simply rand(). Rand is itself an algorithm set to give values uniformly random between 0 and 1. The following loop is run for the Monte Carlo:

MONTE CARLO SCRIPT

```
N    = 30000;
t    = zeros(N,1);  % Initialize long arrays for faster run time.
acc = t;
doPlots   = false; % Suppresses any plotting
runrandom = true;  % Flags SimImpact to run a random impact
rng shuffle        % Ensures a unique random seed for each run
for i = 1:N        % The 30,000 long loop
    SimImpact      % This starts a script which executes a single run
    t(i)   = tdoa.time; % tdoa is a Matlab object generated by
                        % SimImpact and contains the wanted data
    acc(i) = distance(tdoa.hit, tdoa.XY); % This is just Pythagoreans
                   % Theorem. Using Matlab's built in function
end                % t(), acc() will be analyzed for statistical data
```

SIMIMPACT SCRIPT

```
clear tdoa           % Clear tdoa object if it exists already
tdoa = TDOA;         % Create tdoa object
tdoa.makeGrid();     % Create sensor landscape internally
tdoa.randomImpact(); % Set a random coordinate as the impact location
tdoa.spreadSAW();    % Spread the SAW till 3 nodes are activated
tdoa.multilat(tdoa.dT2,tdoa.dT3);
% By the end of this algorithm, the "tdoa" object has collected the
% wanted data
```

MATLAB OBJECT – TDOA

Each TDOA object contains the following information within it:

```
            nodes: [8x2 double]    % Node coordinates
  nodesRegistered: 8               % Number of Nodes
              hit: [0.6760 0.4610] % Hit location
               XY: [0.6710 0.4730] % Resolved location
          hitDist: [8x1 double]    % Hit's distance from each node
             minX: 0
             minY: 0
             maxX: 2
             maxY: 1          % Size of sensor 1"x2"
              inc: 0.001      % Resolution of sensor
              err: 0.0200     % Maximum error bound
               R1: 0.1803     % R1 is a reference and is 0
               R2: 0.5634     %    within algorithm
               R3: 0.6288     % Initial radiuses
            node1: 4
            node2: 7
            node3: 2          % Activated nodes
              dT2: 0.0112     % Time it took to hit 2nd sensor
              dT3: 0.0131     % Time it took to hit 3rd sensor
           t1_REF: 0.0053     % Time it took to hit 1st sensor
```

```
        loops: 174          % Number of loops to find impact
overHeadTime: 0.0033        % Time it takes Matlab to run overhead
        time: 0.0431        % Time Matlab spent in algorithm alone
```

This information, when aggregated from 30,000 independent simulations will help generate statistical diagrams detailing the usefulness of this algorithm and what to expect in real life scenarios.

MONTE CARLO RESULTS

The short scripts and the TDOA object shown above are used to aggregate the following statistics:

ALGORITHM ACCURACY

Accuracy is measured using Pythagorean's theorem $d = \sqrt{(x_1 - x_2)^2 + (y_1 - y_2)^2}$ —through use of the internal Matlab function distance()—between the tdoa.hit coordinate (the actual hit location) and the tdoa.XY coordinate (the resolved hit location). The following histogram shows the accuracy expectation:

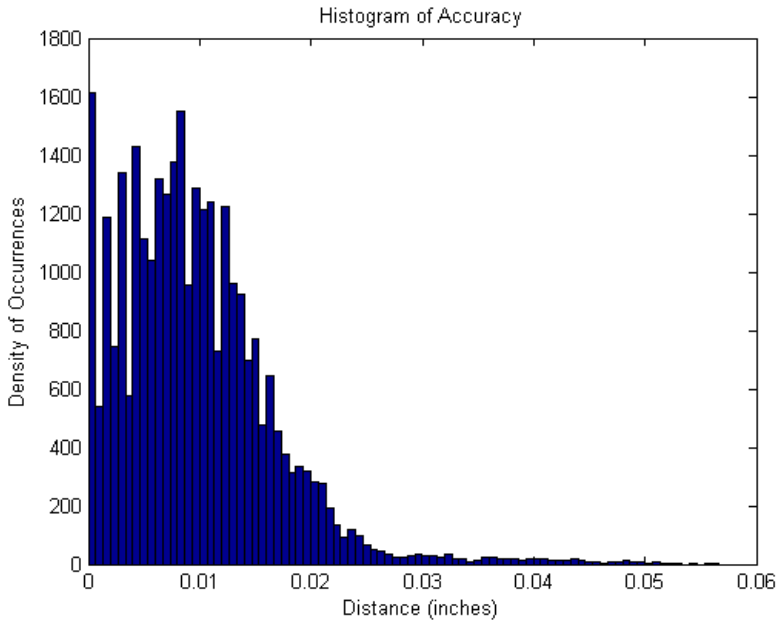

FIGURE 41 - MONTE CARLO ACCURACY HISTOGRAM

This histogram takes all 30,000 results from the distance formula, condenses them into 85 bins where the Y-axis is the density of occurrences and the X-axis is the distance. As can be seen, most of the occurrences are chunked in the 0 – 0.02" range. The vital statistics are:

Mean Distance	0.0097"
Standard Deviation	0.0070"
Maximum Distance	0.0556"
Minimum Distance	0.0000"

TABLE 3 - ALGORITHM ACCURACY STATISTICS

Therefore, this algorithm, with the given error bounds and 0.001" resolution gives very accurate results. One should expect the difference between the resolved hit location and the actual hit location to be on the order of 1 one-hundredths of an inch, and that is rounding up at that. Further, roughly 1600 hits were resolved with 100% accuracy.

ALGORITHM TIME

The algorithm time, found by measuring the number of seconds elapsed in the main multilateration loop and neglecting any overhead or non-mathematical operations, is given with the following histogram:

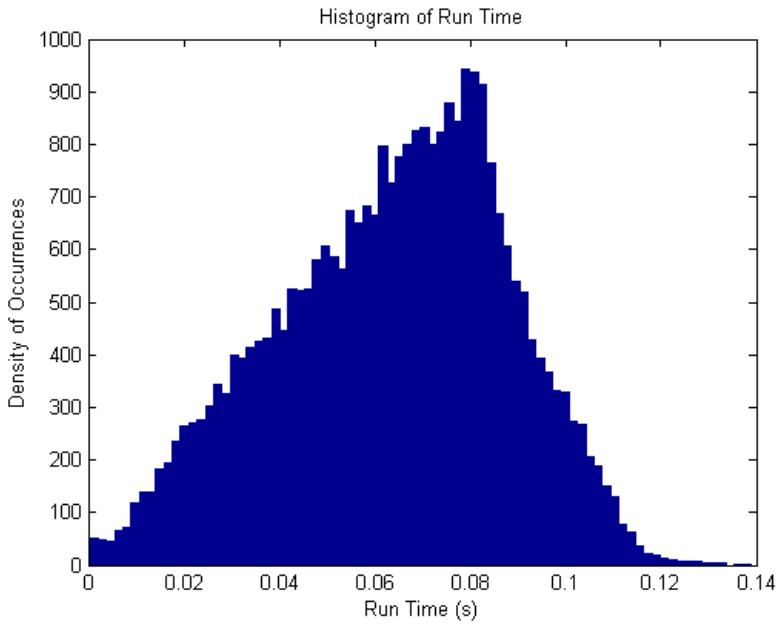

FIGURE 42 - MONTE CARLO TIME HISTOGRAM

The above histogram takes the algorithm time from the 30,000 simulations and organizes them into 200 bins with the Y-axis specifying the density of occurrences and the X-axis specifying the time in seconds. The vital statistics are:

Mean time	0.0637 seconds
Standard Deviation	0.0242 seconds
Maximum time	0.3467 seconds
Minimum time	0.0003 seconds

TABLE 4 - ALGORITHM TIMING STATISTICS

Algorithm time can be a function of many things beyond just the mathematics. Since this process was run on a shared UCLA workstation computer which could have other tasks demanding CPU cycles while the Monte Carlo was running, outliers occurred. The outliers were so sparse that it was purposefully neglected in the histogram and only graphed from 0s to 0.14s, even though the maximum time is 0.3467 seconds. With that said, on a dedicated arithmetic logic unit (ALU) and CPU, one would expect results without the outliers.

The algorithm proves to be sufficiently fast for this application. On average, one can expect results in less than 7 one-hundredths of a second, with a high of about 0.14 seconds and a low being nearly instantaneous.

ALGORITHM FACTORS, CONSIDERATION, AND CONCLUSION

Some factors that were found to affect algorithm timing were the spacing of the nodes. The farther nodes are from each other, the more loops the algorithm must go through. This shows a strong incentive to increase the density of nodes, however increasing the density of nodes will increase the complexity of the sensor, as each node requires careful design to ensure it releases identifiable and unique chirps. The best compromise found is to have 4 nodes per square inch.

The other factor mentioned above is the resolution of the algorithm. The lower the resolution, the higher the error—sometimes the error can be so high, no solution will be found at all. This scenario of not finding any solution can happen when the loop passes over the intersection location by such an amount, that the complex modulus (written about at the top of this section) becomes too large. The largest expected amount of error is 0.1", but in the Monte Carlo, the largest

error was 0.0556”. Failure was common earlier in the algorithm development before the proper tuning of error bounds and resolution were determined; now, of all 30,000 simulations, exactly 0 were failures.

This algorithm has proved to be highly effective in triangulating location, it gives very high accuracy at short time intervals. One could take this same algorithm to other sensor systems too, in fact. All that is needed are unique nodes, about 4 per square inch, and a tactile sensor can be made. If faster response time is wanted, increasing the density of nodes can be used or the error tolerance can be raised slightly. This system could be useful in touchpads that want to have surfaces more resilient to strain and impacts, without compromising the capacitive arrays within them.

FINITE ELEMENT ANALYSIS

Finite Element Analysis (FEA) is the practice of splitting a system into smaller parts that can be looked at linearly and, after analyzing the smaller parts, combined into its whole. Specifically, highly complex partial differential equations describing systems with multiple topologies, geometries, and material properties can be split into tiny shapes that can be solved one-by-one as ordinary differential equations, then once solved, can be combined to form its entire system using methods from Euler or Runga-Kutta[lxix].

In the case of this sensor, there are 7 layers, each adhered to the other, but having separate properties. Each layer shares an impact load, and one of the layers has coupled electromagnetic properties (the PVDF piezoelectric layer). In earlier sections of this report, a 1 MPa load was assumed and its presence was given throughout the sensor—in the case of FEA, a more realistic input load can be analyzed over a specified region. FEA will numerically solve for the stresses at each point of the sensor as well as the voltage response of the PVDF.

The finite element analysis program used was Ansys 13. By using this tool, calibration is made much easier. For example, one can input the thickness of each layer and vary it slightly to find out how much more of a voltage response can be achieved depending on the impact. Ansys also helped give a rudimentary proof of concept—a sensor like this one can produce an electric field on impact and give results that are generally wanted.

In a real design lab, one may test initial experimental parameters in Ansys as a sanity check, then perform live experiments, then go back into Ansys for additional calibration and improvements. Ansys, when used on a supercomputer, could simulate the dynamics of a system as well. Dynamic analysis was found to be impossible on a standard workstation computer due to a lack of computing resources. But, for example, car designers who have access to such high end supercomputers can conduct this analysis and achieve results like such:

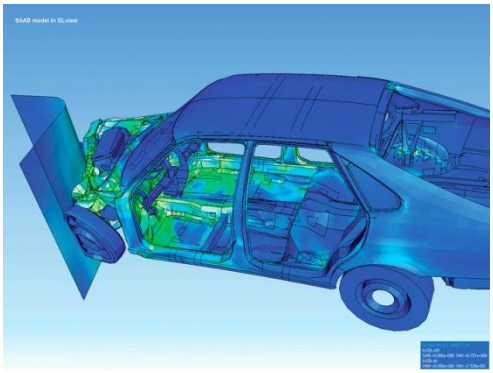

FIGURE 43 – CAR CRASH ANALYSIS USING FEA[lxx]

The following sections will contain many images from the FEA analysis.

IMPACT MODEL

Ansys typically defaults a load to a ramp—that is, a linear function, like $P(t) = m \cdot t$, where the initial value, $P(t_0) = 0$, and $P(t_f) = P_D$ where P_D is the desired pressure value wanted. This ramping method is a reasonable approximation but a more sophisticated function can be used that realistically describes a pressure function. The following pressure function was used in this analysis:

$$P(t) = 10^6 \cdot \exp\left(-\left(\frac{t - 0.0026}{2 \cdot 10^{-7}}\right)^2\right)$$

This pressure value is a Gaussian with peak amplitude of 1 MPa, with a delay of 2.6 millisecond and a pulse width of 400 microseconds—which results in a sigma of about 10^{-7}. The value of 400 microseconds conforms to a safe value impact duration found in the Contact Mechanics section of this report and the 2.6 millisecond delay ensures the pulse starts from low values of P, passes through 1 MPa and ends with low values of P, thus describing a life-like impact.

The reason Gaussian was the chosen function is because it can be easily modified to look like a symmetric impulse, it is a well-known function and used in many applications[lxxi], and it is the

statistical normal distribution, used as the de-facto bell curve. For this, it seemed reasonable to use a Gaussian as the pressure function.

The impact is also focused entirely normal to the sensor with no shearing or other effects—though they could be present in a real life scenario. Just to repeat, the goal of the FEA is to make sure there is a proper voltage response based off of the known material coefficients given in the material properties section of this report.

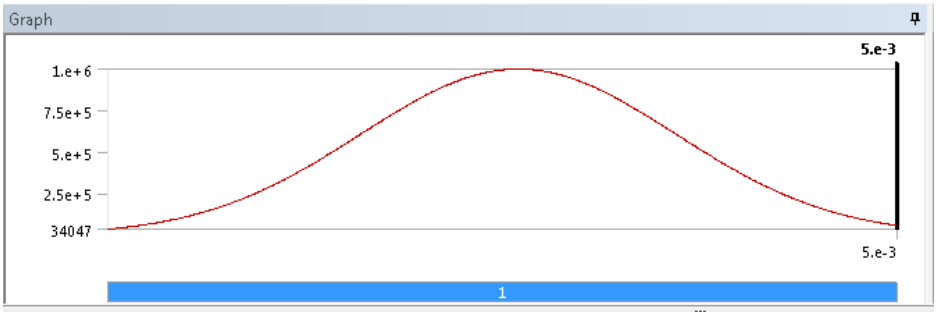

FIGURE 44 – GAUSSIAN PRESSURE LOAD IN ANSYS

The above figure shows how the pressure wave will look. Just for reference, when taking these values into Matlab, the following figure is achieved.

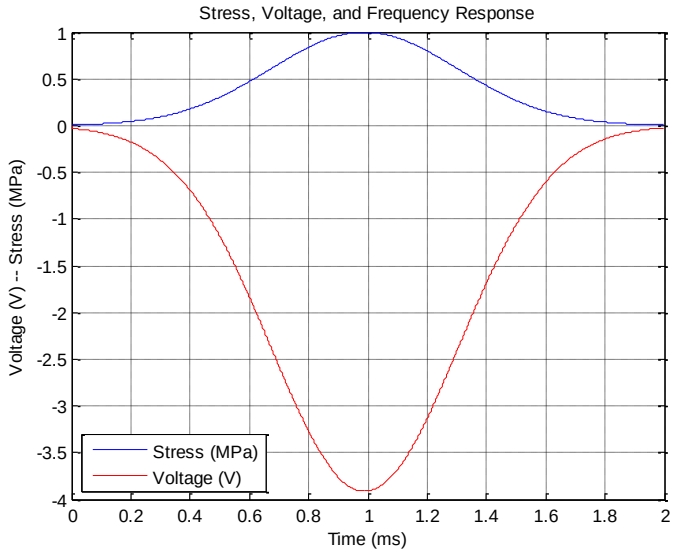

FIGURE 45 – MATLAB STRESS & PRESSURE EXPECTATION

So a voltage magnitude in the 4V range will hopefully be achieved. See the Electrical Loads section of this report for more details on the Matlab piezoelectric effect simulation.

SENSOR MODEL

Within Ansys, specifically its Design Modeler, a near exact representation of the sensor is constructed. Seven layers comprising of the aluminum, copper, kapton and PVDF are layered each of the desired thickness and area of 2" by 1".

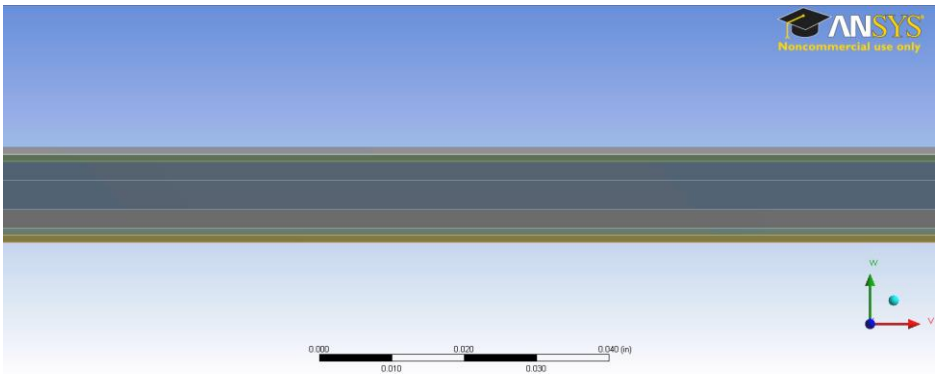

FIGURE 46 – SENSOR SIDE VIEW – ANSYS DESIGN MODELER

The sides view of the sensor—the expectation is a force can be applied at one side and permeate through the thickness.

MESH

The meshes, or the elements of the finite element analysis, are generated automatically by Ansys using the multi-zone mode. The following images show the mesh:

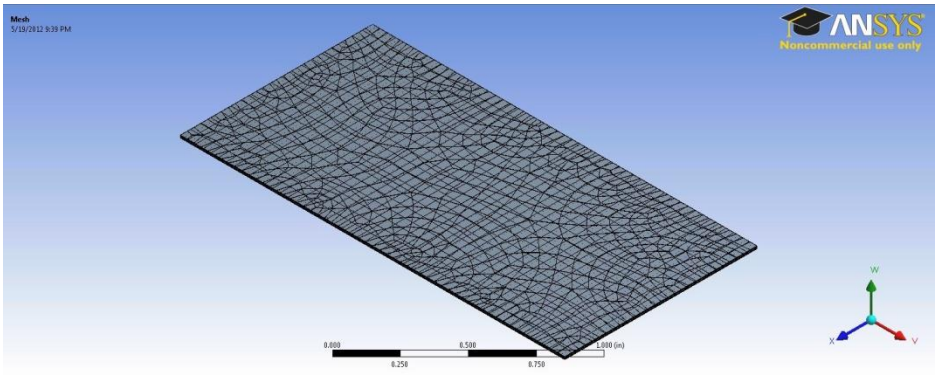

FIGURE 47 – BOTTOM VIEW MESH

The bottom of the sensor is the location of a fixed support, meant to simulate the sensor being adhered to a hard body.

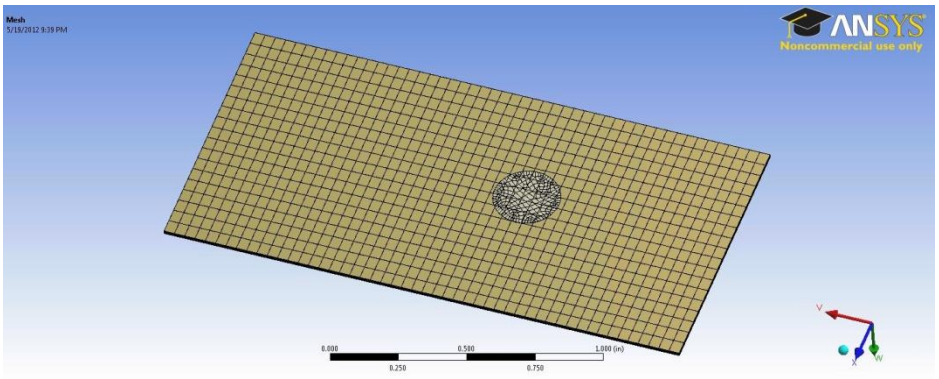

FIGURE 48 – TOP VIEW MESH WITH IMPACT LOCATION AREA SHOWN

The circle on the top view is the location where the impact will occur. Without creating this geometric region, the pressure couldn't only be applied to a face or edge.

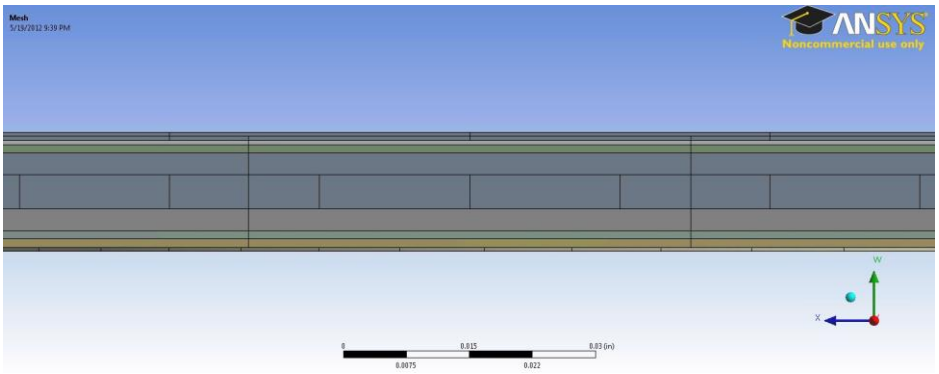

FIGURE 49 – SIDE VIEW MESH

Meshing is a complex topic of itself but for the purposes of this report, automatic meshing appeared to give realistic values.

STATIC STRUCTURAL

Static Structural analysis is a standard method in Ansys which allows the user to take a CAD geometry, apply a mesh, appoint fixed edges or faces (support), and apply a load. The load can be applied as a typical ramp or a function, like a Gaussian (described earlier)

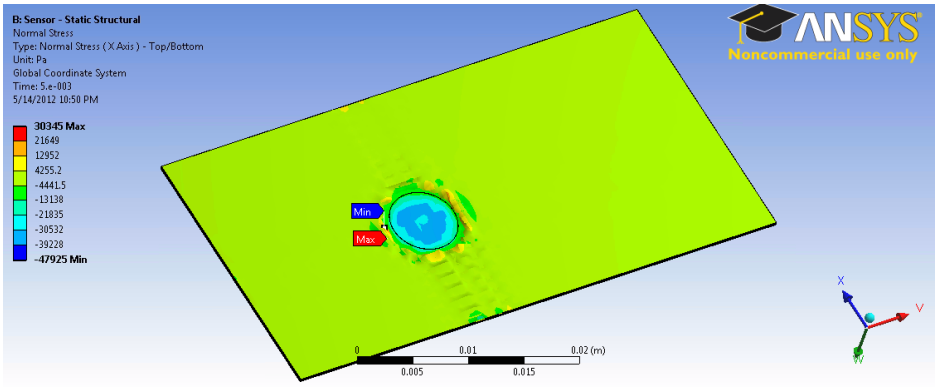

FIGURE 50 – SENSOR IMPACT DEPRESSION – STRESS

This figure shows the sensor after it has been impacted by the object. One can see crests of waves going along the surface, near the depression, as well as significant crests around the depression.

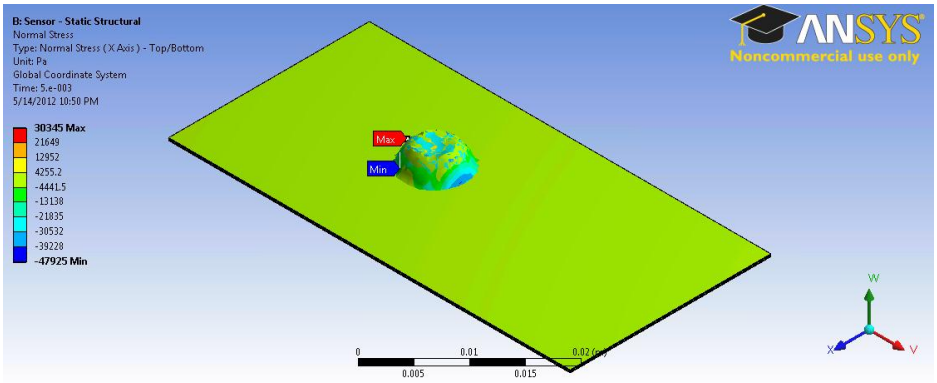

FIGURE 51 – SENSOR IMPACT BULGE – STRESS

This figure shows the results of the same impact but on the other side. Although the depression seems like a big bubble, it is an exaggerated view, as will be seen in the deformation images.

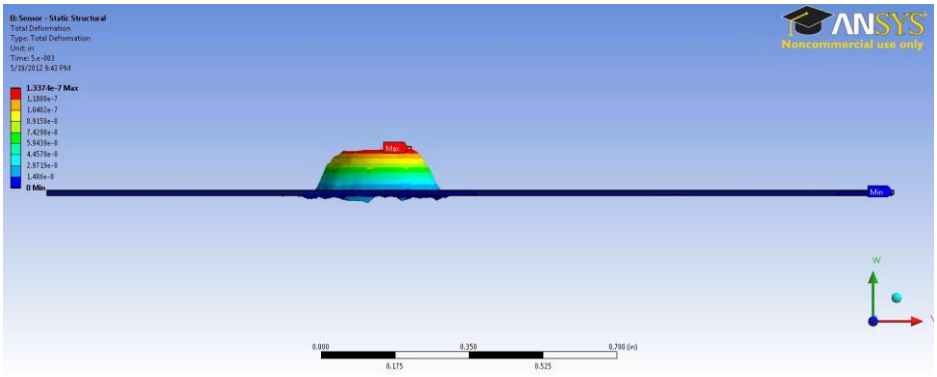

FIGURE 52 - SENSOR IMPACT BULGE (SIDE VIEW) – DEFORMATION

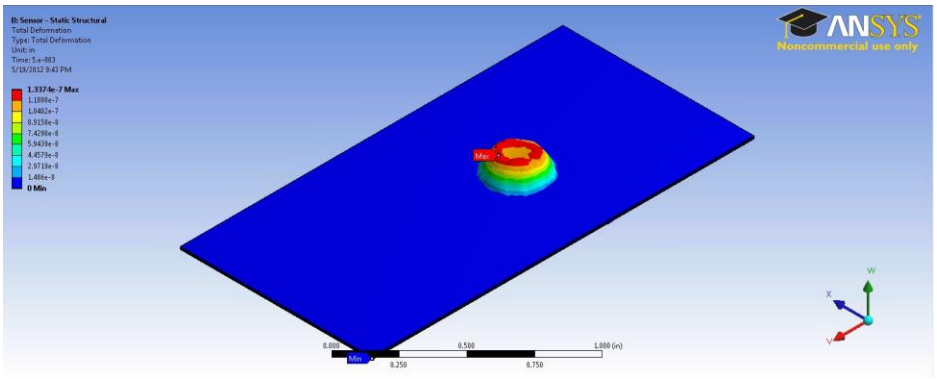

FIGURE 53 – SENSOR IMPACT BULGE (TOP VIEW) - DEFORMATION

This figure shows the deformation is on the order of 10^{-7} meters, or 0.1 micrometers. This differs from the contact mechanics section which gave values of 10^{-5} meters. The contact mechanics section based its results on a theoretical Hertzian solution while FEA is based on the numerical solution to many ordinary differential equations. A proper FEA set up should give more accurate results.

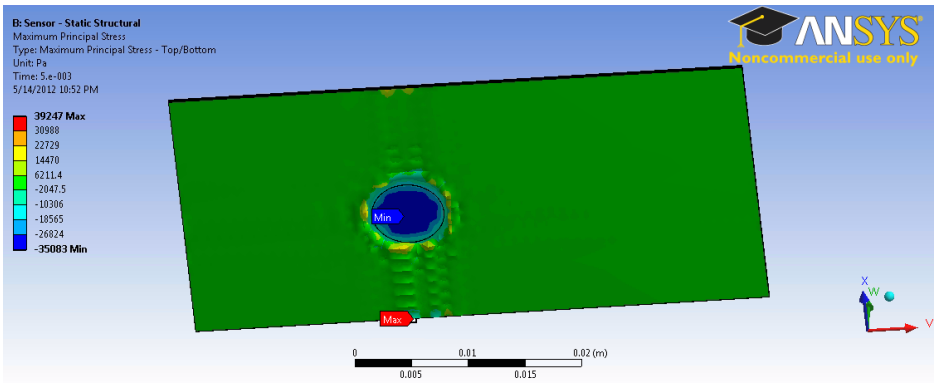

FIGURE 54 – SENSOR IMPACT SAW REVEALED

ELECTRICAL ANALYSIS

Finally, the electrical analysis—the main study in the Ansys simulation. Voltage was found through using the Ansys APDL commands to create the piezoelectric effect programmatically:

```
/NERR,1000000
et,1,226
keyopt,1,1,1001 !Piezo
mp,dens,1,1.78e3 ! Density kg/m
mp,ex,1,2e9 ! Pascal
mp,nuxy,1,0.3
mp,perx,1,106e-12 ! F/m
mp,pery,1,106e-12
mp,perz,1,106e-12
tb,piez,1
tbdata,7,6e-12
tbdata,8,1e-12
tbdata,9,15e-12
ic,1,volt,0
```

The commands are specified within the PVDF layer and the following command is specified in the Solution section of Ansys:

```
plnsol,volt,,2
```

These commands allow an Ansys user to exactly specify the material coefficients in such a way that the graphical Engineering Data module cannot do. The “tb,piez,1” tells Ansys that the material’s piezoelectric coefficient matrix will be specified and tbdata 7, 8, and 9 are d_{33}, d_{31}, and d_{32} respectively. The following images show this voltage response:

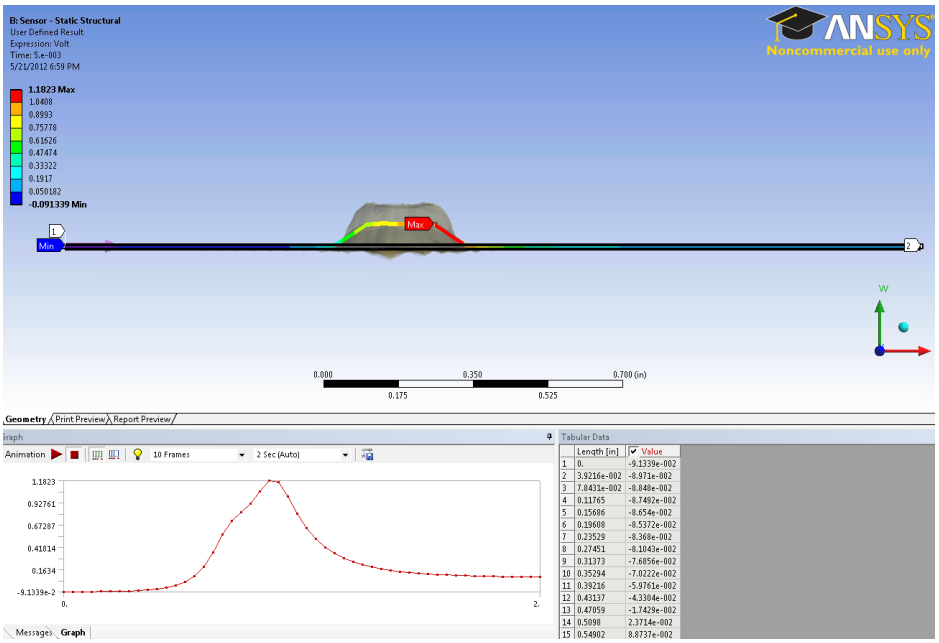

FIGURE 55 – ANSYS VOLTAGE RESPONSE – SIDE VIEW

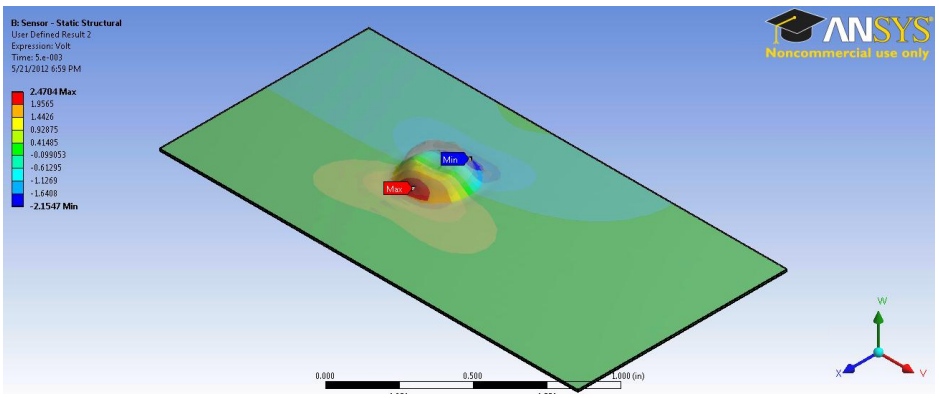

FIGURE 56 - ANSYS VOLTAGE RESPONSE – TOP VIEW

As can be seen, the voltage response is in the 2V range, which conforms quite closely to the Matlab hand analysis.

BLOWN UP SENSOR MODEL

Explicit Dynamic analysis, or rather analyzing a system at small steps in time, was performed on a blown up version of this sensor with the hopes to observe a SAW. Initially, explicit

dynamics was attempted on a geometric, real life dimension version of the sensor itself, but the analysis was estimated to take over 1000 hours, so it was abandoned. Instead, per advice from Professor Lynch, dynamic analysis was performed on a blown up version of the sensor which required only 30 minutes to analyze.

Although analysis on the small scale of the actual sensor could not be performed, the goal of this analysis was not centered on an exact representation, just observation and confirmation of surface acoustic waves.

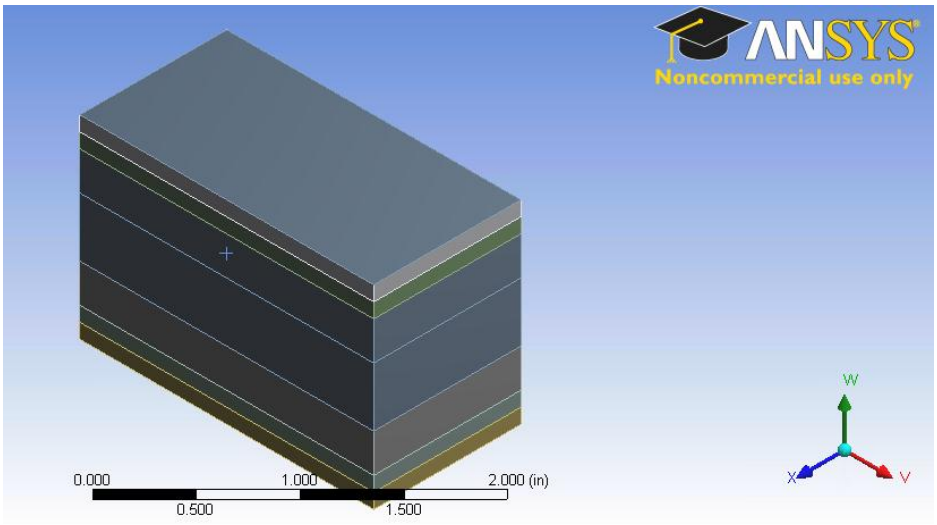

FIGURE 57 - BLOWN UP SENSOR VIEW FOR EXPLICIT DYNAMICS

STATIC STRUCTURAL

Before the dynamic analysis, a check on the static analysis of the blown up sensor model was performed, just to confirm everything was okay before the longer dynamic analysis.

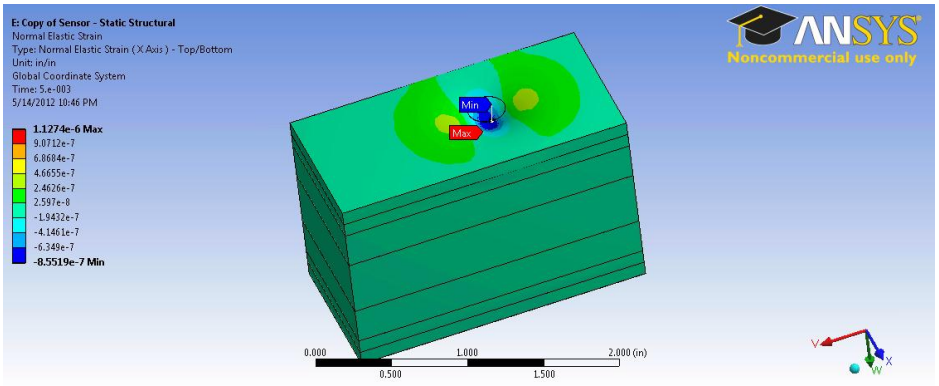

FIGURE 58 - ANALYSIS OF BLOWN UP SENSOR - ELASTIC STRAIN

The above figure shows the elastic strain at the impact region. Since this is a static view, it shows the pressure at varying locations, mostly on the top material. This conforms to the expected outcome of an impact. Recall the image in the surface acoustic wave section of this report showing that much of the wave energy is at the surface.

ELECTRICAL ANALYSIS

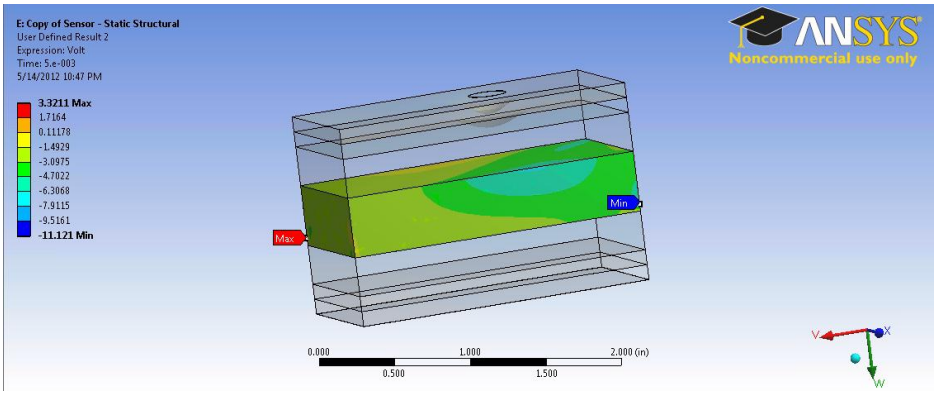

FIGURE 59 - ANALYSIS OF BLOWN UP SENSOR – ELECTRICAL RESPONSE

The above image is the voltage response of the PVDF layer in this blown up sensor. Since the thickness of the PVDF is 10x greater, getting values in this range is expected. At first, it was speculated that the voltage response would be much smaller since the pressure would dissipate, but knowing the piezoelectric equations, the thicker the piezoelectric material, the larger the possible electric field (see Voltage Response Discussion section).

EXPLICIT DYNAMICS

Now that the static structural and electrical analysis on the blown up sensor model has been performed and gave reasonable answers, explicit analysis was performed.

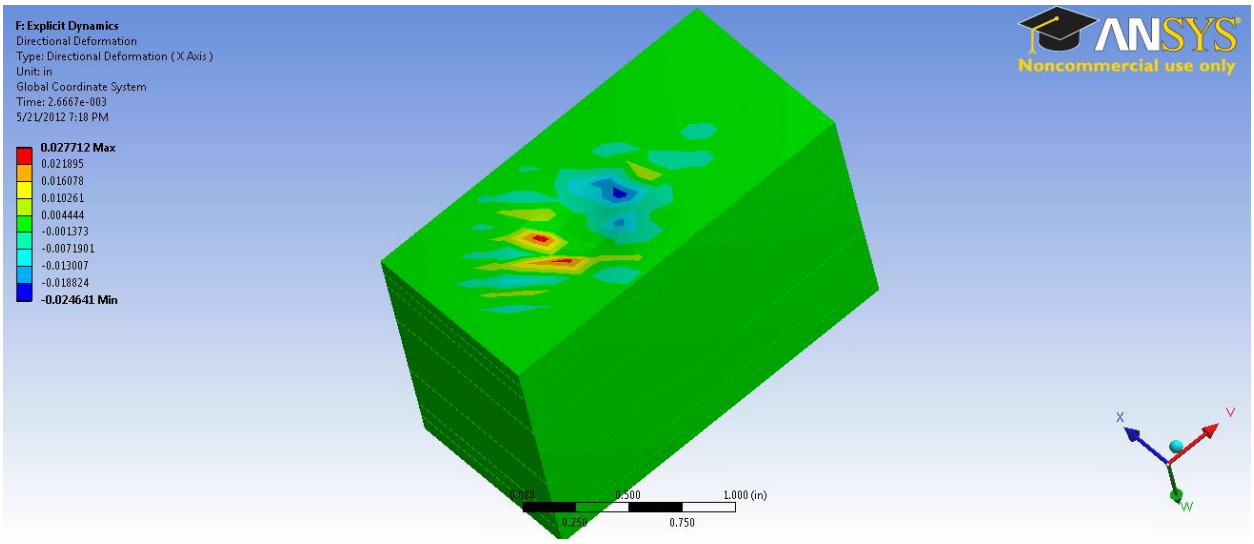

FIGURE 60 - ANALYSIS OF BLOWN UP SENSOR – SAW DYNAMICS – DIRECTIONAL DEFORMATION

This image shows wave flows going through the material. The analysis was short, around 0.008 seconds of model time (though it took at least 30 minutes to perform) because any higher and Ansys gave numerous memory errors. However, this image demonstrated the flow of pressure causing deformation through the sensor. A SAW was produced.

The image above shows wave crests moving through the material with a maximum point on the lower-middle left, which the impact occurred. There are troughs and low points, shown in blue as well.

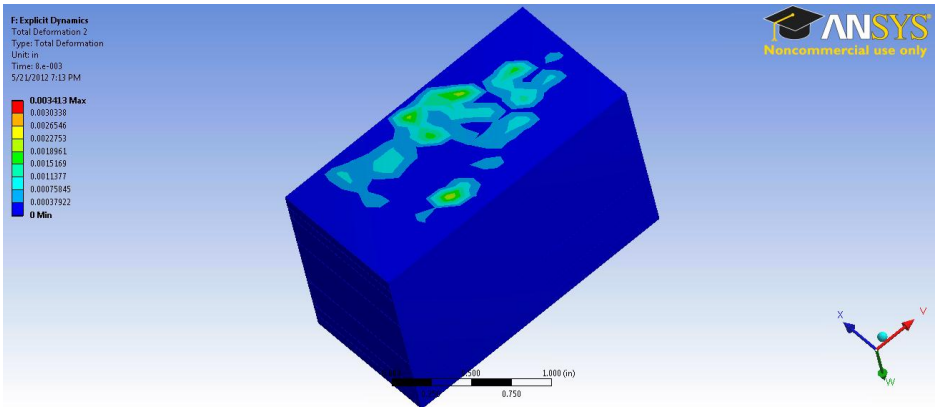

FIGURE 61 - ANALYSIS OF BLOWN UP SENSOR – SAW DYNAMICS – DIRECTIONAL DEFORMATION

The above figure shows total deformation and a pattern of dents in the material as the SAW moves. These images were taken from an Ansys animation as the most representative of the waves.

FUTURE OUTLOOK AND FINAL RESULTS

POSSIBILITIES AND CHALLENGES

Wireless, passive sensing is clearly a possibility, though its level of sophistication may be higher than first anticipated. This makes sense though, if it were simple it would have been done and on large scales already. This report showed the frequency challenges engineers would face, the low power output, the possible diode needs, as well the precision required to avoid parasitic effects. All these represent great challenges and will require non-standard approaches for development.

However, the light at the end of the tunnel is the immense increase in processing power. As processors which can run more intense algorithms become cheaper and fasters, it becomes possible for smaller, lower power system to operate effectively. That is, emitting these tiny chirps from the sensor would be useless unless economical means exist to pick up these signals and make sense of them in real time. For example, the triangulation algorithm is built on running immense equations and performing complex analysis 12 times per loop—and depending on the density of the sensor, the loops can run in the hundreds or thousands, especially if extremely high resolution is wanted. Also, the ability to filter signals mixed with large noise, such as signals in the acoustic range, presents great challenges as well (though these were not discussed in this paper). To perform these calculations, to see low power signals (just barely above 0 dB SNR) will require great processing power and a highly sophisticated middleware system.

These processors are coming into the market now, with Moore's law[lxxii] in effect. Currently, the de-facto low power, high use wireless protocol is Bluetooth which is built on a the IEEE 802.15 framework and utilized an algorithm called frequency hopping spread spectrum (FHSS)[lxxiii,lxxiv] which constitute a complex dance of frequencies hopping between narrow bands to avoid crossovers—in short, this represents high computation complexity with the result of higher effective bandwidth and lower power; with modern processors, this complexity is not an issue. So, as processors become even more powerful, it can be expected that even lower power systems requiring an even more sophisticated backbones will emerge.

Perhaps a low power, passive sensor system like this one can work with such a backbone.

DESIGN ALTERNATIVES

Barring a sophisticated, wireless middleware system, an entirely different design alternative was thought of during this study. This idea was thought of during the study of the frequency limitations and parasitic effects.

The principal of this alternative is based on using very small nodes in a material as the pivot points for the TDOA triangulation algorithm. Simply put, regardless of how the system is structured, it is all geared around finding the unknowns needed to solve the TDOA equations. Thus, instead of this sensor being an external skin, this sensor could be embedded into a material or product.

What if very small piezoelectric sensors could be implanted inside of a composite material, with fibers throughout it, but some fibers acted as wires? Each node was strategically placed around the composite before it was manufactured and solidified. Carefully, the fixed nodes were in such a position to experience the SAW and would send its chirps or signals down the conducting fiber to a wired middleware attached to the composite.

There are some immediate concerns in this system that would need to be overcome, namely making sure the surface of the composite is isotropic, or at least make sure the surface wave spread at equal speeds in all directions. To ensure equal speed, the ratio between the Young's modulus and density of the material must be the same ($v_s = \sqrt{E/\rho}$). Therefore, if a composite that somehow had isotropic properties was unattainable, perhaps one that had varying density could ensure an isotropic wave speed. Or, perhaps a traditional composite is not the right base material. Regardless, as long as the piezoelectric nodes can pick up the wave, the wave has a reliable speed, and a middleware can be non-intrusively attached to the material, this system can work.

The advantage of this system is the reduction of communication sophistication, no need for a skin like material to be adhered to the surface, and it would require less hassle for the end-user in setup and implementation. Some new disadvantages are portability and passiveness; the middleware will need to be attached and powered—though it could be powered by a source like solar. Also, if the piezoelectric material goes bad, the entire piece will need to be replaced since it is embedded.

This design alternative could open the door for entire walls being touch sensitive and advanced security systems integrated into buildings or planes.

CONCLUSION AND NEXT STEPS

The goal of this design study is to set the stage for actual laboratory implementation. This report outlined all the fundamentals from specific materials, geometric arrangements, and a suitable algorithm. However, the finer details will need to be hashed out; for example, what will the exact shape of the capacitive islands be? How will the antenna be shaped and oriented? Will diodes be necessary, and if so, how will they be implemented? Can the diode be silicon based, or will it need to be polymer based? How thick should the PVDF be to consistently achieve the wanted voltage response? And there will be many more questions as these get answered as well.

A wise beginning of a lab implementation may simply be to create a proof of concept with a 3 layer sensor, no capacitive islands, just a full PVDF layer instead with copper on the top and bottom. This implementation would be more like a generic impact sensor, not a location sensor. But, it would prove the concept to the engineer. Once completed, the next step may be to create another single layer sensor, but have the PVDF layer span 10% the size of the sensor. That is, instead of the PVDF being a full, rectangular layer between the copper, it would only sit in the middle. This arrangement would allow an engineer to test the SAW. That is, if an impact occurred on the sensor in a location far from the PVDF, will a significant enough SAW generate that will stimulate the wanted piezoelectric affect in the PVDF?

Once these two fundamental features are consistently replicated, then the task of creating multiple capacitive islands comes to the table. An engineer is to place multiple, separated capacitive islands throughout the Copper and PVDF layer and ensure that a SAW will activate each one.

At this point, the basic fundamentals have been confirmed: an impact will produce a SAW which will activate capacitive nodes. Upon successful completion of this phase, a new set of refinement tasks begin.

The first refinement task is to ensure the geometry of each capacitive island is unique and thus, causes unique but known chirps (or rather, current signatures) to drain. This may require highly precise cutting equipment to ensure the shapes of the capacitive nodes are consistent across many sensor revisions. Once the manufacturing of capacitive nodes is created and they are insured to work properly, the next step is the communication system set up.

In this configuration, the capacitive islands need to drain their current onto an antenna. This antenna must be as tuned and efficient as possible. Although it was alluded to a few times in

previous sections, it will be repeated again—the low frequency response may be a hindrance, and require very special considerations for antenna design, or it may not be reliable at all. At this moment, it is believed that the antenna will be the weakest link in this entire sensor project. However, if a large current spike/chirp is generated, it could overcome this limitation. That is, even if the antenna is extremely inefficient, if a very large current spike can be produced and last long enough for a middleware receiver to pick it up, then the antenna will work just fine. This is why the section on impact duration is so important. Accomplishing the antenna phase will be a great feat and propel an engineer to the finish line. This step will also confirm if diodes will be necessary based on how many repeat chirps are heard, interference, and other behavior that appears faulty.

If it appears diodes will be necessary to electrically isolate each capacitive node, procurement of the proper diode materials (PN junctions) will need to be found as well. This was spoken of briefly in this study, but would need to be further researched if it is required.

However, if the antenna is found to be ineffective in all configurations, then switching to an alternative design may be the best direction to go. Although the design alternative changes the fundamental idea of this passive sensor being skin like and wireless, it will still retain the location sensing ability. See the above section “Design Alternatives” for more details.

Assuming the antenna situation is resolved (either through success or alternatives), the next phase is to marry the sensor to the middleware. The middleware will need to be a state machine with a receiver tuned to work with the chirps the sensor emits. Or, if wireless chirps are not going to be used, then some second stage middleware will need to be hooked up to the material/sensor where it can modulate the wired chirps into a wireless signal. Either case, once the wireless chirps are released, the main middleware will need to act correctly to process the signals and pass them on to either a PDA, Smartphone, or perhaps directly to a 3G or 4G LTE service for cloud processing.

The above paragraphs outline the next steps an engineer would want to take in developing this sensor. Picking the specific manufacturer of PVDF may be the most critical first step, as some PVDF makers do not polarize the film; z-plane polarization is the key to the this sensor, as normal impacts are expected.

Once all these steps are accomplished and pieces of the puzzle resolved, the sensor could very well be a reality.

APPENDIX

SECTION 1 – MATLAB CODE – PIEZOELECTRIC RESPONSE

```
d33  = 15e-12;       % Piezoelectric coefficient
A    = 0.00129032;   % Area of impact in meters (2 sq inches)
R    = 1;            % 1 Ohm as an estimate
er   = 11;           % Dielectric constant of PVDF
e0   = 8.854e-12;    % Epsilon-naught
d    = 2.54e-5;      % Distance between copper layers in meters
C    = er*e0*A/d;    % Capacitance
T3n  = 1e6;          % Impact pressure, 1 MPa
sig  = 10e-9;        % Gaussian Standard deviation
mean = 0.5e-3;       % Centering location
                     % Impact is a Gaussian
T3 = @(t) T3n*exp(-(t-mean).^2/(2*sig));
                     % Voltage equation taken from earlier derivation
V  = @(t) d33*A.*T3(t)./C .*(exp(-t./(R*C))-1);
Fs  = 1e6;           % Sampling frequency
T  = 1/Fs;           % Sample time
L  = 1000;           % Length of signal
t  = (0:L-1)*T;      % Time vector
nt = 1:L;
nf = 1:513;
Vt = V(t);
subplot(211)
plot(t.*1e3,T3(t)./1e6,'b',t.*1e3,Vt,'r')
grid on
title('Stress, Voltage, and Frequency Response')
xlabel('Time (ms)')
ylabel('Voltage (V) -- Stress (MPa)')
legend('Stress (MPa)','Voltage (V)','Location','SouthWest')
NFFT = 2^nextpow2(L); % Next power of 2 from length of T
Vf = fft(Vt,NFFT)/L;
f = Fs/2*linspace(0,1,NFFT/2+1);
subplot(212)
% plot(f./1e6,2*abs(Vf(1:NFFT/2+1)))
semilogx(f(nf),20*log10(2*abs(Vf(nf))),'m')
xlabel('Frequency (Hz)')
ylabel('Voltage (V) - dB')
axis tight
grid on
```

SECTION 2 – TWELVE SOLUTIONS TO THREE CIRCLE SYSTEM

This section gives the equations which form the solution to the three circle system. The following Matlab code will generate all twelve:

```
function [x1_12, y1_12, x1_13, y1_13, x1_23, y1_23,...
    x2_12, y2_12, x2_13, y2_13, x2_23, y2_23] =
symbolicallySolveThreeCircles()
%This function is a reference. It shows how the exact solution is
%determined.
syms x y r_d R_1 R_2 R_3 x_1 y_1 x_2 y_2 x_3 y_3 x_4 y_4 R_4 real positive

eq1 = (x-x_1)^2 + (y-y_1)^2 - (R_1)^2;
eq2 = (x-x_2)^2 + (y-y_2)^2 - (R_2)^2;
eq3 = (x-x_3)^2 + (y-y_3)^2 - (R_3)^2;
xT = x; yT = y;

%%intersection of circles 1 and 2
x = solve(char(eq1-eq2),  x);
y = solve(char(eval(eq1)),y);
x12 = simple(eval(x));
y12 = simple(y);
x = xT; y = yT;

%%Intersection of circles 1 and 3

x = solve(char(eq1-eq3),  x);
y = solve(char(eval(eq1)),y);
x13 = simple(eval(x));
y13 = simple(y);
x = xT; y = yT;

%%Intersections of Circles 2 and 3

x = solve(char(eq2-eq3),  x);
y = solve(char(eval(eq2)),y);
x23 = simple(eval(x));
y23 = simple(y);

%%3 circles
x1_12 = x12(1);
y1_12 = y12(1);
x1_13 = x13(1);
y1_13 = y13(1);
x1_23 = x23(1);
y1_23 = y23(1);

x2_12 = x12(2);
y2_12 = y12(2);
x2_13 = x13(2);
y2_13 = y13(2);
x2_23 = x23(2);
y2_23 = y23(2);
```

When the above code is run, the following come out as the 12 solutions to the three circle system. Six solutions for each possible X-intersection and six solutions for each possible Y-intersection.

```
      x1_12 = (y_1*sqrt((R_1*R_2*2+x_1*x_2*2+y_1*y_2*2+R_1*R_1+R_2*R_2-
x_1*x_1-x_2*x_2-y_1*y_1-y_2*y_2)*(R_1*R_2*2-x_1*x_2*2-y_1*y_2*2-R_1*R_1-
R_2*R_2+x_1*x_1+x_2*x_2+y_1*y_1+y_2*y_2))*(-
1/2)+y_2*sqrt((R_1*R_2*2+x_1*x_2*2+y_1*y_2*2+R_1*R_1+R_2*R_2-x_1*x_1-x_2*x_2-
y_1*y_1-y_2*y_2)*(R_1*R_2*2-x_1*x_2*2-y_1*y_2*2-R_1*R_1-
R_2*R_2+x_1*x_1+x_2*x_2+y_1*y_1+y_2*y_2))*(1/2)-
(R_1*R_1)*x_1*(1/2)+(R_1*R_1)*x_2*(1/2)+(R_2*R_2)*x_1*(1/2)-
(R_2*R_2)*x_2*(1/2)-x_1*(x_2*x_2)*(1/2)-
(x_1*x_1)*x_2*(1/2)+x_1*(y_1*y_1)*(1/2)+x_1*(y_2*y_2)*(1/2)+x_2*(y_1*y_1)*(1/
2)+x_2*(y_2*y_2)*(1/2)+(x_1*x_1*x_1)*(1/2)+(x_2*x_2*x_2)*(1/2)-x_1*y_1*y_2-
x_2*y_1*y_2)/(x_1*x_2*-2-y_1*y_2*2+x_1*x_1+x_2*x_2+y_1*y_1+y_2*y_2)

      x2_12 = (y_1*sqrt((R_1*R_2*2+x_1*x_2*2+y_1*y_2*2+R_1*R_1+R_2*R_2-
x_1*x_1-x_2*x_2-y_1*y_1-y_2*y_2)*(R_1*R_2*2-x_1*x_2*2-y_1*y_2*2-R_1*R_1-
R_2*R_2+x_1*x_1+x_2*x_2+y_1*y_1+y_2*y_2))*(1/2)-
y_2*sqrt((R_1*R_2*2+x_1*x_2*2+y_1*y_2*2+R_1*R_1+R_2*R_2-x_1*x_1-x_2*x_2-
y_1*y_1-y_2*y_2)*(R_1*R_2*2-x_1*x_2*2-y_1*y_2*2-R_1*R_1-
R_2*R_2+x_1*x_1+x_2*x_2+y_1*y_1+y_2*y_2))*(1/2)-
(R_1*R_1)*x_1*(1/2)+(R_1*R_1)*x_2*(1/2)+(R_2*R_2)*x_1*(1/2)-
(R_2*R_2)*x_2*(1/2)-x_1*(x_2*x_2)*(1/2)-
(x_1*x_1)*x_2*(1/2)+x_1*(y_1*y_1)*(1/2)+x_1*(y_2*y_2)*(1/2)+x_2*(y_1*y_1)*(1/
2)+x_2*(y_2*y_2)*(1/2)+(x_1*x_1*x_1)*(1/2)+(x_2*x_2*x_2)*(1/2)-x_1*y_1*y_2-
x_2*y_1*y_2)/(x_1*x_2*-2-y_1*y_2*2+x_1*x_1+x_2*x_2+y_1*y_1+y_2*y_2)

      y1_12 = (x_1*sqrt((R_1*R_2*2+x_1*x_2*2+y_1*y_2*2+R_1*R_1+R_2*R_2-
x_1*x_1-x_2*x_2-y_1*y_1-y_2*y_2)*(R_1*R_2*2-x_1*x_2*2-y_1*y_2*2-R_1*R_1-
R_2*R_2+x_1*x_1+x_2*x_2+y_1*y_1+y_2*y_2))*(1/2)-
x_2*sqrt((R_1*R_2*2+x_1*x_2*2+y_1*y_2*2+R_1*R_1+R_2*R_2-x_1*x_1-x_2*x_2-
y_1*y_1-y_2*y_2)*(R_1*R_2*2-x_1*x_2*2-y_1*y_2*2-R_1*R_1-
R_2*R_2+x_1*x_1+x_2*x_2+y_1*y_1+y_2*y_2))*(1/2)-
(R_1*R_1)*y_1*(1/2)+(R_1*R_1)*y_2*(1/2)+(R_2*R_2)*y_1*(1/2)-
(R_2*R_2)*y_2*(1/2)+(x_1*x_1)*y_1*(1/2)+(x_1*x_1)*y_2*(1/2)+(x_2*x_2)*y_1*(1/
2)+(x_2*x_2)*y_2*(1/2)-y_1*(y_2*y_2)*(1/2)-
(y_1*y_1)*y_2*(1/2)+(y_1*y_1*y_1)*(1/2)+(y_2*y_2*y_2)*(1/2)-x_1*x_2*y_1-
x_1*x_2*y_2)/(x_1*x_2*-2-y_1*y_2*2+x_1*x_1+x_2*x_2+y_1*y_1+y_2*y_2)

      y2_12 = (x_1*sqrt((R_1*R_2*2+x_1*x_2*2+y_1*y_2*2+R_1*R_1+R_2*R_2-
x_1*x_1-x_2*x_2-y_1*y_1-y_2*y_2)*(R_1*R_2*2-x_1*x_2*2-y_1*y_2*2-R_1*R_1-
R_2*R_2+x_1*x_1+x_2*x_2+y_1*y_1+y_2*y_2))*(-
1/2)+x_2*sqrt((R_1*R_2*2+x_1*x_2*2+y_1*y_2*2+R_1*R_1+R_2*R_2-x_1*x_1-x_2*x_2-
y_1*y_1-y_2*y_2)*(R_1*R_2*2-x_1*x_2*2-y_1*y_2*2-R_1*R_1-
R_2*R_2+x_1*x_1+x_2*x_2+y_1*y_1+y_2*y_2))*(1/2)-
(R_1*R_1)*y_1*(1/2)+(R_1*R_1)*y_2*(1/2)+(R_2*R_2)*y_1*(1/2)-
(R_2*R_2)*y_2*(1/2)+(x_1*x_1)*y_1*(1/2)+(x_1*x_1)*y_2*(1/2)+(x_2*x_2)*y_1*(1/
2)+(x_2*x_2)*y_2*(1/2)-y_1*(y_2*y_2)*(1/2)-
(y_1*y_1)*y_2*(1/2)+(y_1*y_1*y_1)*(1/2)+(y_2*y_2*y_2)*(1/2)-x_1*x_2*y_1-
x_1*x_2*y_2)/(x_1*x_2*-2-y_1*y_2*2+x_1*x_1+x_2*x_2+y_1*y_1+y_2*y_2)

      x1_13 = (y_1*sqrt((R_1*R_3*2+x_1*x_3*2+y_1*y_3*2+R_1*R_1+R_3*R_3-
x_1*x_1-x_3*x_3-y_1*y_1-y_3*y_3)*(R_1*R_3*2-x_1*x_3*2-y_1*y_3*2-R_1*R_1-
R_3*R_3+x_1*x_1+x_3*x_3+y_1*y_1+y_3*y_3))*(-
1/2)+y_3*sqrt((R_1*R_3*2+x_1*x_3*2+y_1*y_3*2+R_1*R_1+R_3*R_3-x_1*x_1-x_3*x_3-
```

```
y_1*y_1-y_3*y_3)*(R_1*R_3*2-x_1*x_3*2-y_1*y_3*2-R_1*R_1-
R_3*R_3+x_1*x_1+x_3*x_3+y_1*y_1+y_3*y_3))*(1/2)-
(R_1*R_1)*x_1*(1/2)+(R_1*R_1)*x_3*(1/2)+(R_3*R_3)*x_1*(1/2)-
(R_3*R_3)*x_3*(1/2)-x_1*(x_3*x_3)*(1/2)-
(x_1*x_1)*x_3*(1/2)+x_1*(y_1*y_1)*(1/2)+x_1*(y_3*y_3)*(1/2)+x_3*(y_1*y_1)*(1/
2)+x_3*(y_3*y_3)*(1/2)+(x_1*x_1*x_1)*(1/2)+(x_3*x_3*x_3)*(1/2)-x_1*y_1*y_3-
x_3*y_1*y_3)/(x_1*x_3*-2-y_1*y_3*2+x_1*x_1+x_3*x_3+y_1*y_1+y_3*y_3)

      x2_13 = (y_1*sqrt((R_1*R_3*2+x_1*x_3*2+y_1*y_3*2+R_1*R_1+R_3*R_3-
x_1*x_1-x_3*x_3-y_1*y_1-y_3*y_3)*(R_1*R_3*2-x_1*x_3*2-y_1*y_3*2-R_1*R_1-
R_3*R_3+x_1*x_1+x_3*x_3+y_1*y_1+y_3*y_3))*(1/2)-
y_3*sqrt((R_1*R_3*2+x_1*x_3*2+y_1*y_3*2+R_1*R_1+R_3*R_3-x_1*x_1-x_3*x_3-
y_1*y_1-y_3*y_3)*(R_1*R_3*2-x_1*x_3*2-y_1*y_3*2-R_1*R_1-
R_3*R_3+x_1*x_1+x_3*x_3+y_1*y_1+y_3*y_3))*(1/2)-
(R_1*R_1)*x_1*(1/2)+(R_1*R_1)*x_3*(1/2)+(R_3*R_3)*x_1*(1/2)-
(R_3*R_3)*x_3*(1/2)-x_1*(x_3*x_3)*(1/2)-
(x_1*x_1)*x_3*(1/2)+x_1*(y_1*y_1)*(1/2)+x_1*(y_3*y_3)*(1/2)+x_3*(y_1*y_1)*(1/
2)+x_3*(y_3*y_3)*(1/2)+(x_1*x_1*x_1)*(1/2)+(x_3*x_3*x_3)*(1/2)-x_1*y_1*y_3-
x_3*y_1*y_3)/(x_1*x_3*-2-y_1*y_3*2+x_1*x_1+x_3*x_3+y_1*y_1+y_3*y_3)

      y1_13 = (x_1*sqrt((R_1*R_3*2+x_1*x_3*2+y_1*y_3*2+R_1*R_1+R_3*R_3-
x_1*x_1-x_3*x_3-y_1*y_1-y_3*y_3)*(R_1*R_3*2-x_1*x_3*2-y_1*y_3*2-R_1*R_1-
R_3*R_3+x_1*x_1+x_3*x_3+y_1*y_1+y_3*y_3))*(1/2)-
x_3*sqrt((R_1*R_3*2+x_1*x_3*2+y_1*y_3*2+R_1*R_1+R_3*R_3-x_1*x_1-x_3*x_3-
y_1*y_1-y_3*y_3)*(R_1*R_3*2-x_1*x_3*2-y_1*y_3*2-R_1*R_1-
R_3*R_3+x_1*x_1+x_3*x_3+y_1*y_1+y_3*y_3))*(1/2)-
(R_1*R_1)*y_1*(1/2)+(R_1*R_1)*y_3*(1/2)+(R_3*R_3)*y_1*(1/2)-
(R_3*R_3)*y_3*(1/2)+(x_1*x_1)*y_1*(1/2)+(x_1*x_1)*y_3*(1/2)+(x_3*x_3)*y_1*(1/
2)+(x_3*x_3)*y_3*(1/2)-y_1*(y_3*y_3)*(1/2)-
(y_1*y_1)*y_3*(1/2)+(y_1*y_1*y_1)*(1/2)+(y_3*y_3*y_3)*(1/2)-x_1*x_3*y_1-
x_1*x_3*y_3)/(x_1*x_3*-2-y_1*y_3*2+x_1*x_1+x_3*x_3+y_1*y_1+y_3*y_3)

      y2_13 = (x_1*sqrt((R_1*R_3*2+x_1*x_3*2+y_1*y_3*2+R_1*R_1+R_3*R_3-
x_1*x_1-x_3*x_3-y_1*y_1-y_3*y_3)*(R_1*R_3*2-x_1*x_3*2-y_1*y_3*2-R_1*R_1-
R_3*R_3+x_1*x_1+x_3*x_3+y_1*y_1+y_3*y_3))*(-
1/2)+x_3*sqrt((R_1*R_3*2+x_1*x_3*2+y_1*y_3*2+R_1*R_1+R_3*R_3-x_1*x_1-x_3*x_3-
y_1*y_1-y_3*y_3)*(R_1*R_3*2-x_1*x_3*2-y_1*y_3*2-R_1*R_1-
R_3*R_3+x_1*x_1+x_3*x_3+y_1*y_1+y_3*y_3))*(1/2)-
(R_1*R_1)*y_1*(1/2)+(R_1*R_1)*y_3*(1/2)+(R_3*R_3)*y_1*(1/2)-
(R_3*R_3)*y_3*(1/2)+(x_1*x_1)*y_1*(1/2)+(x_1*x_1)*y_3*(1/2)+(x_3*x_3)*y_1*(1/
2)+(x_3*x_3)*y_3*(1/2)-y_1*(y_3*y_3)*(1/2)-
(y_1*y_1)*y_3*(1/2)+(y_1*y_1*y_1)*(1/2)+(y_3*y_3*y_3)*(1/2)-x_1*x_3*y_1-
x_1*x_3*y_3)/(x_1*x_3*-2-y_1*y_3*2+x_1*x_1+x_3*x_3+y_1*y_1+y_3*y_3)

      x1_23 = (y_2*sqrt((R_2*R_3*2+x_2*x_3*2+y_2*y_3*2+R_2*R_2+R_3*R_3-
x_2*x_2-x_3*x_3-y_2*y_2-y_3*y_3)*(R_2*R_3*2-x_2*x_3*2-y_2*y_3*2-R_2*R_2-
R_3*R_3+x_2*x_2+x_3*x_3+y_2*y_2+y_3*y_3))*(-
1/2)+y_3*sqrt((R_2*R_3*2+x_2*x_3*2+y_2*y_3*2+R_2*R_2+R_3*R_3-x_2*x_2-x_3*x_3-
y_2*y_2-y_3*y_3)*(R_2*R_3*2-x_2*x_3*2-y_2*y_3*2-R_2*R_2-
R_3*R_3+x_2*x_2+x_3*x_3+y_2*y_2+y_3*y_3))*(1/2)-
(R_2*R_2)*x_2*(1/2)+(R_2*R_2)*x_3*(1/2)+(R_3*R_3)*x_2*(1/2)-
(R_3*R_3)*x_3*(1/2)-x_2*(x_3*x_3)*(1/2)-
(x_2*x_2)*x_3*(1/2)+x_2*(y_2*y_2)*(1/2)+x_2*(y_3*y_3)*(1/2)+x_3*(y_2*y_2)*(1/
2)+x_3*(y_3*y_3)*(1/2)+(x_2*x_2*x_2)*(1/2)+(x_3*x_3*x_3)*(1/2)-x_2*y_2*y_3-
x_3*y_2*y_3)/(x_2*x_3*-2-y_2*y_3*2+x_2*x_2+x_3*x_3+y_2*y_2+y_3*y_3)
```

```
      x2_23 = (y_2*sqrt((R_2*R_3*2+x_2*x_3*2+y_2*y_3*2+R_2*R_2+R_3*R_3-
x_2*x_2-x_3*x_3-y_2*y_2-y_3*y_3)*(R_2*R_3*2-x_2*x_3*2-y_2*y_3*2-R_2*R_2-
R_3*R_3+x_2*x_2+x_3*x_3+y_2*y_2+y_3*y_3))*(1/2)-
y_3*sqrt((R_2*R_3*2+x_2*x_3*2+y_2*y_3*2+R_2*R_2+R_3*R_3-x_2*x_2-x_3*x_3-
y_2*y_2-y_3*y_3)*(R_2*R_3*2-x_2*x_3*2-y_2*y_3*2-R_2*R_2-
R_3*R_3+x_2*x_2+x_3*x_3+y_2*y_2+y_3*y_3))*(1/2)-
(R_2*R_2)*x_2*(1/2)+(R_2*R_2)*x_3*(1/2)+(R_3*R_3)*x_2*(1/2)-
(R_3*R_3)*x_3*(1/2)-x_2*(x_3*x_3)*(1/2)-
(x_2*x_2)*x_3*(1/2)+x_2*(y_2*y_2)*(1/2)+x_2*(y_3*y_3)*(1/2)+x_3*(y_2*y_2)*(1/
2)+x_3*(y_3*y_3)*(1/2)+(x_2*x_2*x_2)*(1/2)+(x_3*x_3*x_3)*(1/2)-x_2*y_2*y_3-
x_3*y_2*y_3)/(x_2*x_3*-2-y_2*y_3*2+x_2*x_2+x_3*x_3+y_2*y_2+y_3*y_3)

      y1_23 = (x_2*sqrt((R_2*R_3*2+x_2*x_3*2+y_2*y_3*2+R_2*R_2+R_3*R_3-
x_2*x_2-x_3*x_3-y_2*y_2-y_3*y_3)*(R_2*R_3*2-x_2*x_3*2-y_2*y_3*2-R_2*R_2-
R_3*R_3+x_2*x_2+x_3*x_3+y_2*y_2+y_3*y_3))*(1/2)-
x_3*sqrt((R_2*R_3*2+x_2*x_3*2+y_2*y_3*2+R_2*R_2+R_3*R_3-x_2*x_2-x_3*x_3-
y_2*y_2-y_3*y_3)*(R_2*R_3*2-x_2*x_3*2-y_2*y_3*2-R_2*R_2-
R_3*R_3+x_2*x_2+x_3*x_3+y_2*y_2+y_3*y_3))*(1/2)-
(R_2*R_2)*y_2*(1/2)+(R_2*R_2)*y_3*(1/2)+(R_3*R_3)*y_2*(1/2)-
(R_3*R_3)*y_3*(1/2)+(x_2*x_2)*y_2*(1/2)+(x_2*x_2)*y_3*(1/2)+(x_3*x_3)*y_2*(1/
2)+(x_3*x_3)*y_3*(1/2)-y_2*(y_3*y_3)*(1/2)-
(y_2*y_2)*y_3*(1/2)+(y_2*y_2*y_2)*(1/2)+(y_3*y_3*y_3)*(1/2)-x_2*x_3*y_2-
x_2*x_3*y_3)/(x_2*x_3*-2-y_2*y_3*2+x_2*x_2+x_3*x_3+y_2*y_2+y_3*y_3)

      y2_23 = (x_2*sqrt((R_2*R_3*2+x_2*x_3*2+y_2*y_3*2+R_2*R_2+R_3*R_3-
x_2*x_2-x_3*x_3-y_2*y_2-y_3*y_3)*(R_2*R_3*2-x_2*x_3*2-y_2*y_3*2-R_2*R_2-
R_3*R_3+x_2*x_2+x_3*x_3+y_2*y_2+y_3*y_3))*(-
1/2)+x_3*sqrt((R_2*R_3*2+x_2*x_3*2+y_2*y_3*2+R_2*R_2+R_3*R_3-x_2*x_2-x_3*x_3-
y_2*y_2-y_3*y_3)*(R_2*R_3*2-x_2*x_3*2-y_2*y_3*2-R_2*R_2-
R_3*R_3+x_2*x_2+x_3*x_3+y_2*y_2+y_3*y_3))*(1/2)-
(R_2*R_2)*y_2*(1/2)+(R_2*R_2)*y_3*(1/2)+(R_3*R_3)*y_2*(1/2)-
(R_3*R_3)*y_3*(1/2)+(x_2*x_2)*y_2*(1/2)+(x_2*x_2)*y_3*(1/2)+(x_3*x_3)*y_2*(1/
2)+(x_3*x_3)*y_3*(1/2)-y_2*(y_3*y_3)*(1/2)-
(y_2*y_2)*y_3*(1/2)+(y_2*y_2*y_2)*(1/2)+(y_3*y_3*y_3)*(1/2)-x_2*x_3*y_2-
x_2*x_3*y_3)/(x_2*x_3*-2-y_2*y_3*2+x_2*x_2+x_3*x_3+y_2*y_2+y_3*y_3)
```

Although the above pages of equations would be nearly impossible for a human to perform by hand in any reasonable amount of time, a modern computer chip sees this as nothing more than a set of basic addition, multiplication, and square roots. This can be performed fast and in nearly real time, depending on the number of loops it has to go through.

SECTION 3 – MULTILATERATION LOOP

```
for k = 1:tries
    %Exact solutions to the 3-circle intercept equations. 6 possibilities
    %Assume no sensor overlap. Complex solutions imply no intercept.
    %Since the equations are second order polynomials, xys1 is solution
    %space for the (+) --- Analogous to the quadratic formula
    A = tic;

    [xys1 xys2] = TDOA.solveThreeCircles(x_1, x_2, x_3, y_1, y_2, y_3,
        R_1, R_2, R_3);

    if mod(k,plot_incs) == 0 && obj.doPlots
        p{1}(:,1) = xys1(:,1); %x1_12, x1_13, x1_23
        p{2}(:,1) = xys1(:,2); %y1_12, y1_13, y1_23
        p{3}(:,1) = xys2(:,1); %x2_12, x2_13, x2_23
        p{4}(:,1) = xys2(:,2); %y2_12, y2_13, y2_23
        obj.plotTriProgress(x_1,y_1,x_2,y_2,x_3,y_3,...
            R_1,R_2,R_3,p);
        pause(eps);
    end

    %p       - the increments index
    %p{n}(i) - For n = 1,2:
    %                 i = 1 is the x,y intercept of Circ 1,2 (first)
    %                 i = 2 is the x,y intercept of Circ 1,3 (first)
    %                 i = 3 is the x,y intercept of Circ 2,3 (first)
    %           - For n = 3,4:
    %                 i = 1 is the x,y intercept of Circ 1,2 (second)
    %                 i = 2 is the x,y intercept of Circ 1,3 (second)
    %                 i = 3 is the x,y intercept of Circ 2,3 (second)
    %
    % If p{n}{i} is imaginary, there is no solution.
    % i well be a be either 1,2,3 or 1,2,4 or 1,3,4, or 2,3,4
    % as one of the circles

    %p cells are used for plotting below:

    x1_12 = xys1(1,1); %p{1}(1)
    x1_13 = xys1(2,1); %p{1}(2}
    x1_23 = xys1(3,1); %p{1}(3}
    y1_12 = xys1(1,2); %p{2}(1}
    y1_13 = xys1(2,2); %p{2}(2}
    y1_23 = xys1(3,2); %p{2}(3}

    x2_12 = xys2(1,1); %p{3}(1)
    x2_13 = xys2(2,1); %p{3}(2)
    x2_23 = xys2(3,1); %p{3}(3)
    y2_12 = xys2(1,2); %p{4}(1)
    y2_13 = xys2(2,2); %p{4}(2)
    y2_23 = xys2(3,2); %p{4}(3)

    %Based on this solution, the first real intercept from the first
    %hit sensor will be the target location.
```

```
    X = [x1_12, x1_13, x1_23;
        x2_12, x2_13, x2_23];

    Y = [y1_12, y1_13, y1_23;
        y2_12, y2_13, y2_23];

    X = round(X./obj.inc).*obj.inc;
    Y = round(Y./obj.inc).*obj.inc;

    found = obj.findInterceptPt(X,Y);
    %increase R's incrementally for each iteration.
    %this needs to be here to be within the tic/toc. Otherwise, at end.
    R_1 = R_1 + incT;
    R_2 = R_2 + incT;
    R_3 = R_3 + incT;

    B = toc(A);
    time_cum = time_cum + B;

    if found
        if obj.doPlots
            obj.registerHit(obj.hit); %register original hit again to make it
more pronouced on graph.
            plot(X(found), Y(found), 'ro', 'LineWidth',5);
            obj.addframe();
            pause(eps)
        end
        obj.XY = [X(found), Y(found)];
        break
    end
end
```

SECTION 4 – CLASSICAL LAMINATION THEORY

This section was removed from the report and placed in the appendix, as it was determined to be unnecessary. Classical lamination theory deals with stress on the sides of a ply, not normal to the ply. Therefore it may not be useful; however in the off chance that it could serve some purpose in deeper analysis of the sensor, it has been preserved in the appendix.

Classical Lamination Theory (CLT) is the theory that the material properties of thin laminas can be combined such that that the full laminate's stress-strain relation can be solved using a single matrix equation. CLT is an approximation, but simplifies a 3 dimensional elasticity problem to a solvable two-dimensional mechanics of deformable bodies' problem[lxxv]. CLT is taught in the UCLA course MAE 166C, "Design of Composite Structures" by Professor Gregory Carman and the book "Mechanics of Composite Materials" by Robert Jones with its focus on composites, with materials having anisotropic and orthotropic Young's modulus, but the theory can be ported to this sensor since isotropic materials can be represented mathematically just like anisotropic materials and the layers of the sensor can be looked at as laminas, forming a final laminate.

The goal of CLT is to discern the level of strain each layer of the laminate will experience so one can get an understanding of failure and damage.

This notion of laminas falls right in line with the goal of this sensor—to be able to withstand high impacts due to proper lamination and at the same time utilize the piezoelectric effect. Therefore, CLT analysis will be used here to help calibrate the sensor's loading ability.

To derive the equations of CLT, one must combine the Young's modulus of each material, taking into account the material's position in the laminate. The following equation summarizes the theory:

$$\begin{Bmatrix} N \\ M \end{Bmatrix} = \begin{bmatrix} A & B \\ B & D \end{bmatrix} \begin{Bmatrix} \varepsilon^0 \\ \kappa \end{Bmatrix}$$

The above equation is made up of the following terms (all assumes plane stress or rather, no relevant thickness component in the individual lamina):

- N – Vector with components in the X, Y, and XY shearing direction. Notice, it does not include the normal Z direction. It has units of Newton per meter. It is mathematically defined as $N_i = \int_{thickness} \sigma_i dz$. This definition means that N_i is the stress multiplied by the thickness over each differential unit of the thickness, specifically force per unit width. This is why the units are Newton per meter, and not just Pascal.
- M – Vector with components in the X, Y, and XY shearing direction. It has units of moment per meter, or more specifically moment per unit width. Moment is Newton-meters, so even though the meter units in the numerator and dominator cancel out, the ability to describe the situation diminishes with that reduction. M specifies how much the laminate bends in accordance with its load. $M_i = \int_{thickness} \sigma_i \cdot z \cdot dz$
- ε^0 - Vector containing components of the mid-plane strain on the lamina
- κ - Vector containing components of the mid-plane curvature the lamina experiences
- A – Extensional stiffness matrix made up of the summation of each term in a materials Young's modulus: $A_{mp} = \sum_{i=1}^{n} \left(\overline{Q}_{mp}\right)^i \left(z_i - z_{i-1}\right)$.
    - $\left(\overline{Q}_{mp}\right)^i$ Represents each term in the inverse, reduced Young's modulus (i.e., compliance matrix). That is, $\overline{Q}_{11} = -E/\left(\nu^2 - 1\right)$ and $\overline{Q}_{12} = -E\nu/\left(\nu^2 - 1\right)$ etc, just as the plain strain compliance matrix specifies. The bar of the $\overline{Q}$ means that the matrix is oriented with the stress
    - $\overline{Q} = \begin{pmatrix} \frac{E}{1-\nu^2} & \frac{E\nu}{1-\nu^2} & 0 \\ \frac{E\nu}{1-\nu^2} & \frac{E}{1-\nu^2} & 0 \\ 0 & 0 & \frac{E}{2(\nu+1)} \end{pmatrix}$
    - $\left(z_i - z_{i-1}\right)$ Represents the thickness of each layer.
    - Summing everything together for each layer and each Compliance matrix—assuming 7 layers and 9 terms, it involves 63 operations.
    - When A is multiplied by the strain vector, components relating to stress on the lamina are found.

- B – Bending-extension coupling stiffness matrix made up similarly to the A matrix, only it is not multiplying each term of the Young's modulus by the thickness, but the square difference of the thickness. $B_{mp} = \frac{1}{2}\sum_{i=1}^{n}\left(\overline{Q}_{mp}\right)^{i}\left(z_i^2 - z_{i-1}^2\right)$
  - The Q and z terms are similar to the A matrix formula.
  - The B matrix, when multiplied by the strain gives components of the bending moment of the lamina
  - Also, when B matrix is multiplied by the mid-plane curvature vector, components relating to stress on the lamina are found.
    - This coupling stiffness really means that one cannot pull on a laminate without causing some bending as well, and vice-versa[lxxvi].
  - Again, with 7 layers, this requires up to 63 operations.
- D – Bending stiffness matrix similar to A and B, only it is multiplying each terms of the Young's modulus by the cube difference of the thickness $D_{mp} = \frac{1}{3}\sum_{i=1}^{n}\left(\overline{Q}_{mp}\right)^{i}\left(z_i^3 - z_{i-1}^3\right)$
  - The Q and z terms are similar to A and B matrix formula
  - The D matrix, when multiplied by mid-plane curvature gives components of the bending moment of the lamina
  - This matrix also requires 63 operations to obtain.

In deriving A, B, and D, then multiplying each term by the strain and curvature, up to 225 calculations must be performed to relate the lamina's strain and mid-plane curvature to stress and bending moment. Therefore, use of Matlab will be solely used in these calculations. The full matrix equation is:

$$\begin{Bmatrix} N_x \\ N_y \\ N_{xy} \\ M_x \\ M_y \\ M_{xy} \end{Bmatrix} = \begin{bmatrix} A_{11} & A_{12} & A_{16} & B_{11} & B_{12} & B_{16} \\ A_{12} & A_{22} & A_{26} & B_{12} & B_{22} & B_{26} \\ A_{16} & A_{26} & A_{66} & B_{16} & B_{26} & B_{66} \\ B_{11} & B_{12} & B_{16} & D_{11} & D_{12} & D_{16} \\ B_{12} & B_{22} & B_{26} & D_{12} & D_{22} & D_{26} \\ B_{16} & B_{26} & B_{66} & D_{16} & D_{26} & D_{66} \end{bmatrix} \begin{Bmatrix} \varepsilon_x^0 \\ \varepsilon_y^0 \\ \gamma_{xy}^0 \\ \kappa_x \\ \kappa_y \\ \kappa_{xy} \end{Bmatrix}$$

FIGURE 62 - CLASSIC LAMINATION THEORY MATRIX EQUATION

CLT APPLIED TO SENSOR

In applying CLT to this sensor, it is apparent that the inputs to the equation above should be stress, not strain (as stress will be estimated as 1 MPa over an area of roughly 0.2 square inches. Therefore, the equation that will be used will be:

$$\begin{Bmatrix} \varepsilon^0 \\ \kappa \end{Bmatrix} = \begin{bmatrix} A & B \\ B & D \end{bmatrix}^{-1} \begin{Bmatrix} N \\ M \end{Bmatrix}$$

Again, this operation would be immense by hand, as the matrix to be inverted is a 6x6, so only Matlab will be used to perform calculations. The following Matlab code is placed here in instead of the appendix since the lines help explain CLT and lead to the result:

```
% Material properties - All units in SI.
Ea = 70e9;  % Aluminum
va = 0.35;

Ec = 119e9; % Copper
vc = 0.34;

Ek = 2.5e9; % Kapton
vk = 0.34;

Ep = 3.2e9; % PVDF
vp = 0.35;

% Compliance Matrix Function - Plain Strain Reduction
% No longer used since can't apply normal stress!
Q = @(E,v) [E/(1-v^2) E*v/(1-v^2) 0;
          E*v/(1-v^2)   E/(1-v^2) 0;
                   0           0 E/(2*(v+1))];

in = 0.0254;    % 1 inch = 0.0254 meters
zb = 1*in;      % thickness of back support
za = 0.001 *in; % thickness of Aluminum
zc = 0.0026*in; % thickness of Copper
zk = 0.001 *in; % thickness of Kapton
zp = 0.004 *in; % thickness of PVDF

z = [-zb-za-zk-zc;  % If including back support
        -za-zk-zc;
           -zk-zc;
              -zc;
                0;
               zp;
             zc+zp;
           zk+zc+zp;
      za+zk+zc+zp]; % Thickness array - Top
```

```
% abd function gives A, B, and D depending on input.

abd = @(p) (Q(Ea,va).*(z(2)^p-z(1)^p) + ...  Al - Back Suppoer
            Q(Ea,va).*(z(3)^p-z(2)^p) + ...  Al - Bottom Layer
            Q(Ek,vk).*(z(4)^p-z(3)^p) + ...  Kapton - Bottom Layer
            Q(Ec,vc).*(z(5)^p-z(4)^p) + ...  Copper - Bottom Layer
            Q(Ep,vp).*(z(6)^p-z(5)^p) + ...  PVDF - Dielectric Layer
            Q(Ec,vc).*(z(7)^p-z(6)^p) + ...  Copper - Top Layer
            Q(Ek,vk).*(z(8)^p-z(7)^p) + ...  Kapton - Top Layer
            Q(Ea,va).*(z(9)^p-z(8)^p))./p; % Al - Top Layer

A = abd(1);
B = abd(2);
D = abd(3);
ABD = [A B; B D];

% N, M Vectors defined.
P  = 1e6;                % Pressure of impact on side - [N/m^2]
t  = (za+zk+zc)*2+zp+zb; % Thickness of Laminate      - [m]
N  = [P*t; 0; 0];        % [Nx; Ny; Nxy] - [N/m]
M  = [  0; 0; 0];        % [Mx; My; Mxy] - [mN/m]
NM = [  N; M];

str_curv = ABD\NM; % same as inv(ABD)*NM

m_strain    = str_curv(1:6);
m_curvature = str_curv(7:12);
```

$$\begin{Bmatrix} N \\ M \end{Bmatrix} = \begin{Bmatrix} 0.000056158 \\ -0.000019636 \\ 0 \\ 0.003300998 \\ -0.001154208 \\ 0 \end{Bmatrix} \rightarrow \begin{pmatrix} N_x \\ N_y \\ N_{xy} \\ M_x \\ M_Y \\ M_{xy} \end{pmatrix}$$

FIGURE 63 - CONCLUSION OF CLT - STRESS AND BENDING MOMENT

In the above code, I do the following:

1- Define the material properties – Young's modulus and Poisson ratio, E and ν
2- Create an anonymous function, Q, that takes as its arguments the material properties, E and ν.
    - This function generates a compliance matrix.
3- Define the thickness array
    - Include the payload thickness too, as the support.

4- Create an anonymous function, abd, that takes as its argument the denominator of the outside multiplier, which also serve as the term to power the thickness differences.
5- Create the A, B, D matrices by utilizing the abd function.
6- Define the N, M vectors. In this case, only N_x = 1 MPa, the rest are 0.
7- Solve for the strain-curvature vector by using numerical methods that are equivalent to inv(ABD)*NM;
8- Extract out the strain and curvature parts

CLT RESULTS

The resultant mid-plane strain and curvature acting on the laminate are shown in figure 8. These values tell one how much compression and bending will occur on the laminate when exposed to a 1 MPa impact load. Since the results of CLT are only mid-plane strains and curvatures, the idea is to take these values as the starting point for finding out the specific stresses in each ply. That is, what is the specific stress on the PVDF, and hence, what is the specific strain on the PVDF. Knowing this will help refine the expectation on the piezoelectric effect.

This noted strain relation looks like this:

$$\begin{bmatrix} \varepsilon_x \\ \varepsilon_y \\ \gamma_{xy} \end{bmatrix} = \begin{bmatrix} \varepsilon_x^\circ \\ \varepsilon_y^\circ \\ \gamma_{xy}^\circ \end{bmatrix} + z \begin{bmatrix} \kappa_x \\ \kappa_y \\ \kappa_{xy} \end{bmatrix}$$ lxxvii

Since ε^0 and κ, the mid-plane strain and curvatures were found, then the individual strains on each respective layer can be determined. By knowing the strain on each individual ply, failure analysis can be performed as well. The stresses found on each ply are:

```
strain_al_b  = m_strain + za.*m_curvature;
strain_kap_b = m_strain + zk.*m_curvature;
strain_cu_b  = m_strain + zc.*m_curvature;
strain_pvdf  = m_strain + zp.*m_curvature;
strain_cu_t  = m_strain + zc.*m_curvature;
strain_kap_t = m_strain + zk.*m_curvature;
strain_al_t  = m_strain + za.*m_curvature;

strains      = [strain_al_b strain_kap_b strain_cu_b ...
    strain_pvdf strain_cu_t strain_kap_t strain_al_t];

stress_al_b  = Q(Ea,va)*strain_al_b;
stress_kap_b = Q(Ek,vk)*strain_kap_b;
stress_cu_b  = Q(Ec,vc)*strain_cu_b;
```

```
stress_pvdf  = Q(Ep,vp)*strain_pvdf;
stress_cu_t  = Q(Ec,vc)*strain_cu_t;
stress_kap_t = Q(Ek,vk)*strain_kap_t;
stress_al_t  = Q(Ea,va)*strain_al_t;

stresses     = [stress_al_b stress_kap_b stress_cu_b ...
    stress_pvdf stress_cu_t stress_kap_t stress_al_t]


% stresses =
%
%   1.0e+006 *
%
%     3.9375    0.1401    6.6838    0.1808    6.6838    0.1401    3.9375
%     0.0015   -0.0015   -0.0732    0.0001   -0.0732   -0.0015    0.0015
%          0         0         0         0         0         0         0
```

Where the far left is the bottom aluminum layer, bottom kapton layer, bottom copper layer, pvdf layer, top copper layer, top kapton layer, and top aluminum layer.

CLT AND FAILURE

Now that the stress on the side of the laminate is determined, a failure analysis using distortion energy theory can be applied once again:

```
distortion_energy = @(s) 1/2*((s(1)-s(2))^2+(s(2)-s(3))^2+(s(3)-s(1))^2);
sf_al = 125e6; % When squared: 1.5625e+016
sf_cu = 220e6; % When squared: 4.8400e+016
sf_ka = 231e6; % When squared: 5.3361e+016
sf_pv = 240e6; % When squared: 5.7600e+016
ss = [1e6 0 0];
fail_al_t = distortion_energy(stress_al_t);  % 1.7860e+012
fail_ka_t = distortion_energy(stress_kap_t); % 2.2858e+009
fail_cu_t = distortion_energy(stress_cu_t);  % 3.5041e+012
fail_pv   = distortion_energy(stress_pvdf);  % 1.6619e+009
fail_cu_b = distortion_energy(stress_cu_b);  % 3.5041e+012
fail_ka_b = distortion_energy(stress_kap_b); % 2.2858e+009
fail_al_b = distortion_energy(stress_al_b);  % 1.7860e+012

does_al_t_fail = fail_al_t >= sf_al^2; % False
does_ka_t_fail = fail_ka_t >= sf_ka^2; % False
does_cu_t_fail = fail_cu_t >= sf_cu^2; % False
does_pvdf_fail = fail_pv   >= sf_pv^2; % False
does_cu_b_fail = fail_cu_b >= sf_cu^2; % False
does_ka_b_fail = fail_ka_b >= sf_ka^2; % False
does_al_b_fail = fail_al_b >= sf_al^2; % False
```

And once again this comes out to be false for each condition. A 1 MPa load on the sides will not cause failure.

REFERENCES

- Polh, A. "A Review of Wireless SAW Sensors" Ultrasonics, Ferroelectrics and Frequency Control. IEEE Transactions on Vol. 47, PP: 317-332, 2000
- Fu, Q. Luo, W. Wang, Y. Wang, J. Zhou, D. "Simulation of Wireless Passive SAW Sensors Based on FEM/BEM Model" Ultrasonics Symposium, 2008. IUS 2008 IEEE. Digital Object Identifier pp 1861 – 1864, 2008
- Sherrit, S. Wiederick, H. D. Mukherjee, B. K. Sayer, M. "An accurate equivalent circuit for the unloaded piezoelectric vibrator in the thickness mode" Journal of Physics D: Applied Physics, Vol. 30, Number 16., 1997
- Elvin, N. G. Elivin A. A. "A General Equivalent Circuit Model for Piezoelectric Generators" Journal of Intelligent Material System sand Structures, Vol 20, 2009
- Bucher, R. Misra, D. "A Synthesizable Low Power VHDL Model of the Exact Solution of the Three Dimensional Hyperbolic Positioning System" New Jersey Center for Wireless Telecommunications, US, pp 225-228, 2002
- Lee, H. Cooper, R. Wang, K. Liang, H. "Nano-Scale Characterization of Piezoelectric Polymer (Polyvinylidene Difluouride, PVDF)" Sensors 2008 ISSN 1424-8220. Pp 7359 – 7368
- Takeuchi, M. Matsuzawa, S. Tairaku, K. Takatsu C. "Piezoelectric Generator as Power Supply for RFID-Tags and Applications" Ultrasonics Symposium, 2007. IEEE. PP 2558 – 2561. Year 2007.
- "Interfacing PIezo Film to Electronics" Measurement Specialists Inc. www.meas-spec.com. © March 2006
- Gamelin, T. W. "Complex Analysis" 1st Edition, Springer. Year 2001 ISBN-13: 978-0387950693
- Collins, J. A. "Failure of Materials in Mechanical Design. Analysis, Prediction, Prevention" 2nd Edition. John Wiley & Sons. Year 1993. ISBN-13: 978-0471558910
- Jones, R M. "Mechanics of Composite Materials" 2nd Edition, Virginia Polytechnic Institute and State University, PP 190 – 221. Year 1999. ISBN-13: 978-1560327127
- Tillett, J. P. A. "A Study of the Impact on Spheres of Plates" Imperial Chemical Industries Limited, Butterwick Research laboratories, Welwyn, Herts. 1954

ENDNOTES

Reference links to dynamic pages, such as Wikipedia, are provided as permanent links. That is, the exact page I used in my reference is placed here, with the *&oldid* parameter pointing to the exact page I used.

[i] Pohl, A. "A Review of Wireless SAW Sensors" FIG 1
[ii] Pohl, A. "A Review of Wireless SAW Sensors" PP 2-3
[iii] Takeuchi, M. "Piezoelectric Generator as Power Supply for RFID-Tags and Applications" PP 1-2
[iv] Takeuchi, M. "Piezoelectric Generator as Power Supply for RFID-Tags and Applications" FIG 5
[v] http://en.wikipedia.org/w/index.php?title=Aluminium&oldid=486162534
[vi] http://en.wikipedia.org/w/index.php?title=6061_aluminium_alloy&oldid=487703010#Mechanical_properties
[vii] http://www2.dupont.com/Kapton/en_US/assets/downloads/pdf/HN_datasheet.pdf
[viii] http://www.pleo.com/dupont/kap_thick.htm
[ix] http://en.wikipedia.org/w/index.php?title=Copper&oldid=487988472
[x] http://en.wikipedia.org/w/index.php?title=Ultimate_tensile_strength&oldid=486839019#Typical_tensile_strengths
[xi] http://en.wikipedia.org/w/index.php?title=Electrical_resistivity_and_conductivity&oldid=487606017#Resistivity_of_various_materials
[xii] http://www.piezotech.fr/image/documents/22-31-32-33-piezotech-piezoelectric-films-leaflet.pdf
[xiii] http://www.texcal.us/coaxialwire/pvdfproperties.html
[xiv] http://en.wikipedia.org/w/index.php?title=Polyvinylidene_fluoride&oldid=488360049
[xv] Lee, H. "Nano-Scale Characterization of Piezoelectric Polymer PVDF" PP 7359
[xvi] Lee, H. "Nano-Scale Characterization of Piezoelectric Polymer PVDF" FIG 3
[xvii] Lee, H. "Nano-Scale Characterization of Piezoelectric Polymer PVDF" FIG 5
[xviii] Lee, H. "Nano-Scale Characterization of Piezoelectric Polymer PVDF" FIG 6
[xix] http://en.wikipedia.org/w/index.php?title=Ferroelectric_polymers&oldid=463921193#Study_of_the_structure_of_PVDF
[xx] http://en.wikipedia.org/w/index.php?title=Ferroelectric_polymers&oldid=463921193#Study_of_the_structure_of_PVDF
[xxi] http://en.wikipedia.org/w/index.php?title=Hamilton%27s_principle&oldid=491528400
[xxii] http://en.wikipedia.org/w/index.php?title=Lagrangian&oldid=492194569
[xxiii] Hashimoto, K Y. "Surface Acoustic Wave Devises in Telecommunications" EQ A.22
[xxiv] http://en.wikipedia.org/w/index.php?title=Piezoelectricity&oldid=489647464#Mathematical_description
[xxv] Elvin, N. G. "A General Equivalent Circuit Model for Piezoelectric Generators" PP 2
[xxvi] Hashimoto, K Y. "Surface Acoustic Wave Devises in Telecommunications" PP 276
[xxvii] http://en.wikipedia.org/w/index.php?title=Poisson%27s_ratio&oldid=482777337#Transversely_isotropic_materials
[xxviii] http://en.wikipedia.org/w/index.php?title=Contact_mechanics&oldid=492545325#History
[xxix] http://en.wikipedia.org/w/index.php?title=Contact_mechanics&oldid=492545325#Contact_between_a_sphere_and_an_elastic_half-space
[xxx] Jones, R M. "Mechanics of Composite Materials" PP 126-132
[xxxi] Jones, R M. "Mechanics of Composite Materials" FIG 3.9
[xxxii] Jones, R M. "Mechanics of Composite Materials" EQ 3.19
[xxxiii] http://www.tms.org/pubs/journals/JOM/9902/Schulson-9902.html
[xxxiv] Tillett, J. P. A. "A Study of the Impact on Spheres of Plates" PP 677-678
[xxxv] http://en.wikipedia.org/w/index.php?title=Clarence_Zener&oldid=471125281
[xxxvi] Tillett, J. P. A. "A Study of the Impact on Spheres of Plates" EQ 1
[xxxvii] Tillett, J. P. A. "A Study of the Impact on Spheres of Plates" EQ 2
[xxxviii] Tillett, J. P. A. "A Study of the Impact on Spheres of Plates" FIG 6
[xxxix] http://en.wikipedia.org/w/index.php?title=Acoustic_resonance&oldid=491058894
[xl] http://en.wikipedia.org/w/index.php?title=Acoustic_resonance&oldid=491058894#Closed
[xli] http://www.youtube.com/watch?v=00I2uXDxbaE&feature=player_detailpage
[xlii] Collins, J. A. "Failure of Materials in Mechanical Design" PP 151
[xliii] Collins, J. A. "Failure of Materials in Mechanical Design" PP 154-155
[xliv] Collins, J. A. "Failure of Materials in Mechanical Design" FIG 6.6

[xlv] http://en.wikipedia.org/w/index.php?title=Seismic_wave&oldid=486627582
[xlvi] http://en.wikipedia.org/w/index.php?title=Young%27s_modulus&oldid=486379640#Relation_among_elastic_constants
[xlvii] http://www.geo.mtu.edu/UPSeis/waves.html
[xlviii] Hashimoto, K Y. "Surface Acoustic Wave Devises in Telecommunications" Figures 1.29 & 1.30
[xlix] Hashimoto, K Y. "Surface Acoustic Wave Devises in Telecommunications" EQ 1.11
[l] Hashimoto, K Y. "Surface Acoustic Wave Devises in Telecommunications" PP 18-19
[li] http://en.wikipedia.org/w/index.php?title=Rayleigh_wave&oldid=490885772#Rayleigh_wave_dispersion
[lii] http://earthquake.usgs.gov/learn/glossary/?term=Rayleigh%20wave
[liii] Hashimoto, K Y. "Surface Acoustic Wave Devises in Telecommunications" PP 135, FIG 5.15
[liv] Hashimoto, K Y. "Surface Acoustic Wave Devises in Telecommunications" FIG 5.11
[lv] http://en.wikipedia.org/w/index.php?title=SPICE&oldid=476975144
[lvi] http://en.wikipedia.org/w/index.php?title=Transmission_line&oldid=488412329#Applicability
[lvii] http://en.wikipedia.org/w/index.php?title=Transmission_line&oldid=483323578#Explanation
[lviii] http://en.wikipedia.org/w/index.php?title=Capacitor&oldid=491043430#AC_circuits
[lix] http://en.wikipedia.org/w/index.php?title=Diode&oldid=491465949
[lx] http://en.wikipedia.org/w/index.php?title=Silicon&oldid=492146012#Physical
[lxi] http://en.wikipedia.org/w/index.php?title=P%E2%80%93n_junction&oldid=491558039
[lxii] http://en.wikipedia.org/w/index.php?title=Semiconductor_device&oldid=486067369#Semiconductor_device_materials
[lxiii] http://en.wikipedia.org/w/index.php?title=Band_gap&oldid=487590655#List_of_band_gaps
[lxiv] http://en.wikipedia.org/w/index.php?title=OLED&oldid=492030773
[lxv] http://en.wikipedia.org/w/index.php?title=Organic_semiconductor&oldid=492139035#Charge_transport_in_disordered_organic_semiconductors
[lxvi] http://en.wikipedia.org/w/index.php?title=Complex_number&oldid=490548997#Complex_analysis
[lxvii] Gamelin, T. W. "Complex Analysis" PP 5-6
[lxviii] http://en.wikipedia.org/w/index.php?title=Complex_number&oldid=490548997#Absolute_value_and_argument
[lxix] http://en.wikipedia.org/w/index.php?title=Finite_element_method&oldid=492042214
[lxx] http://en.wikipedia.org/w/index.php?title=Finite_element_method&oldid=492042214#Application
[lxxi] http://en.wikipedia.org/w/index.php?title=Gaussian_function&oldid=493052770#Applications
[lxxii] http://en.wikipedia.org/w/index.php?title=Moore%27s_law&oldid=493152165
[lxxiii] http://en.wikipedia.org/w/index.php?title=Bluetooth&oldid=493961450#Specifications_and_features
[lxxiv] http://en.wikipedia.org/w/index.php?title=Frequency-hopping_spread_spectrum&oldid=492480079
[lxxv] Jones, R M. "Mechanics of Composite Materials" PP 190
[lxxvi] Jones, R M. "Mechanics of Composite Materials" PP 198
[lxxvii] Jones, R M. "Mechanics of Composite Materials" EQ 4.13